

Spatial and Temporal Variability of Subsidence:

Fort Bend County, Texas

A Thesis Presented to
the Faculty of the Department of Earth and Atmospheric Sciences
University of Houston

In Partial Fulfillment
of the Requirements for the Degree
Master of Science

By

Rebecca L. Neill

December 2015

Spatial and Temporal Variability of Subsidence:

Fort Bend County, Texas

Rebecca L. Neill

APPROVED:

Dr. Guoquan Wang, Chairman

Dr. Shuhab D. Khan

Dr. Hyongki Lee

Dean Wells, College of Natural Science and Mathematics

Acknowledgements

My special thanks go to Dr. Guoquan Wang for his guidance, patience, and support throughout this project. I would also like to thank my committee for their continued involvement in my project. I have learned to think critically and better communicate my stance under their direction. Special thanks go to Mark Kasmarek at the United States Geological Survey and Cliff Middleton of the National Geodetic Survey for providing the raw data and offering valuable feedback.

As the HoustonNet GPS network was coming to life, Guoquan Wang, his students, and I spent a lot of time performing station reconnaissance, collecting data and installing new instrumentation. It was an intense time of learning both the mechanics and relevance of the work being done in the area. Special thanks go to all of my colleagues, both past and present, for continuing to explore and grasp the new (and old) ideas being presented in our field of research.

Finally, I would like to deeply thank my family and fiancé for their continued support. Cathy, Sarah, and Austin- thank you for contributing to my work in your own unique ways- you have kept me moving forward as I worked to obtain the necessary skills to finish this work. Ultimately, I dedicate this work to my father, who encouraged me to do the thing I would never have done for myself. Thank you.

Spatial and Temporal Variability of Subsidence:

Fort Bend County, Texas

An Abstract of a Thesis

Presented to

the Faculty of the Department of Earth and Atmospheric Sciences

University of Houston

In Partial Fulfillment

of the Requirements for the Degree

Master of Science

By

Rebecca L. Neill

December 2015

Abstract

This study presents new geodetic data revealing the evolution and magnitude of land subsidence in Fort Bend County (FBC) through 2014. Subsidence in the greater Houston metropolitan area has been monitored since 1926 and several generations of maps have portrayed more than three meters of subsidence. Recent studies indicate that the land surface has stabilized or rebounded up to 2.0 centimeters in southeast Houston, coincident with aquifer levels recovering to approximately 30 meters below land surface.

FBC, located west of Houston, was chosen to study the early drivers of subsidence. GPS stations co-located with monitoring wells across the county indicate that periodic subsidence can occur when the potentiometric surface is more than 30 meters below land surface, whether groundwater levels are rising, falling or remain stable. Nine out of the fifteen GPS stations in FBC recorded more than one centimeter of subsidence during the drought of 2011.

The potentiometric surface across FBC shows a strong correlation with areas of subsidence where the hydraulic head is more than 30 meters below land surface. In 2011, the Rosenberg and Simonton GPS stations experienced 3.0 and 4.0 centimeters of subsidence, respectively. Farther to the west, where hydraulic head is less than 30 meters BLS, GPS stations are stable.

Further investigation of Rosenberg indicates that groundwater levels *and* the rate of groundwater withdrawal controls subsidence, affecting all three-directional components. The TXRO and PA10 GPS stations show 5.0 centimeters inelastic deformation occurred from 2005 through 2013 in both the horizontal and vertical

directions. This deformation correlates with periods of increased rates of groundwater withdrawal, indicating that localized pumping can create independent subsidence.

Observational data were acquired from sixteen high-precision Global Positioning System (GPS) stations, with three or more years of data, in FBC. Data were processed using the GIPSY/OASIS v. 6.3 software package developed by NASA's Jet Propulsion Laboratory (JPL). Global position coordinates were transformed from the IGS08 reference frame to the Stable Houston Reference Frame (SHRF) using a 14-parameter Helmert transformation. Groundwater-level changes were analyzed for the period from 2005 to 2014 utilizing sixty-five USGS monitoring wells.

Table of Contents

Table of Contents.....	vii
Index of Figures.....	viii
Index of Tables.....	viii
1 Introduction.....	1
2 Study Area.....	8
2.1 Location and Instrumentation.....	8
2.2 Regional Geology.....	11
2.3 Hydrostratigraphy.....	16
3 Groundwater.....	19
3.1 Movement of Water in the Gulf Coast Aquifer System.....	19
3.2 Aquifer Mechanics.....	23
3.3 History of Subsidence in the Houston Area.....	27
3.4 Monitoring Aquifer Levels.....	30
4 GPS Positioning.....	33
4.1 GPS as a Surveying Tool.....	34
4.2 GPS Data Processing.....	36
4.3 Sources of Error and Accuracy.....	39
4.4 Reference Frame.....	46
5 Results.....	55
5.1 Groundwater Withdrawal.....	55
5.2 Groundwater Levels.....	58
5.3 GPS Measured Surface Deformation.....	63
6 Groundwater Levels and Surface Deformation.....	67
6.1 Spatial Variability of Subsidence in Relation to Hydraulic Head.....	68
6.2 Temporal Variability of Subsidence in Richmond and Rosenberg.....	74
6.3 Groundwater Levels in Relation to Geologic Features.....	80
7 Conclusions.....	82
8 References.....	84
9 Appendix I: Groundwater Levels.....	92
Appendix II: GPS Timeseries.....	107

Index of Figures

Figure 1-1 Groundwater Withdrawals in 2010 and FBC Aquifer Levels.....	3
Figure 2-1 Location of Monitoring Equipment	10
Figure 2-2 Geology Surrounding Fort Bend County	13
Figure 2-3 Cross-section A-A'	17
Figure 3-1 Movement of Groundwater in the Gulf Coast Aquifer System	21
Figure 3-2 Principal Stresses within the Aquifer System	25
Figure 3-3 FBC Monitoring Well Depths and Groundwater Levels in 2011	31
Figure 4-1 PAM Station Set-up	35
Figure 4-2 Outlier Identification and Removal.....	43
Figure 4-3 2011 Offset: PAM vs. CORS Time-Series	45
Figure 4-4 Location of Nine SHRF Reference Stations	49
Figure 4-5 PA04 Displacement Time-series in Three Reference Frames	54
Figure 5-1 Groundwater Withdrawal History by Regulatory Area	55
Figure 5-2 Annual Groundwater Withdrawal Data: City of Rosenberg Well #7	57
Figure 5-3 Groundwater Level Maps: Fort Bend County.....	59
Figure 5-4 Chicot and Evangeline Aquifer Level Changes.....	60
Figure 5-5 2011 Groundwater Levels Graph: Fort Bend County	61
Figure 5-6 GPS Observations: 2005-2014.....	64
Figure 5-7 GPS Observations: 2011-2012.....	65
Figure 6-1 2011 Potentiometric Surface and Land Surface Deformation	68
Figure 6-2 Smithers Lake: Surface Deformation and Groundwater Levels.	70
Figure 6-3 Arcola: PA40 and JY-65-29-709	72
Figure 6-4 Aerial View of PA61 in Simonton	73
Figure 6-5 TXRO and PA10 Surface Deformation	75
Figure 6-6 Evangeline Aquifer Level Changes: 2005-2014.....	76
Figure 6-7 Monthly Groundwater Withdrawal at CoR Well #7	77
Figure 6-8 Rosenberg Groundwater Levels and Surface Displacement.....	77
Figure 6-9 Groundwater levels for the Chicot and Evangeline Aquifers.	81

Index of Tables

Table 2-1 Hydrostratigraphic Column	16
Table 4-1 Vertical Shift from Antenna Change on 2011.025	44
Table 4-2 14-parameter Helmert Transformation from IGS08 to NAD83 and SHRF	53
Table 5-1 Groundwater Consumption by Area.....	56
Table 6-1 Changes in Rosenberg Groundwater Withdrawal and Aquifer Levels	78

1 Introduction

Fort Bend County (FBC) is located adjacent to Houston, an historic area of land surface subsidence due to fluid (oil, gas, or water) withdrawal. The first documented case of subsidence and faulting in the Houston area was at Goose Creek Oil Field in 1926 (Pratt and Johnson, 1926). Differential subsidence, horizontal displacements and faulting associated with oil and gas extractions from shallow fields were studied by Yerkes and Castle in 1969. Current production in FBC targets older, Oligocene-aged sediments, and is therefore disregarded in this shallow-subsidence study.

Land surface subsidence occurs naturally on a geologic timescale as sediments compact and dewater with burial. This process can be expedited by anthropogenic activities such as oil and gas extraction, groundwater withdrawal, and mining of sulfur around salt domes (Galloway and Burbey, 2011; Gabrysch, 1984). Subsidence induced by groundwater withdrawal is a known problem around the world. Both dry, arid parts of America that rely on groundwater for irrigation like the San Joaquin Valley, and densely populated metropolitan areas like Houston, Texas are significantly affected.

The Houston metropolitan area (Houston-Sugarland-Baytown) population was ranked as having the sixth largest population for a metropolitan area in the 2010 census (U.S. Census Bureau, 2012). The area's aquifer system has an abundant supply of potable groundwater (Kasmarek and Strom, 2002), purified by filtering through alternating layers of sand and clay over hundreds to thousands of years (Fogg, 1986). Before 1962, the aquifer was under artesian conditions (Wesselman, 1972) meaning wells would flow freely because aquifer pressures exceeded surface pressure.

From the late 19th to early 20th centuries, FBC was a sparsely populated agricultural community. However, over the past twenty years, it has become a booming center of residential development. Groundwater was initially developed in FBC for agricultural irrigation, and more recently for municipal supply. The large volumes being extracted since 1990 have caused major declines in potentiometric surface in and around Houston (Figure 1-1; Maupin et al., 2014). There is a corresponding, regional deepening of the potentiometric surface on the eastern half of FBC that can be attributed to both the increased rate of withdrawal in FBC and the large volumes of water being extracted to the east in Harris County.

The rate of groundwater withdrawal is three times greater in Harris County, than seen for FBC, (Figure 1-1). A strong correlation between population density, groundwater consumption, and subsidence is illustrated in Figure 1-1. The eastern, urbanized region of FBC consumed 70 million gallons per day more than the western, agricultural region in 2013. As population increases, conservation districts across the state are tasked with regulating sustainable development of the groundwater resources, (Theis, 1940).

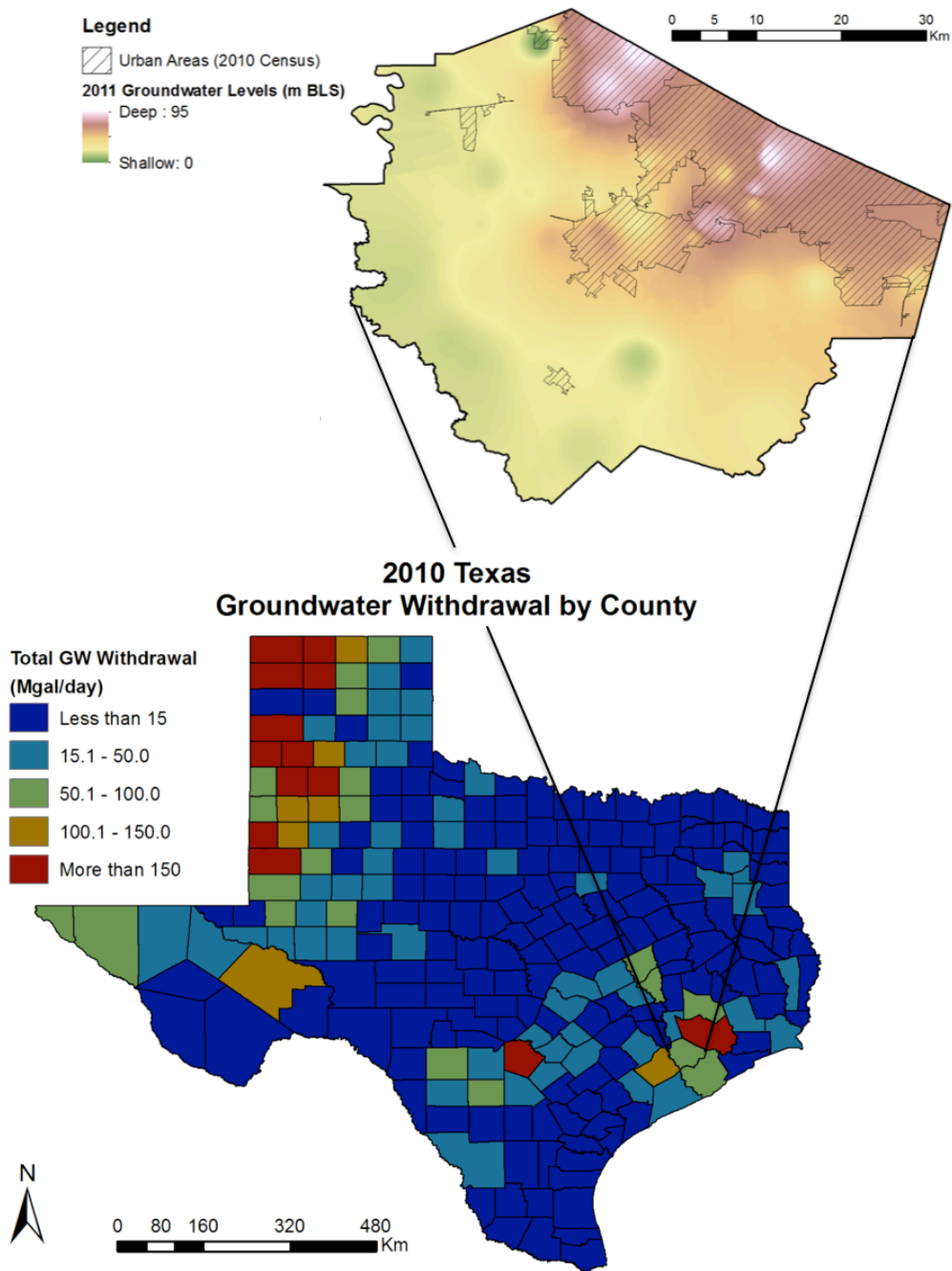


Figure 1-1 Groundwater Withdrawals in 2010 and FBC Aquifer Levels.

The lower map shows groundwater-withdrawal rates across Texas, by county. Fort Bend County extracts 76.96 million gallons per day (Mgal/day), while Harris County used 239.0 Mgal/day. Fort Bend County is expanded, showing aquifer levels in relation to urban areas. Data sources: 2010 Groundwater withdrawals (Maupin et al., 2014), Groundwater levels (USGS Groundwater Watch, 2014), Urban Areas (U.S. Census Bureau, 2010).

Subsidence is driven by aquifer characteristics and anthropogenic activities, e.g. oil and gas extraction, groundwater withdrawal, mining of sulfur around the salt domes. The first documented case of subsidence and faulting in the Houston area occurred at Goose Creek Oil Field in 1926 (Pratt and Johnson). Oil and gas were extracted from shallow, unconsolidated sediments (Yerkes and Castle, 1969), while most modern production in FBC targets deeper, Oligocene-aged sediments.

Development of surface and groundwater supplies can manipulate coastal processes through starving the sediment supply (dams), controlling flooding which would recharge aquifers over a broad area, and deposit clay-rich organic sediments to fields. Subsidence induced by groundwater withdrawal significantly impacts the Gulf Coast by flooding and the degrading of infrastructure (shifting foundations, road, and pipelines). Subsidence in coastal areas has resulted in land being inundated by bay waters (Galloway and Burbey, 2011), while episodic rainfalls or hurricanes leading to flooding more significantly affect inland locations.

For example, in 2001, tropical storm Allison stalled over Houston, raining about 90 centimeters (36 inches) over four days (Grant and Rodriguez, 2006). The bayous backed up near downtown and the Medical Center, causing significant flooding and damage. The problem of subsidence has begun to affect a larger geographic area, not just Houston, as population and development increases to the north and west of Houston. For example, Jersey Village, in northwest Houston has subsided 3 meters (~9.8 feet) in elevation due to fluid withdrawal (Kasmarek et al., 2014).

Groundwater is extracted from Miocene to Holocene-aged units to supply water for municipal, industrial, commercial, and agricultural purposes in FBC. A pertinent issue to recognize as the county tries to decrease consumption and the associated negative effects of surface deformation and flooding as groundwater resources are more heavily relied on to water lawns or maintain crops in time of drought. There is also a strong correlation between urban areas, as defined by the 2010 U.S. Census, and areas of significant drawdown within the aquifer.

FBC offers a unique opportunity to study the changing aquifer stress patterns in areas that were historically considered stable. This report analyzes groundwater and GPS data from January 2005 through January 2014, focusing on time periods of significant change. Demand for groundwater within FBC is related to land use. The two regulatory areas within the district, Area A and Area B, reflect the more urbanized and agricultural regions, respectively.

Each year, the municipalities consume five to six times more groundwater than agricultural irrigation in all of FBC (Figure 1-3; FBSD, 2013). Countywide groundwater withdrawals increased 31% from 2010 to 2011 due to drought (FBSD, 2013). The aquifer resources were significantly strained as precipitation, or recharge into the system, was less than half of the annual average.

Surface deformation is a function of the soil moisture content, involving clays with strong-shrink and -swell properties (Kasmarek et al., 2014). Slowly shifting ground adversely affects infrastructure in developed areas causing structural instability and damage to buildings, roadways, and pipelines. During the 2011 drought, subsurface

pipelines broke causing the loss of 18 billion gallons of water from June through October of 2011 (Houston Chronicle, 2011).

A reliable network of GPS stations already exists with sufficient-data history to conduct this study. Eighteen GPS sites exist in FBC, including seventeen Port-A-Measure Stations (PAMS) owned and operated by the Fort Bend Subsidence District (FBSD) and one Continuously Operating Reference Station (CORS) from the National Geodetic Survey (NGS). To minimize the influence of seasonal signals on velocity patterns within a time-series, only sixteen GPS stations with three years of data or more were used.

Researchers have traditionally treated subsidence as a one-dimensional problem occurring only in the vertical direction, and considered the horizontal components to be insignificant (Holzer, 1984). While the original paradigm holds true for most stations, GPS stations in the Rosenberg area recorded horizontal displacements of greater magnitude than the vertical, suggesting all three components should be studied to effectively understand deformation trends in FBC. Measured horizontal displacements in FBC are generally elastic and minor, ranging from 2.0 to 4.0 centimeters per year.

Surface deformation has been attributed to natural tectonic processes as no aerial correlation was found between the orientation of fault offset and known areas of subsidence in a 2010 LiDAR study of Houston (Engelkemeir et al., 2010). No work has been published on the tectonic activity in Fort Bend County at this time.

In summary, the goal of this study is to determine whether there is a regional control on subsidence and to quantify three-dimensional deformation in FBC as the aquifer is subjected to an increased demand with urban development. First, the history

and characteristics of the aquifer will be examined, including current monitoring efforts aided by the USGS. Next, surface deformation as recorded by GPS will be analyzed for spatial and temporal trends. Correlations and anomalies between the two datasets will be discussed to describe potential mechanisms driving compaction within the aquifer. This report confirms that subsidence is not just an historical issue in Houston, but is continuing to affect an ever-growing area.

2 Study Area

The study area is contained within a single county that has its own groundwater conservation district, so the regulations are fairly uniform. The Houston metropolitan area and Gulf Coast aquifer system extend far beyond the county borders, making this study a detailed analysis of a part of the larger system. An understanding of the Gulf Coast's depositional history and aquifer characteristics are necessary to better understand the relationship between groundwater withdrawal and subsidence (Gabrysch and Bonnet, 1975).

2.1 Location and Instrumentation

Fort Bend County (FBC), located 90 kilometers (km) inland and 45 km southwest of the city of Houston, covers 2,295 km² of the Texas Coastal Plain. Elevations range from 76 meters in the north to 15 meters above mean sea level in the south. Topography is relatively flat, sloping gently toward the Gulf of Mexico. The Brazos River channel is the most abrupt change in topography, cutting northwest to southeast across the county.

Minor changes to topography can alter drainage patterns. The coastal prairie is pockmarked with wetlands, low-lying areas prone to periodic flooding. Wetlands act as a buffer to major flooding in flat lying areas and filter impurities as water passes to the ocean (Hardinsky et al., 1986). In an effort to preserve this valuable national resource, a policy of "no-net loss" of wetlands was adopted as the federal wetland protection policy (U.S. EPA, 1990).

Many new neighborhoods are built on drained wetlands and include a retention pond to offset the lost drainage area. Flooding in FBC is mainly mitigated through

groundwater regulations and the use of levees. Large stretches of coastal prairie and farmland are quickly being developed into sprawling suburban communities with high demand for groundwater resources.

Groundwater is considered a private property right within the state of Texas, whereas surface water (lakes and rivers) is state owned and regulated. Texas State Legislature created Fort Bend Subsidence District (FBSD) in 1989 to regulate groundwater usage contributing to subsidence and flooding (FBSD, 2013). The district is subdivided into three regulatory “areas” (Figure 2-1) with unique regulations and groundwater reduction plans, addressing the past and future potential of subsidence, present and forecasted population growth, and surface water availability to help meet total demand in each respective area.

The FBSD Groundwater Regulatory Plan (FBSD, 2013) aims to reduce countywide reliance on groundwater through conversion to surface-water resources. FBSD Area A (30% conversion from 2014 – 2024) encompasses the eastern, most populous region. The Richmond/ Rosenberg Sub-Area (30% conversion from 2016-2024) is at the center of FBC. Both of these areas will aim for 60% conversion by 2025 and thereafter. The western, rural and agriculture-rich region of the county is classified as Area B (100% groundwater). “Percentage conversion” indicates the portion of total groundwater demand to be replaced with surface water.

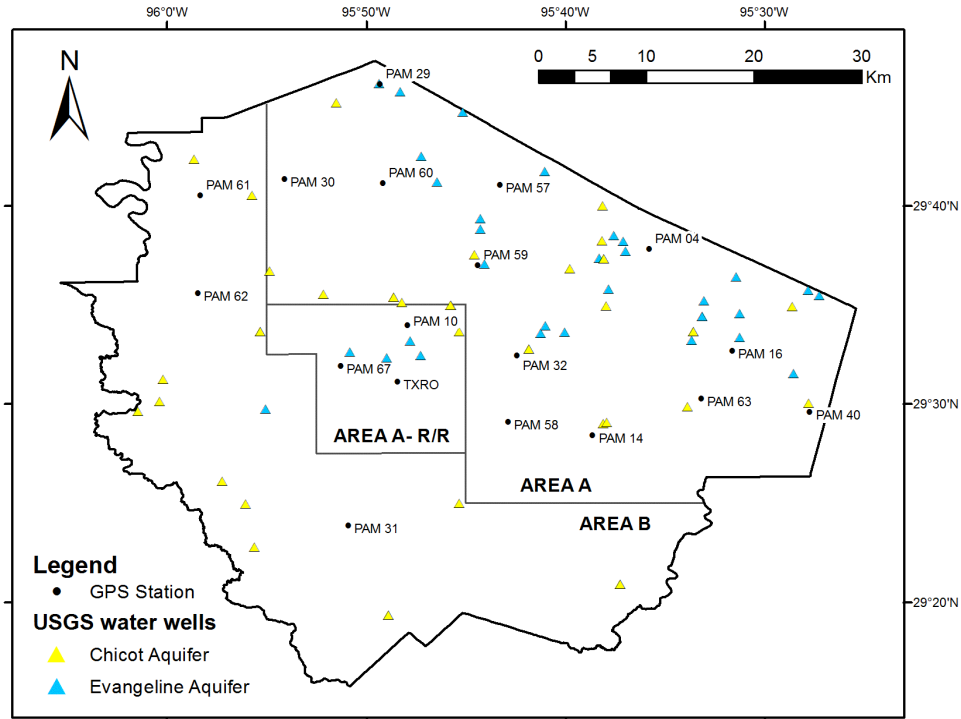


Figure 2-1 Location of Monitoring Equipment.

This map shows the boundaries for three regulatory areas within Fort Bend County. GPS stations are indicated by a black dot, yellow triangles refer to monitoring wells screened in the Chicot aquifer and blue to the Evangeline aquifer. Data provided by the FBSD and USGS Groundwater Watch.

At present, there is one Continuously Operating Reference Station (CORS) and seventeen Port-A-Measure Stations (PAMS) that have permanent stand pipes, but the actual positioning instrumentation is rotated regularly amongst the different locations. This means that the temporal resolution at older sites has decreased as spatial-data density increases with the addition of new PAMS. Sites were installed at different intervals, so data histories vary across the network. The oldest station (PA04) dates back to 1994, whereas the youngest station was installed less than two years ago. Blewitt and Lavalée (2002) determined that three years of data is necessary for reliable results. Therefore, only the sixteen stations installed by 2011 were included in this study.

2.2 Regional Geology

Fort Bend County is located on the Texas Coastal Plain, a thick wedge of alternating fluvial-deltaic to shallow marine deposits. The coastal plain forms a monocline approximately 110 to 145 km wide, extending from Mexico to Florida. Along the Texas coast, deposits of heterogeneous, clay to gravel sized sediments form interfingered units that are thinly bedded and not laterally extensive. Heterogeneous sediments are underlain by actively deforming Jurassic salt and growth faults throughout the region. Geologic complexity within the study area results from the region's depositional and tectonic history, which will be explained further.

The Gulf of Mexico opened with the breakup of Pangea. Salt layers were deposited with thinning of the continental crust during the Jurassic period (Bird et al., 2005). The Gulf of Mexico developed into a passive rift margin during the late Triassic (Chowdhury and Turco, 2006). A rich sediment supply from the young Rocky Mountains fed streams leading to the Gulf of Mexico basin. Deposits accumulated to be several kilometers thick (Galloway, 2001), building out the shoreline to its modern extent. The modern coast is approximately the same as previous highstand coastlines (Knox et al., 2006).

The sediment column was deposited and subsequently reworked through eustatic sea-level change, long-shore currents, and fluvial-deltaic systems (Galloway, 2001). Complex relationships result from a system of fluvial-deltaic and shallow-marine sediments being alternately deposited and reworked through a series of sea-level changes (Kreitler et al., 1977). The depositional environment is a function of sea level.

The last ice age (22,000-16,000 years ago) fixed huge volumes of water on the continents as glaciers (Anderson and Rodriguez, 2001). During this time, the estimated sea level was 120 meters below its modern level, causing sediments to be deposited about 120 km farther south (Burkett et al., 2002; Anderson and Rodriguez, 2001). The drop in sea level also allowed saline waters to be flushed out of the aquifers to considerable depths (Fetter, 2001).

As the glaciers melted, the sea level rose quickly at a rate of approximately five centimeters per year (Burkett et al., 2002). The corresponding transgression (inland migration) of the shoreline proceeded at about five meters per year (Anderson and Rodriguez, 2001). Isostatic adjustments caused the land surface to elevate and the basin to subside, resulting in a progressive thickening of the sedimentary wedge (Chowdhury and Turco, 2006). Recently –within the past 4,000 years– the sea level has risen at a relatively slow rate of less than three millimeters per year to the modern coastline.

Multiple rivers cut perpendicular to the coastline, carrying sediment directly to the Gulf of Mexico. A network of barrier islands developed from the interaction of sediment supply and long-shore currents. Alluvial till fills many relict incised valleys that were cut and filled during alternating highstand and lowstand system tracts, respectively (Shah et al., 2007). A geologic map of the region shows units outcropping roughly parallel to the coastline, (Figure 2-2).

The Brazos River Alluvium, Lissie and Beaumont Formation are present at the surface in FBC. Both the Lissie and Beaumont formations were deposited in fluvial-deltaic systems and are therefore laterally discontinuous, with slightly different

compositions resulting from the depositional mechanisms, environments and time periods of deposition (Meyer, 1939).

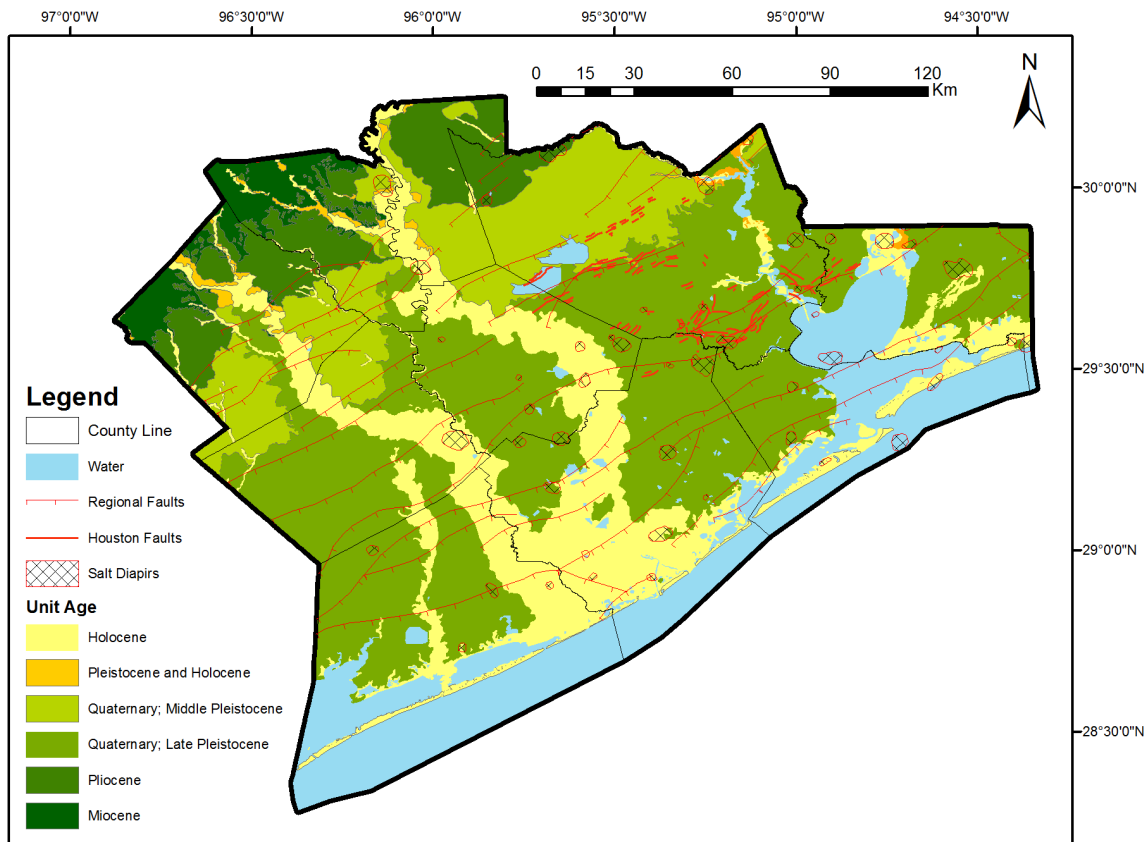


Figure 2-2 Geology Surrounding Fort Bend County. This figure shows the geologic units by age for part of the Texas Gulf Coast. Units dip and thicken toward the coast (Kasmarek et al., 2014). Regional faults from Ewing, 1991; Houston faults from Shah and Lanning-Rush, 2005; salt diapirs from Huffman et al., 2004; regional geology from USGS, 2012.

The sedimentary deposits that developed the Texas coast are interpreted to represent the varying influence of fluvial-deltaic to shallow marine depositional environments. The character of the deposits varied in response to climate, eustatic sea level, and sediment supply (Chowdhury and Turco, 2006). In summary: during a time of sea-level fall, shoreface deposits and the associated rivers supplying the sediment advanced across the continental shelf; as sea level began to rise, rivers reworked deposits

as the shoreface stepped back to a highstand position. This process explains the alternating sequence of coarse-grained fluvial-deltaic (aquifer) and fine-grained brackish-marine (confining) sediments present in the same place (Kasmarek and Strom, 2002).

Fault and Salt Deformation

Both subsidence and faulting are forms of surface motion that can induce slow, imperceptible damage to buildings and roads (Holzer and Gabrysch, 1987). Pratt and Johnson (1926) documented the first occurrence of human-induced faulting in the region, where oil and gas withdrawal accompanied localized subsidence. In general, Gulf Coast regional faults parallel the coastline (Ewing, 1991). In contrast, localized faulting related to collapsed salt domes or oil and gas fields (Pratt and Johnson, 1926) may exhibit arc to radial patterns (Van Siclen, 1968).

Regional faults along the Gulf Coast are aseismic, meaning there is no sudden release of stress, but rather a slow creep. Offset along faults is about one to three centimeters per year (Holzer and Gabrysch, 1987; Buckley et al., 2003; Shah and Lanning-Rush, 2005), making them difficult to identify since erosion will conceal the scarp. LiDAR or structural damage observations are the most effective methods of identifying scarps in an urbanized area (Engelkemeir and Khan, 2008).

The Gulf Coast region was deformed through salt diapirism and growth faulting (Engelkemeir et al., 2010) as the accumulated Cenozoic overburden began to mobilize the Louann salt, a ductile material that can deform and rise due to density differences (Ewing, 1983). A salt diapir can have little or no surface expression whether it is shallow or sits thousands of meters below the surface. Eight salt domes are present in FBC with

depths ranging from 85 to over 2800 meters below land surface (BLS) (Huffman et al., 2004). Six domes are shallow enough to penetrate the Chicot and Evangeline aquifers (Hamlin, 2006), potentially impeding flow and affecting groundwater quality.

Regional faults are listric growth faults; *listric* means displacement increases with depth as the fault angle shallows and *growth* indicates offset is caused by rapid sedimentation along a failure plane coeval with deposition (Ewing, 1991). Kreitler (1977) found that growth faults around Houston could act as hydraulic barriers, isolating (at least partially) the lateral affects of drawdown within the aquifer. Offset along faults within the study area do not demonstrate great enough displacement to completely isolate sand-rich units within the aquifer (Jorgensen, 1975; Kasmarek and Strom, 2002).

Shelf-margin growth faults developed before the modern configuration of salt domes existed (Ewing, 1983). Faulting within Tertiary deposits along the Gulf of Mexico is due to unstable depositional surfaces and differing sediment types (Ewing, 1991). The continental-shelf break indicates a change in depositional environment, moving from coarser materials deposited on the gently dipping shelf to fine grained materials deposited on the continental slope. Fort Bend and Harris County are situated above the Oligocene shelf-margin break (Winker, 1982; Ewing, 1991).

2.3 Hydrostratigraphy

This section focuses on the hydrologic units supplying water for most of the industrial, municipal, agricultural, and commercial demand in FBC. The Gulf Coast aquifer system extends across the coastal plains from western Florida down into Mexico. Units dip (slightly more than the land surface gradient) and thicken towards the coast (Figure 2-3), ranging from 600 to 800 meters in thickness (Wesselman, 1972).

Regionally, the aquifer system includes units from the surface to the Oligocene-aged Frio Formation, but is locally limited to the depth of fresh water (Baker, 1979). This study follows the naming scheme proposed by Baker (1979) for the hydrologic units. Table 2-1 shows the relationship between stratigraphic and hydrologic units within the study area.

Table 2-1 Hydrostratigraphic Column (after Baker, 1979)

Period	Epoch	Stratigraphic Unit	Hydrologic Unit (Baker, 1979)	
Quaternary	Holocene	Alluvium	Brazos River Alluvium	Gulf Coast aquifer system
	Pleistocene	Beaumont Clay	Chicot Aquifer	
		Lissie Formation		
		Willis Sand		
Neogene	Pliocene	Goliad Sand	Evangeline Aquifer	
	Miocene	Fleming Formation	Burkeville confining unit	
		Oakville Sandstone	Jasper Aquifer	

The primary hydrogeologic units within the study area are, from oldest to youngest, the: Jasper aquifer, Burkeville confining unit, Evangeline aquifer, and Chicot aquifer. The Jasper aquifer is potable up dip and being developed in Montgomery County. The Burkeville, a part of the Fleming Formation, is a regionally extensive, clay-dominated layer (Jorgenson, 1975). Kasmarek and Strom (2002) defines the freshwater

limit to be at or near the base of Miocene-aged sediments in northern FBC, and Pliocene aged sediments to the south. For this study, the base of the aquifer system in FBC will be defined as the Burkeville confining unit, which caps the briny waters that have infiltrated the aquifer system at depth.

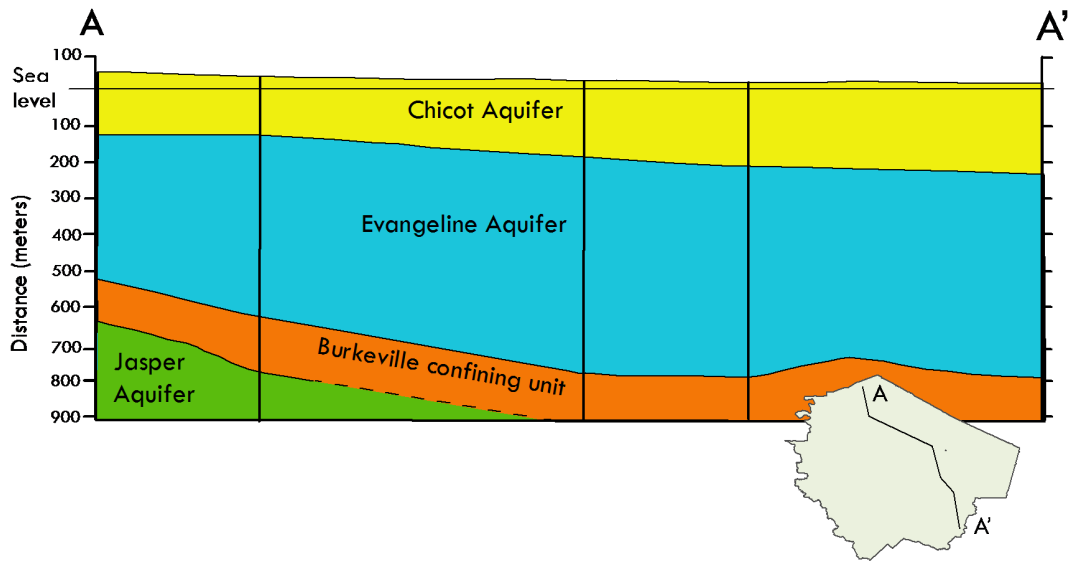


Figure 2-3 Cross-section A-A' (after Wesselman, 1972) showing aquifer thicknesses beneath Fort Bend County. Vertical exaggeration is 1:10.

The Evangeline aquifer is composed of the Pliocene-aged Goliad Formation, composed of about thirty-three to forty percent sand (Wesselman, 1972). The top of the Evangeline aquifer is defined by a single flooding surface, ranging from 120 to 230 meters below sea level (Wesselman, 1972). The Chicot and Evangeline aquifers are hydraulically connected, meaning that changes in the hydraulic head of one will affect the other (Jorgenson, 1975).

The shallower Chicot aquifer is composed of Holocene to Pleistocene-aged sediments. Electric well logs interpreted by Wesselman (1972) characterized the Chicot unit as having thirty to seventy-five percent sand (increasing from east to northwest).

Groundwater wells are intentionally screened in and produce from these thick, sand-rich intervals.

Laterally discontinuous interbeds make up the remaining seventy to twenty-five percent of the section. Leake and Prudic (1991) defined an interbed as having (1) a significantly lower hydraulic conductivity than the surrounding units, (2) sufficient permeability and porosity to permit fluid flow, (3) lateral discontinuity, i.e., is not a regional confining layer, and (4) a larger horizontal extent compared to the vertical thickness. The abundance of interbeds is integral to explaining the mechanism driving inelastic compaction, which will be discussed further in the following chapter.

3 Groundwater

3.1 Movement of Water in the Gulf Coast Aquifer System

FBC is situated halfway between the natural zone of recharge about 145 kilometers inland and discharge near the coast. Recharge to the aquifer system comes mainly from rainfall that enters the system where sandy units are exposed at the surface northeast of the study area. The rate and direction of regional groundwater flow is controlled by the depositional pattern, lithology, and potentiometric surface within an aquifer (Kreitler et al., 1977).

A natural flow system develops when there is a regional slope and topographic relief is relatively insignificant (Fetter, 2001). Prior to development of the aquifer, regional groundwater flow followed the depositional pattern down-dip and perpendicular to the coast (Kasmarek et al., 2014). Extracting groundwater from aquifers is the primary means of affecting the potentiometric surface (in a confined system) or the water table (in an unconfined system).

An unconfined aquifer is open to the affects of atmospheric pressure. Water trickles through the unsaturated zone till it reaches the saturated zone. This interface is called the water table, a surface faintly that faintly reflects overlying topography. The hydraulic head at a point is the sum of elevation, z , above a datum, and the weight of the overlying water column, h_p , or pressure head (Fetter, 2001).

$$h = z + h_p$$

Changes in hydraulic head will cause the water table to fluctuate until equilibrium is established (Williams and Williamson, 1989). In a confined aquifer, which has a non-

porous layer sealing the units below from the affects of the atmosphere, the hydraulic head is a function of pressure *within* the aquifer. The potentiometric surface represents the slope of the hydraulic gradient in a confined system. A method for measuring this parameter is explained later in this chapter.

Shallow, or localized, flow generally enters the aquifer system through an outcrop or unconfined portion of the aquifer (Young et al., 2014). Local flow within the Gulf Coast aquifer system is largely controlled by lithology and topography. Clay-rich lenses will keep water in shallow zones with a short flow path to areas of discharge, like springs and streams (Kasmarek et al., 2014). Intermediate flow zones feed into larger rivers and basins. Once water reaches the deep regional system, it will either be tapped by a well, or flow to distal areas where water will be discharged into the Gulf of Mexico at the down-gradient limits of the aquifer.

Kasmarek and Robinson (2004) explain that the transition from water table to potentiometric surface is incrementally a function of depth, but it is difficult to assign a specific depth range to each zone. Essentially, the uppermost parts of the aquifer experience unconfined conditions, intermediate sections are semi-confined, and deep zones behave as a confined system.

The aquifer system in FBC was still under artesian conditions in Wesselman's (1972) report for the Texas Water Development Board. Wells under artesian conditions flow freely and do not require a pump to bring water to the surface. Discharge can also occur naturally into lakes, rivers, and the ocean, or artificially through pumping wells, as seen in Figure 3-1 (after Oden and Delin, 2013).

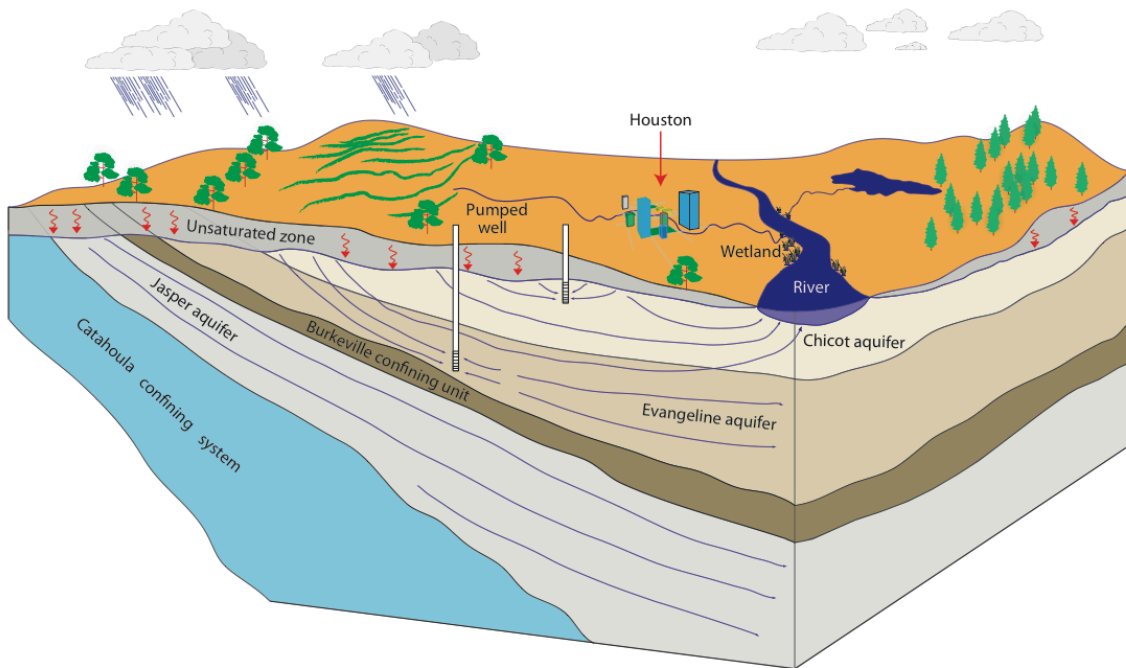


Figure 3-1 Movement of Groundwater in the Gulf Coast Aquifer System.
(Modified from Oden and Delin, 2013).

The Chicot aquifer can be distinguished from the Evangeline aquifer by a clear increase in hydraulic conductivity, as reported by Jorgenson (1975) and Baker (1979), which is a function of increasing-sand content (Young et al., 2014). The two aquifers are hydraulically connected, meaning that changes in the hydraulic head of one will affect the other (Jorgenson, 1975). Vertical-head gradients have increased as a result of pumping,

inducing downward flow from shallow zones into the deeper regional-flow systems, capturing in storage groundwater that would have discharged naturally (Gabrysch, 1969).

Water levels will fluctuate in response to seasonal variations in recharge and discharge rates. Modeling of the Trinity River Basin lead Nolan et al. (2007) to conclude that *surface* recharge rates can be strongly affected by air temperature, runoff, and precipitation rates. Kasmarek and Strom (2002) calculated a typical recharge rate in the Houston area to be about six inches per year. The flow rate at depth is estimated to be one foot (0.3 meters) per day in both the lateral and vertical directions, regardless of current climate conditions (Kasmarek, 2015, *personal communication*). The Gulf Coast aquifer system is so thick and laterally extensive, that impeding flow in one direction (e.g., interbedding or salt domes) will induce radial flow from the surrounding aquifer.

Localized drawdown of the water table or potentiometric surface, referred to as a cone of depression, will result when the rate of withdrawal at a well exceeds the rate of recharge (Fetter, 2001). Theis (1940) found that the rate of pumping would affect the depth of a cone of depression, but not the radius or lateral extent. A cone of depression over 150 meters deep has developed beneath Houston (Campbell et al., 2014). Aquifer-levels were significantly depressed up to 90 meters BLS are visible on the eastern edge of FBC, as seen in Figure 1-1.

3.2 Aquifer Mechanics

Groundwater withdrawal has caused over eighty percent of subsidence in America (Galloway et al., 1999). Either high-pumping rates at a single location or multiple closely-spaced wells can cause drastic pressure declines within the aquifer and a subsequent drop of the potentiometric surface (Kasmarek and Strom, 2002). The combined weight of overlying sediments, interstitial fluids, and the atmosphere at any depth within the aquifer is referred to as overburden. The force exerted by the aquifer to counterbalance the overburden comes from both the aquifer matrix and the pressure exerted by pore fluids (Bawden et al., 2012).

Sandstone aquifers generally consist of discontinuous-sand lenses, which are complexly distributed in a matrix of less permeable materials, such as clay and silt (Fogg, 1986). Each material has a unique hydraulic conductivity, which is the measure of a rock's ability to transmit water (Fetter, 2001). Clays for example, can have rather large pore spaces, but they are not well connected, making clay less transmissive than sand. Fogg (1986) found that flow within the aquifer is controlled not by the hydraulic conductivity, but rather the interconnectedness and continuity of the sand bodies.

Groundwater withdrawal can cause both elastic and inelastic compaction within the aquifer, depending on the lithology. Extraction of groundwater from sand-rich intervals can cause reversible compaction as water levels recover (Kasmarek et al., 2014). Rebound was observed by Kasmarek et al. (2014) at the Baytown and Clear Lake extensometers in response to the elimination of groundwater extraction. Kasmarek et al.

(2014) suggest the land surface rebound was driven by recovering water levels in southeast Harris County.

Water that has been in the aquifer for long periods is considered to be “in storage.” This can refer to water in the deep, sand-rich, regional system or the tight-pore spaces of clays. Inelastic compaction is attributed to the presence of clay lenses storing water in tiny pore spaces that are much less connected than sandy intervals (Kasmarek et al., 2014; Gabrysch and Bonnet, 1975). The storage and compressibility of an aquifer depends on the stress history and characteristics of porous media within the aquifer.

In a closed aquifer system, groundwater extraction will cause aquifer pressure to decrease. As the interstitial fluid pressure decreases, the aquifer will experience an equal increase in effective stress (Galloway et al., 1999). The removal of water from storage within clay interbeds can be induced if the hydraulic gradient is favorable between fast-draining (high transmissivity) sands and low-permeability (low transmissivity) clays (Fetter, 2001).

As water is released from storage in the clay matrix, overburden stress will cause the clay matrix to collapse. Clay grains preferentially realign perpendicular to the overburden stress, resulting in irreversible or inelastic compaction, (Figure 3-2). Even as groundwater levels are reestablished, much of the porosity has been lost. Gabrysch and Bonnet (1975) estimated only ten percent of the height lost to inelastic compaction would be restored with the theoretical re-establishment of artesian conditions within the aquifer.

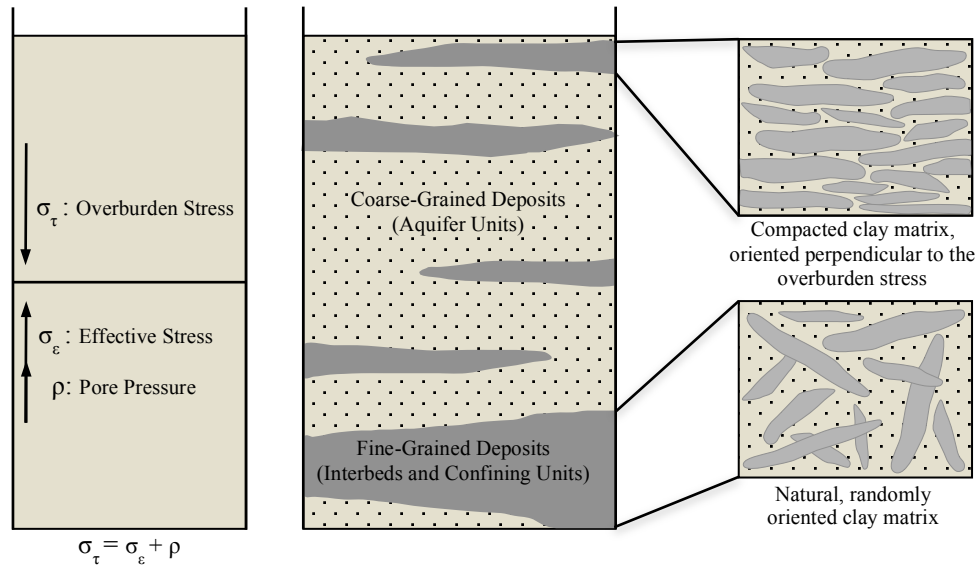


Figure 3-2 Principal Stresses within the Aquifer System.

This figure shows the relationship between compaction and changes in the subsurface stress regime in response to fluid withdrawal. The weight of overlying sediment (σ_{τ}) is equal to the force exerted by the sediment matrix (σ_{e}) and interstitial fluids (ρ) below. In a confined aquifer, groundwater withdrawal causes a uniform decrease in pore pressure and an equal increase in the effective stress (Leake and Prudic, 1991). The change in pressure, and increased effective stress, causes water to be expelled from storage (in the fine-grained layers) and the clay matrix to collapse. Figure modeled after Galloway et al. (1999).

Factors such as the age of the sediment, clay content, and previous drawdown-levels will affect the amount of aquifer compaction or subsidence observed at a given location. Kasmarek et al. (2014) suggests that subsidence is a localized phenomenon, meaning rates of compaction cannot be extrapolated or inferred across an area because groundwater withdrawal rates, local lithology, and compressibility of sediments are unique to each location.

Additionally, the rate at which groundwater is extracted, the porosity, and permeability of the unit will affect the rate of dewatering (Galloway and Burbey, 2011). Previous studies (Burbey et al., 2006; Warner, 2003; etc.) address three-dimensional

strain within an unconsolidated aquifer. The dewatering process changes stress patterns on the sediment matrix, as each material has a unique transmissivity. Gulf Coast-aquifer units are more transmissive in the horizontal direction than vertical causing the transmissivity to be dampened by abrupt changes in lithology (Fetter, 2001).

Pumping rates exert more control on rates of subsidence than actual volumes of water extracted (Ortega, 2013). For example, a set volume of water is continuously pumped over a month, the next month the same set volume is pumped over a period of two weeks and pumping ceases for the second half of the month. Both scenarios are expected to result in subsidence, but the latter example has been shown to produce a more-rapid subsidence (Ortega, 2013).

3.3 History of Subsidence in the Houston Area

Land-surface deformation refers to changes to the surface of the earth caused by subsurface processes. Subsidence is negative land-surface deformation, a process naturally occurring on a geologic-time scale. Subsidence along the Gulf Coast can be attributed to three main processes:

- 1) Consolidation and compaction of sediments. Younger sediments are more susceptible to compaction as they have been exposed to less-overburden stress and subsequent dewatering. Older sediments are still susceptible, but at lower rates. Marshy sediments, rich in organic materials, will also compact rapidly when drained for development (agricultural or urban). Carbon-rich soils will oxidize as the sediments desiccate, releasing CO₂ into the atmosphere with associated mass and volume loss to the soil (Dixon and Dokka, 2008). This process tends to vary spatially in association with clay to sand ratios, organic content, burial depth, and groundwater withdrawal.
- 2) Subsidence due to mass loading or isostasy. Flexure of the continental crust has been attributed to the increasing sediment load in the Gulf of Mexico basin (Jurkowski and Brown, 1984), while González and Tornqvist (2006) suggest that the crust is still rebounding in response to the Larentide Ice Sheet melting.
- 3) Tectonic subsidence in the form of gravity sliding. Gulfward, or down slope, movement of deltaic sediments due to gravitational loading is thought to connect to actively-deforming subsurface salt (Dokka et al., 2006). Engelkemeir and Khan (2008) have identified hundreds of surface faults in the Houston metropolitan area using LiDAR, implying that neotectonics are still actively deforming the region. Many GPS

stations in FBC are assumed to be stable regarding tectonic motion because many stations are located on the up-thrown side of regional faults mapped by Ewing (1991).

Traditional methods for quantifying rates of compaction were based on the stratigraphic record. Until the latter half of the 20th century, subsidence estimates assumed relative coastal stability and were reported on millennial scale or time-averaged rates referenced to chronostratigraphic data. Paine (1993) calculated long-term, natural rates of subsidence for the Texas Gulf Coast to be, on average, 0.05 millimeters per year.

Rapid subsidence was first observed in the Houston area at Goose Creek Oil Field, where oil and gas withdrawal caused localized faulting and a rapid drop in ground level (Pratt and Johnson, 1926). Various early workers (e.g., Winslow and Doyle, 1954; Holzer and Johnson, 1985; etc.) found a strong correlation between groundwater withdrawal and aquifer compaction. The United States Geological Survey (USGS) correlated artesian pressure declines within the aquifer system to pronounced regional subsidence (Kasmarek et al., 2014). Gabrysch (1969) postulated that the recovery of water levels would decrease the rate of subsidence and possibly allow for rebound of the land surface to occur.

The USGS then began to install a network of extensometers in the Houston area to monitor aquifer compaction, and implement regulations limiting groundwater withdrawal. There was a corresponding effort by the Texas Water Development Board in the 1960's and 1970's to increase surface water supplies by creating local reservoirs (e.g., Lakes Livingston, Conroe, and Houston) to serve the greater Houston metropolitan area.

It is difficult to discern between the various processes without a deep-seated monument to constrain the interval of compaction and the controlling mechanism. Previous studies by Ortega (2013) and Burrough (2013) utilized the Addicks and Southwest Extensometers in Harris County to study subsidence related to groundwater withdrawal. Results indicated that surface deformation recorded at GPS stations corresponded with the aquifer compaction rates recorded by nearby extensometers. Therefore, this paper assumes that the observed surface deformation is representative of aquifer compaction and *subsidence* will refer to compaction of aquifer sediments due to groundwater withdrawal.

Modern measuring techniques include leveling, GPS, InSAR and LiDAR; each of which can be referenced to a localized or geocentric datum. For Houston, and surrounding developed areas, geodetic data show that the present average rate of subsidence in Sugarland (20 millimeters per year) is much faster than undeveloped areas to the west (less than 7 millimeters per year or below the instrument's detection limit). Many parts of Houston experience five to ten millimeters of vertical motion every year, whereas the Addicks site is sinking fifty millimeters per year (Bawden et al., 2012), a rate two to three orders of magnitude greater than the historic rate from the rock record. Such a pronounced acceleration of geologic processes has been attributed to fluid extraction from young sediments in the Gulf Coast region (Kasmarek et al., 2014).

3.4 Monitoring Aquifer Levels

The health of an aquifer is primarily monitored through monitoring groundwater levels and maintained through pumping regulations. In the Gulf Coast Aquifer system, the groundwater levels and pumping rates are closely related. Groundwater levels indicate the health of an aquifer, which is controlled by groundwater-extraction rates.

The primary source for groundwater-level measurements used in this study is the USGS Groundwater Watch website. Groundwater levels were measured from USGS piezometers after the methods described by Kasmarek et al. (2014). A piezometer is a monitoring well, open to atmospheric pressure, used to measure the hydraulic head of an aquifer at a specific location (Fetter, 2001). The hydraulic head, or potentiometric surface, is the elevation to which water will rise, representing the pressure within the aquifer at the screened depth.

Aquifers are dynamic and constantly change to maintain equilibrium, with flow patterns changing in response to pumping. Any pumping near a monitoring well causes water levels in the immediate vicinity to fluctuate. Therefore, hydrologic technicians take measurements when water levels are static- two hours to one day after withdrawal has stopped at a nearby pumping station (USGS Groundwater Watch, 2014).

Sixty-five monitoring wells in Fort Bend County have measurements dating back to 2005, and were used in this study. Groundwater levels are collected annually between December and February when water usage is less intense and aquifer levels are more stable. There are about ten data points for each well site over the nine-year observation period from 2005 to 2014. The sampling rate is much less regular than the GPS sampling

rate, and therefore correlating trends between groundwater levels and subsidence are limited to the stable-wintertime conditions.

Extracting groundwater from aquifers is the primary means of affecting the hydraulic head (in a confined system) or the water table (in an open system). Wells within the Chicot and Evangeline aquifers are screened at depths ranging from 80 to 600 meters below land surface (BLS). The Evangeline is assumed to be under confined conditions at the depths screened within the study area, while Chicot wells in FBC are either semi-confined to confined (Kasmarek et al., 2014). Figure 3-3 shows the correlation between groundwater levels (hydraulic head) in 2011 and the depth at which the respective well is screened.

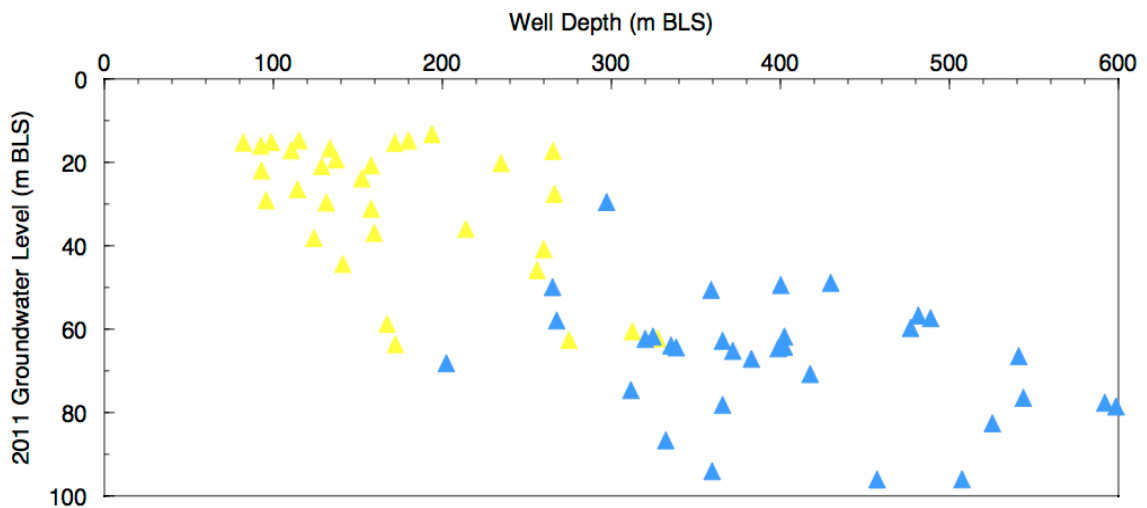


Figure 3-3 FBC Monitoring Well Depths and Groundwater Levels in 2011. This plot shows a correlation between the depth to which a well is screened and the hydraulic head of the aquifer at that depth. There is a rough correlation between deeper wells and a lower hydraulic head within the respective aquifer (Chicot- yellow triangles, Evangeline- blue triangles).

Pumping wells are intentionally drilled to sandy, water-producing intervals. High volume pumping stations that provide large volumes of water for municipal utility districts are typically finished in deeper intervals to eliminate the possibility of running

dry. There is correlation between deeper wells and a deeper potentiometric surface measurement observed in Figure 3-3. The USGS-monitoring wells were not always located directly adjacent to a pumping well, and are therefore interpreted to represent regional trends.

Groundwater level maps were created using water-level data and the Inverse Distance Weighting (IDW) interpolation method to produce a raster surface using ArcGIS version 10.0. The IDW method interpolates values between each data point based on the input values. The resulting surface is therefore only as deep as the input values reach and will neglect any unmeasured areas with a deeper potentiometric surface due to drawdown or the overlapping effects of pumping in areas that are not being monitored.

Groundwater level changes in the Chicot and Evangeline aquifers were analyzed separately rather than as a unit because of the varying depths and properties of the aquifers. There are over a thousand groundwater pumping wells being monitored by the FBSD (2015, *personal communication*). Rosenberg was chosen for a site-specific survey, since drawdown within the aquifer beneath this area appears to be independent of any cumulative effects from the long history of withdrawal in the Houston area. Twelve meters of drawdown within the aquifer was observed from 2005 to 2014 at a USGS monitoring well near the city of Rosenberg. Pumping data were obtained for analysis at a municipal-supply well closest to this monitoring well.

4 GPS Positioning

Global Positioning System (GPS) technology has been applied to surveying and scientific applications since its advent in the early 1990's. This study utilizes GPS data collected by the Fort Bend Subsidence District (FBSD), which were then processed to create time-series dating back to 1994. Since then, a network of eighteen GPS stations has been installed in the study area to augment spatial resolution.

In further support of this effort, the National Science Foundation recently awarded the University of Houston a grant to establish a dense, real-time GPS network (HoustonNet). Ten of over forty stations installed in the greater Houston metropolitan area are located in Fort Bend County (FBC). The HoustonNet stations will be used to monitor hazards relating to natural processes such as land-surface subsidence, active faulting, and salt diapirism in addition to hurricane forecasting.

All data were uniformly post-processed using the Jet Propulsion Laboratory's GIPSY-OASIS II software version 6.3. This software employs the Precise Point Positioning (PPP) method, yielding sub-centimeter accuracy results. Data accuracy and outliers were determined and eliminated if greater than two times the standard deviation (2σ). Initial results from GIPSY are provided within the Earth-Centered, Earth-Fixed International GNSS Service (IGS08) reference frame.

A local reference frame, the Stable Houston Reference Frame (SHRF), was established using nine GPS stations; results were then translated from IGS08 to SHRF using a 14-parameter Helmert transformation. The SHRF sites surrounding the study area were selected using criteria outlined in this chapter. The stable reference frame highlights

intra-regional processes by eliminating dominant and consistent signals attributed to crustal motion. All positions are reported within the SHRF, and the collection of time-series is available in Appendix II.

4.1 GPS as a Surveying Tool

The United States' Department of Defense began developing GPS technology in the early seventies (El-Rabbany, 2006). A diverse array of industries has since found applications for the technology ranging from the real-time navigation of cars to measuring the soil moisture content of crops. Scientific applications include monitoring tectonic motions from slow uplifts to instantaneous earthquakes.

GPS instruments are able to measure ground-surface motions much more frequently than traditional land-surveying techniques, and maintain a comparable range of error. The spatial and temporal variability of surface deformation can be constrained by installing multiple, permanent, or campaign style GPS stations over an area.

Fort Bend Subsidence District (FBSD) has a network of permanent GPS stations that utilize a rotating set of equipment. Permanent monumentation at each site includes a concrete pad with a pole anchored six meters into the ground. An opening at the center of the pad allows the pole to slip freely. This helps avoid any superficial shrink-swell motions associated with fluctuating soil-moisture content and highly-expansive clays.

A GPS antenna is fixed on top of the pole three meters above the land surface to avoid the effects of multipath from surrounding objects. The rotating set of equipment includes a Trimble antenna, paired with a Trimble NetR9 receiver, pictured in Figure 4-1

(Cliff Middleton, *personal communication*, 2014). The rotating GPS instrumentation, referred to as Port-A-Measure Stations (PAMS), collect data at each location for seven to ten days before being moved to the next station. An antenna is collecting data at a single site for six to seven weeks out of the year, or about twelve percent of the time. A general understanding of how the instrument works, and the associated processing method, is necessary to understand and interpret GPS data.



Figure 4-1 PAM Station Set-up.
This photo shows PAM04 in Sugarland. The solar panel, battery and GPS receiver are attached to a fixed pole on the left, while the GPS antenna is mounted on the pole with a slip joint on the right.

4.2 GPS Data Processing

Obtaining an accurate position using the Global Positioning System (GPS) requires a processing method to account for meaningful variables affecting the accuracy of a position. Results can either compromise on accuracy and be produced in real-time (rapid), or post-processed to obtain high accuracy results. To utilize either method correctly, one must understand the technical aspects of how to get a position using GPS.

Global Positioning System (GPS) defines a position through triangulation. The orbit and position of each satellite is geocentric, or referenced to the center of the earth. By measuring the travel time of radio signals, a pseudo-range from satellite to receiver is calculated within a few seconds. An actual distance is derived from the pseudo-range by multiplying travel time by the speed of light ($c=3.0 \times 10^8$ m/s). The range is then used to determine the position at the intersection of all four spheres, resulting in one unique point on the surface of the earth. This method relies on an accurate travel time and knowing exactly when the satellite sent the radio signal, which is dependent on synchronous clocks. GPS satellites are equipped with incredibly precise clocks made of cesium, resonating at a known and uniform frequency.

Each satellite sends out its signal on two carrier frequencies. The L1 carrier transmits a pseudo-random code and status message, while L2 carries more precise coding that is specifically for military use. Any discrepancies between the clocks in orbit and on earth will introduce error. These errors are monitored by the Department of Defense and corrections are communicated back to satellites.

Since 2005, satellites have been equipped to transmit a second signal (L2C) that is available to civilians, thereby improving the accuracy of measurements. The L2C signal created the ability to directly measure and remove errors related to ionospheric delay. Accuracy is further increased through post-processing the data, which utilizes satellite paths and eliminates several sources of noise and error.

Raw GPS data are provided in a binary format, and must be processed to produce meaningful results. Converting data from the receiver specific format to the standardized **Receiver Independent Exchange (RINEX)** file format is necessary prior to processing. Observation files (*.120) include time, satellite, C1 (distance), P2 (distance), L1 (cycles), and L2 (cycles). RINEX was developed for the easy exchange of GPS data and archiving.

Two main methods have been established for post-processing raw data to produce a positional time-series- differential (relative positioning) and precise-point positioning, or PPP (absolute positioning). The differential method measures the relative distance between a pair of stations with a short baseline on the scale of hundreds of kilometers (Eckl et al., 2001). The relative positioning method measures single-frequency, pseudo-range numbers, yielding sub-meter accuracy positions at best (Rizos et al., 2012).

Networks of reference receiver stations, such as the Continuously Operating Reference Stations (CORS), were established to facilitate more-accurate positioning using the differential method. The two paired stations will have a set of shared errors in their signals that can be canceled out, except multipath.

Precise Point Positioning (PPP) is a processing method that has been developed over the past two decades for the measurement of *individual* GPS station motions. The

Global Navigation Satellite System's (GNSS) PPP method requires a single receiver, removing the need for another station nearby. This is advantageous in remote locations that lack infrastructure, because it does not require the same dense and costly infrastructure as differential GPS. Though, according to Rizos et al. (2012), if CORS are present, they could be used to enhance PPP, especially regarding real-time applications.

There is a dense GPS network already in place within the Houston metropolitan area. Localized phenomena near the reference station can bias results when using the differential method. Determining the position of a station utilizing the PPP method eliminates the possibility of this kind of anomaly. This study employs the PPP method to study land subsidence; reasoning and methodology are described below.

GPS data were initially formatted specifically to the receiver type and converted to a standard Receiver Independent Exchange (RINEX) format. Receivers collect a data sample every 30 seconds. The PPP method averages the 2,880 positions collected over a 24-hour period to produce a daily solution. Averaging is an effective way to minimize any minor noise in the signal due to atmospheric conditions or multipath since GPS orbits are designed to circumnavigate the globe twice a day (Blewitt, 2002).

Data were then post-processed using GIPSY/OASIS v.6.3, a software package developed by NASA's Jet Propulsion Laboratory (JPL). The GIPSY data processing method employs PPP, which compares the L1/L2 bands at a single receiver to eliminate differences in carrier-phase velocity (Wang et al., 2013). The absolute positioning method allows users to get a position from a single receiver with dual-frequency (L1 and

L2) P-code processing capabilities (Rizos et al., 2012). This method uses the difference between the L1 and L2 bands to eliminate atmospheric noise.

Minute horizontal and vertical motions are discernible using high-resolution GPS receivers. This sensitivity is associated with more noise, which requires a longer time-series to define a trend. The positional time-series was required to have an observation period of three or more years to minimize the influence of seasonal signals on interpretation (Blewitt, 2002).

4.3 Sources of Error and Accuracy

Generally, the main sources of error for a GPS system stem from an inaccurate satellite clock (time) or ephemeris (satellite position), phase ambiguity bias, or signal delay from traveling through Earth's atmosphere. These errors may be estimated, corrected or reduced using the detailed processing techniques discussed in this study.

Finalized station positions are highly dependent upon the travel time of a signal. When inaccuracies are introduced into this fundamental function, error will result. Travel time, in turn, depends on the accuracy of satellite clocks. GPS satellites have atomic clocks made of cesium, which are accurate to the nanosecond. Multipath is caused by signals reflecting off surfaces near the antenna resulting in a longer travel time; clocks that are out of synch will introduce errors into the signal-travel time as well. Noise from the receiver and pseudo-random number can also reduce accuracy.

Ephemeris error is introduced when the actual position of a satellite strays from the predicted or modeled path. Though the ephemeris error is a fixed distance between the predicted and true positions, the effects vary depending on the viewing angle of each

individual receiver. Short-baseline observations can be very useful in this particular situation (El-Rabbany, 2006). As distance between stations decreased, accuracy of the ephemeris estimation was found to improve as the distance decreased between monitoring stations. Producing accurate positions are therefore dependent on precise ephemeris data, which was obtained from the International GNSS Service (IGS).

In order to process carrier phase data for a GPS station, one must estimate the number of wavelengths between a transmitter and receiver (Remondi, 1985). Remondi (1985) explains that satellites transmit carrier signals, which are then stripped of modulations so that the waveform may be isolated and used to calculate distances. In theory, the number of cycles or wavelengths transmitted and received will increase with time in a linear fashion. In other words, signal propagation proceeds at a constant rate, but since the GPS system is in motion, it does not behave in linear manner. The process of estimating an accurate number of phase cycles was termed “bias-optimization” by Blewitt (1989), who suggested that the reliability of data could be improved through large GPS networks with differing baselines.

The ionosphere, ranging from 50 to 500 km in altitude, creates the most significant source of error. Radio signals can travel from the satellite to receiver at varying speeds due to atmospheric conditions, referring to both the different atmospheric layers and weather events. Corrections must take into account the properties of the troposphere and ionosphere, and estimate how long the signal takes to pass through each.

Tropospheric (0 – 50 km altitude) delays result from both hydrostatic and wet parameters (Davis et al., 1985). Hydrostatic delay occurs when dry gases and the non-

dipole component of water vapor are present. It is strongly correlated to surface pressure and accounts for about ninety percent of the observed delay (Bar-Sever et al., 1998). On the other hand, wet delay, a product of the water vapor dipole, is much more variable (Bar-Sever et al., 1998; Davis et al., 1985).

Tropospheric delay varies both along the zenith path and in the azimuthal (horizontal) directions encompassing a receiver (Bar-Sever et al., 1998). Horizontal variation was found to decrease in magnitude as elevations approached the zenith. Bar-Sever et al. (1998) ascertained that the accuracy, or “repeatability, of coordinates improved when gradients were modeled using a random-walk process and a relatively low-elevation cutoff of seven degrees.” This method was applied to this study.

GIPSY utilizes the Vienna Mapping Function (VMF) created by Boehm and Schuh (2006) to model tropospheric delays. Mapping functions are generally used to define the correlation between signal delay and elevation angle (Davis et al., 1985). Vertical accuracy, or repeatability, of GPS were clearly improved through the use of VMF (Bertinger et al., 2010).

As the signal continues traveling, it will encounter ionospheric delays, which have been organized into first- and second-order delays. The larger first-order delays depend upon factors such as satellite elevation, solar activity, local season, and time of day (Kedar et al., 2003). Minor second-order delays are on the scale of millimeter to centimeter errors, but as the accuracy of GPS solutions improve, these small errors can become significant. Correcting for second-order ionospheric delays can reduce

movements associated with seasonal variability, and thereby improve the precision of results (Kedar et al., 2003).

Since station positions are initially reported within the geocentric IGS08 reference frame, any force periodically displacing Earth's center of mass must be accounted for. Solar and lunar tides can cause displacement of both the ocean and solid earth. Earth's tidal pattern is regular and predictable; large enough volumes of water are displaced from one side of Earth to the other that it causes a minute shift in Earth's center of mass, affecting the accuracy of satellite positions.

This study utilizes a program called Ocean Tide Loading that models the affect of tides on satellite positions. It has been made available online through the Onsala Space Observatory at Chalmers University in Sweden (Bos and Scherneck, 2011). The FES2004 atlas tidal model was used. FES (Finite Element Solutions) 2004 uses algorithms to calculate the primary diurnal and semi-diurnal tides. Atlas then combines the modeled values with altitude data from altimetry satellites (Lyard et al., 2006).

Multipath is caused by signals bouncing off objects in the environment immediately surrounding a station, inadvertently prolonging the signal travel time and producing a false distance. Proximal objects like trees, buildings or a parked car will decrease signal accuracy. This may produce anomalous results, depending on the satellite angle, season (foliage), or something as simple as a point (car) that gets averaged out.

When a source of noise cannot be modeled or corrected for, it results in an anomalous position that must be systematically removed. GIPSY outputs a sigma value for each-daily-position coordinate produced through the program. The sigma value

indicates the average amount of noise in each direction at every point. Sigma is therefore an effective measurement for removing outliers from within the context of the entire dataset. Averaging the daily results will eliminate some minor errors, but if an anomalous noise source is present for an extended amount of time, high frequency measurements will exhibit more variability.

Outliers were systematically identified and removed through an approach modified from previous studies (Firuzabidi and King, 2012; Wang, 2013). Firuzabidi and King (2012) implemented a study in central Italy to understand the relationship between each position's precision, observational timespan, and reference station location. Within their local reference frame, any position coordinate with a sigma value greater than two times the average sigma value was considered to be an outlier. Similarly, the data for each directional component was de-trended, the standard deviation calculated, and any position value greater than two times the standard deviation was removed, (Figure 4-2).

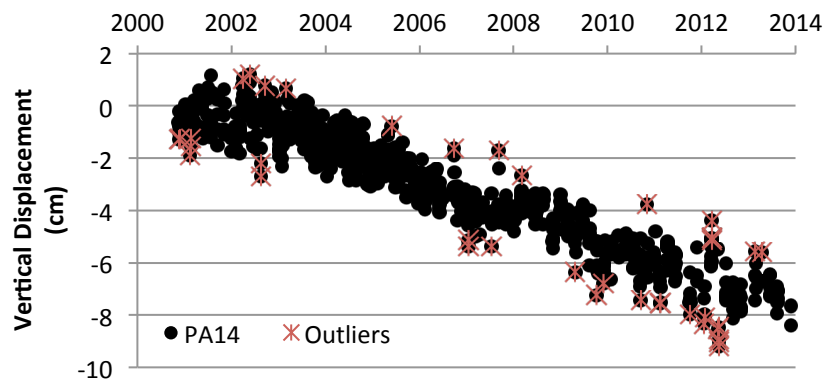


Figure 4-2 Outlier Identification and Removal.

This plot shows the contrasting-data record resulting from the elimination of outliers. Black dots represent the complete time-series generated by GIPSY, outliers (greater than 2 times the standard deviation) are crossed out.

2011 Antenna Change

Multiple PAM stations plotted within the Stable Houston Reference Frame showed an anomalous rebound at the beginning of 2011. An equipment change took place on 2011.025 across the PAM network that was accounted for in the processing method. All PAMS employed the TRM41249.00 antenna through 2011.025, and were switched to TRM57971.00 on 2011.026 (Middleton, *personal communication*, 2014).

The two antenna models have about a fifteen-millimeter difference in the L1 phase center height, which will only manifest in the vertical component and should not affect horizontal components. Large offsets, ranging from about one to four centimeters in the vertical component, remained after processing. As such, displacements caused by the antenna change were removed manually for each station, by the amount shown in table 4-1.

Table 4-1: Vertical Shift from Antenna Change on 2011.025

Station	Vertical Δ (cm)	Station	Vertical Δ (cm)
PA04	-2.8	PA32	-2.3
PA10	-4.3	PA40	-2.4
PA14	0.0	PA57	-4.0
PA16	-2.6	PA58	-1.5
PA29	0.0	PA59	-1.2
PA30	0.0	PA61	0.0
PA31	-3.0	PA62	0.0

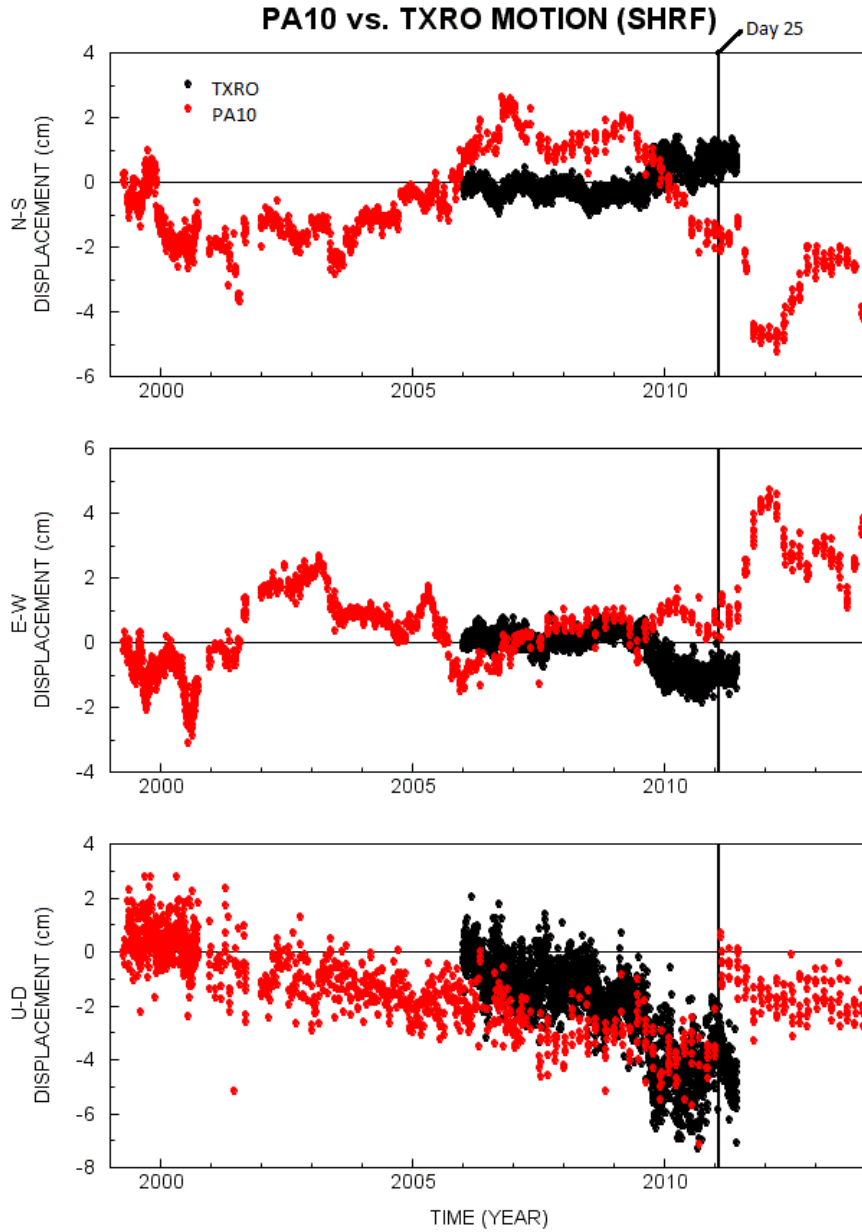


Figure 4-3 2011 Offset: PAM vs. CORS Time-Series.

A vertical offset of about 4.3 centimeters was recorded at PA10, while a nearby CORS recorded a positive vertical jump of about 3.0 cm around the same time. Vertical offset at the PA10 is attributed to an equipment change, though the same explanation cannot be applied to TXRO.

4.4 Reference Frame

A position is, by definition, reported relative to an established point or frame of reference. A reference frame may be celestial or terrestrial (global, regional, national, or local) (Matsuzaka, 2012). A reference frame can aid the understanding of how changes to Earth's surface relate to the underlying geologic processes (Bawden et al., 2012). In order to produce meaningful results when working with GPS data, it is essential to choose a stable-reference frame appropriate to the scale of the project.

For example, if plate tectonics are being studied, a global reference frame should be chosen. In such a case, one plate will be “fixed” and all other plate motions are described relative to the fixed plate. The North American Datum of 1983 (NAD83) (Schwarz, 1989; Soler and Snay, 2004) is a regional or continental-scale reference frame that fixes the North American tectonic plate motion, highlighting intra-continental processes. Subsidence is a localized to regional-scale phenomenon, commonly linked to localized groundwater withdrawal practices unique to the climate and urbanization of a given area (Galloway and Burbey, 2011).

GPS velocity vectors and surface positions in the Houston metropolitan area have historically been reported relative to CORS mounted on stable, deep-seated extensometers. An alternative to the baseline-pair method involves the use of multiple stable sites to establish a local reference frame. Observations from stable sites in the region can be used to determine the orientation, origin, scale, and time-derivatives of these parameters (Wang et al., 2013). Any observation within this reference frame will more readily display internal or localized deformation.

GPS data processing using GIPSY-OASIS v. 6.3 yields solutions referred to the geocentric International GNSS Service (IGS) reference frame of 2008 (IGS08). The most current version offered at the time of data processing, IGS08 (2001-04-17 through 2012-10-06) was used for this study. Subsequent revisions, or realizations to the IGS reference frame are GPS-based, using fifty well-established stations around the world (Soler and Snay, 2004). Modern GPS coordinate frames provide very accurate and reliable solutions achieved by the precise orbits (ephemerides) distributed by IGS (Soler and Snay, 2004). High-precision GPS relies on GNSS satellites and International Terrestrial Reference Frame (ITRF) solutions. The IGS began using ITRF precision products in 1994 (Kouba, 2002).

As ITRF coordinates improved with time, and subsequent realizations were released, updated IGS products are also released. This ensures that precise orbit and clock corrections are in step with any changes to ITRF. Since 2000, IGS began defining their own global reference frame, which is still based on the most recent realization of the ITRF (Ray et al., 2011). For example, IGS replaced the IGS05 reference frame in 2011 with IGS08, which is referenced to ITRF08.

Positions are actualized as X, Y, and Z components in a geocentric reference frame. Solutions are then converted to latitude, longitude, and ellipsoid height. Ellipsoid height is defined as the distance to a point measured perpendicular to the ellipsoid surface (Wang and Soler, 2014). All results (Appendix II) are reported as displacement in the Northing, Easting, and Vertical directions. When no displacement occurs, or it is within the calculated error of the instrument, the station is considered to be stable in that

direction. If a significant change in position was observed, then the velocity (speed and direction) can be derived from the time-series. Since this study of subsidence encompasses a whole county, all three components were taken into account.

Global positions were transformed into a localized reference frame- the Stable Houston Reference Frame (SHRF). The SHRF (Wang et al., 2013) was realized using nine CORS surrounding the Houston area that have a long and stable history. Each station's coordinates were transformed into the localized reference frame, displacement values were calculated with respect to the initial position, and a time-series was created for analysis. Solutions within the SHRF are able to achieve 2-3 mm horizontal accuracy and 6-7 mm vertical accuracy (Wang et al., 2013).

Previous studies in the area have utilized the double differencing (DD) or baseline-pair technique, eliminating the need to determine the scale of a reference frame. DD will normalize any displacements shared between the two stations such as tectonic motion, faulting or compaction. There is also the potential for muting important information, or propagating error throughout the whole dataset. For example, data may need to be eliminated from a whole study due to localized or anomalous motion at a reference station (Bawden et al., 2012).

Utilizing the precise point position (PPP) method within this stable reference frame eliminated the possibility of losing data due to site-specific motion. Instead, each point was referenced to a stable reference frame for the Houston area, which effectively averaged and fixed the localized motion in three dimensions. Nine stable "frame" sites in the region surrounding Houston were required by Wang, et al. (2013) to have:

1. Begun operation before 2006
2. Collected data for more than seven years, with data gaps less than 5 month long
3. A standard error less than 0.1 mm/year for velocities referenced to IGS08
4. No discernible motion upon visual inspection of the vertical time-series.
5. Good lateral distribution to reduce “network effect”

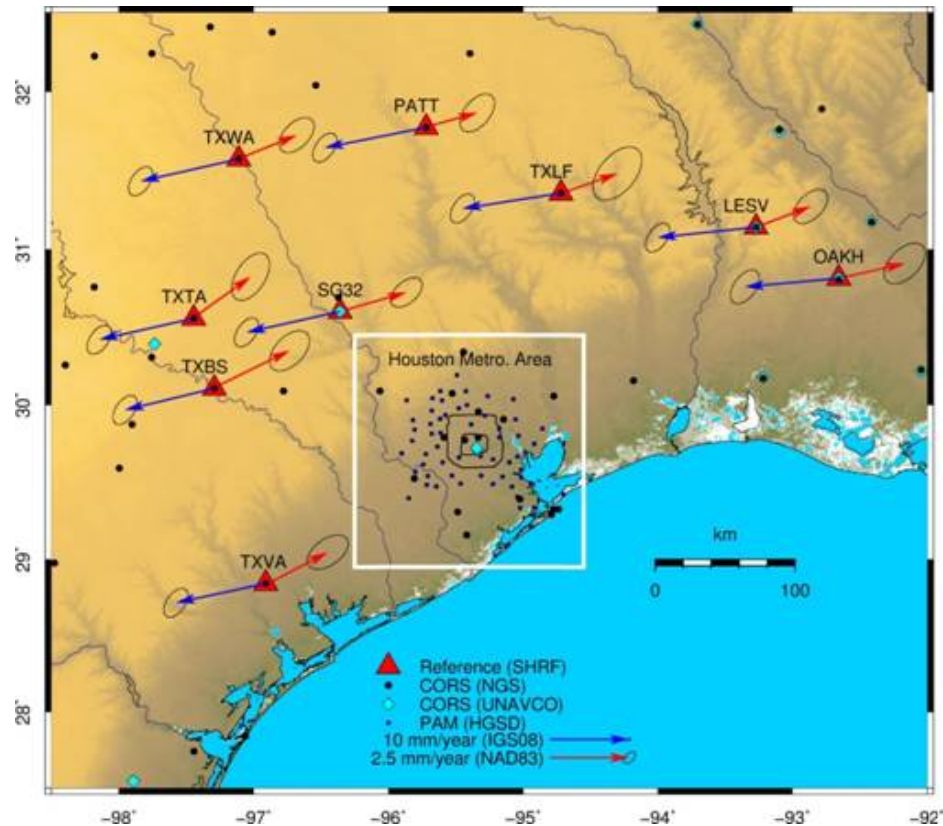


Figure 4-4 Location of Nine SHRF Reference Stations.
 Nine long-term CORS across Texas and Louisiana were used to construct the Stable Houston Reference Frame. Black dots indicate the location of PAM and COR stations within the Houston metropolitan area.

A reference frame's most important mathematical and physical parameters are the origin, scale, orientation, and the change of these properties over time (Wang et al., 2013). A Helmert Transformation, which accounts for each parameter, was used to translate coordinates from an IGS08 reference frame into the SHRF following the methodology of previous studies (e.g., Soler and Snay, 2004; Pearson et al., 2010; Wang et al., 2013).

A 14-parameter similarity transformation, which includes three translations, three rotations, one scale and the respective rates, was utilized in this study. Parameters (Table 4-2) are defined with respect to time, and can be solved for using a set of unique, individual points with known coordinates in each reference system preceding and following the transformation. Since there are seven parameters that need to be determined, at least one coordinate and two points must be known. This enables a system of seven linear equations with seven unknowns to be solved.

Three common points will fulfill the minimum requirements mathematically, but observational errors at each point make it almost impossible to satisfy the parameters. In practice, adding additional points will increase the solution accuracy. Known IGS08 coordinates of a GPS site are related to their corresponding SHRF coordinates by a similarity transformation that is determined using the following equations (Snay, 1999):

$$X(t)_{SHRF} = T_x(t) + [1 + s(t)] \cdot X(t)_{IGS08} + R_z(t) \cdot Y(t)_{IGS08} - R_y(t) \cdot Z(t)_{IGS08}$$

$$Y(t)_{SHRF} = T_y(t) - R_z(t) \cdot X(t)_{IGS08} + [1 + s(t)] \cdot Y(t)_{IGS08} + R_x(t) \cdot Z(t)_{IGS08} \quad (\text{eqn 1})$$

$$Z(t)_{SHRF} = T_z(t) + R_y(t) \cdot X(t)_{IGS08} - R_x(t) \cdot Y(t)_{IGS08} + [1 + s(t)] \cdot Z(t)_{IGS08}$$

These equations show $X(t)_{SHRF}$, $Y(t)_{SHRF}$, and $Z(t)_{SHRF}$ indicating the X , Y , and Z position coordinates, at time t , for the ground station within the SHRF. Similarly, $X(t)_{IGS08}$, $Y(t)_{IGS08}$, and $Z(t)_{IGS08}$ represent the respective position coordinates, of the same station, within the IGS08 reference frame.

Equation 1 (Wang et al., 2013; Soler and Snay, 2004) demonstrates X , Y , and Z position coordinates in IGS08 being transformed into the SHRF as a function of time using:

$T_x(t)$, $T_y(t)$, $T_z(t)$ *translation* along the x -, y -, and z -axis, respectively, at time t ;
 $R_x(t)$, $R_y(t)$, $R_z(t)$ counterclockwise, positive *rotation* about respective axes, at time t ;
 $s(t)$ a differential *scale factor* between IGS08 and SHRF, at time t .

Approximated equations are sufficient due to the small magnitudes of the three rotations. Note that each of the seven parameters is represented as a function of time. These time-related functions are assumed to be linear, as expressed by Pearson and Snay (2013):

$$T_x(t) = T_x(t_0) + T'_x \cdot (t-t_0)$$

$$T_y(t) = T_y(t_0) + T'_y \cdot (t-t_0)$$

$$T_z(t) = T_z(t_0) + T'_z \cdot (t-t_0)$$

$$R_x(t) = R_x(t_0) + R'_x \cdot (t-t_0)$$

$$R_y(t) = R_y(t_0) + R'_y \cdot (t-t_0)$$

$$R_z(t) = R_z(t_0) + R'_z \cdot (t-t_0)$$

$$s(t) = s(t_0) + s' \cdot (t-t_0)$$

In the aforementioned equations, t_0 symbolizes a pre-specified value of time. All seven parameters that are a function of t_0 are constant. Therefore, $T_x(t_0)$, $T_y(t_0)$, $T_z(t_0)$, $R_x(t_0)$, $R_y(t_0)$, $R_z(t_0)$ and $s(t_0)$ are also constants. The SHRF transformation from IGS08 uses 2012.0 as t_0 . The other seven quantities (T'_x , T'_y , T'_z , R'_x , R'_y , R'_z , and s') representing rates of change, or velocities, as a function of time (after Pearson and Snay, 2013) are also constant.

Table 4-2 shows the values used for the fourteen parameters used to transform the IGS08 coordinates into the NAD83 reference frame, and IGS08 to the SHRF. The long data history available in the vicinity of the Houston metropolitan area allowed the SHRF transformation to account for all seven parameters and their respective time derivatives. The results for both transformations are visible in Figure 4-5, a time-series of PA04.

Table 4-2: 14-parameter Helmert Transformation from IGS08 to NAD83 and SHRF

Transformation Parameters	Unit	IGS08 to SHRF $t_0 = 2012.0$	IGS08 to NAD83 (2011) $t_0 = 1997.0$
$T_x(t_0)$	cm	0	99.34300
$T_y(t_0)$	cm	0	-190.3310
$T_z(t_0)$	cm	0	-52.65500
$R_x(t_0)^*$	mas**	0	25.91467
$R_y(t_0)$	mas	0	9.42645
$R_z(t_0)$	mas	0	11.59935
$s(t_0)$	ppb***	0	1.71504
dT_x	cm/year	-1.0725	0.07900
dT_y	cm/year	-1.05876	-0.06000
dT_z	cm/year	-3.54574	-0.13400
dR_x	mas/year	1.1572	0.06667
dR_y	mas/year	-0.93885	-0.75744
dR_z	mas/year	-0.33224	-0.05133
ds	ppb/year	1.3722	-0.10201

*Counterclockwise rotations of axes are positive.
**mas= milliarc second
radians to mas coefficient: 206264806.24709636;
mas to radians coefficient: 4.848137E-09.
***ppb = parts per billion

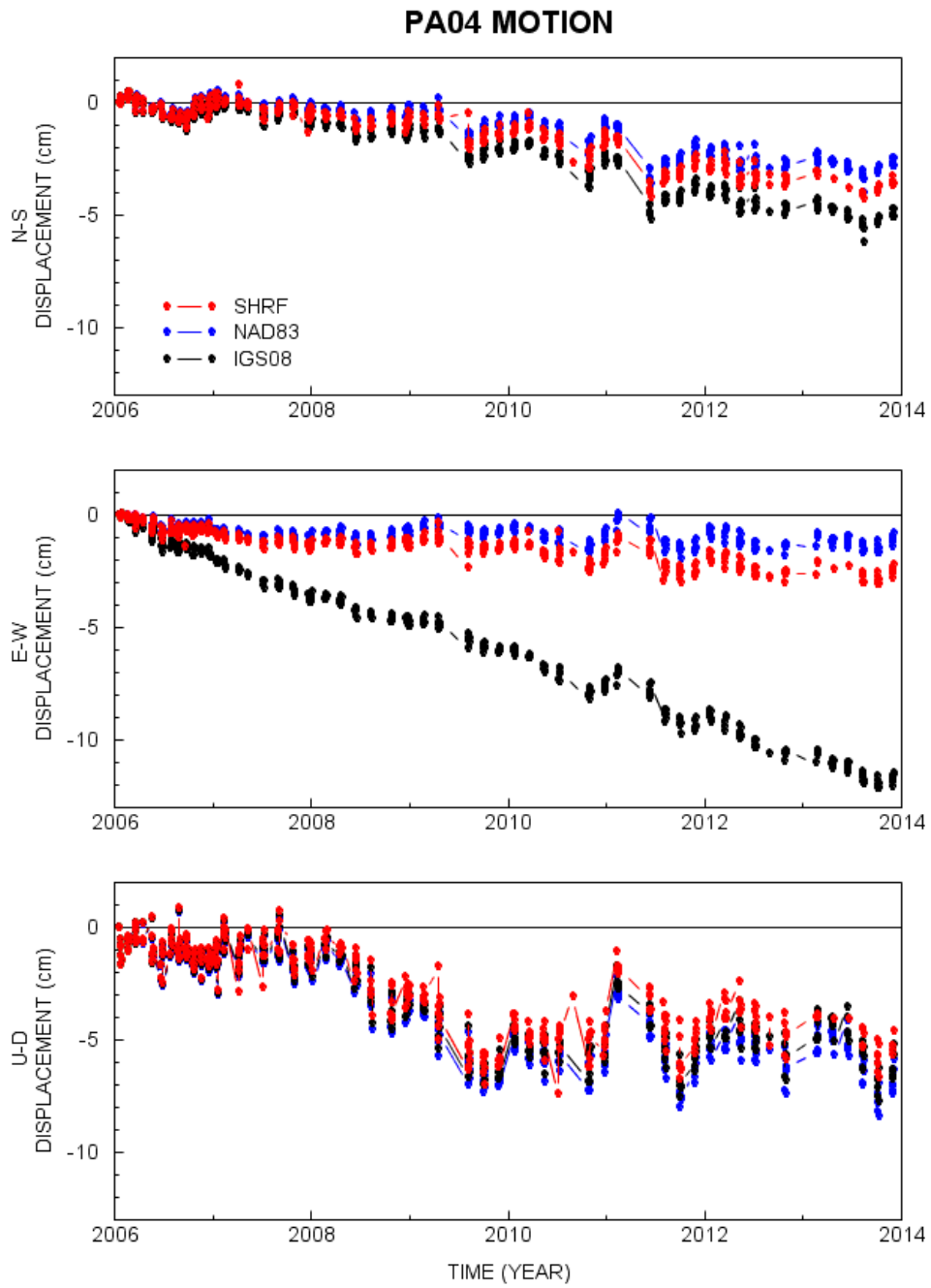


Figure 4-5 PA04 Displacement Time-series in Three Reference Frames.

5 Results

5.1 Groundwater Withdrawal

As population grows with development in Fort Bend County (FBC), increased water demand places strain on the aquifer system. In 2010, fresh groundwater withdrawal accounted for 63% of the community's needs (U.S. Census Bureau, 2010). Fort Bend Subsidence District (FBSD) regulations required a 30% conversion to surface water supplies by 2016 for all of Area A in an effort to mitigate subsidence and ensure ample water supplies for future generations. Groundwater pumping history across the three regulatory areas within FBSD is shown in Figure 5-1 (FBSD, 2013).

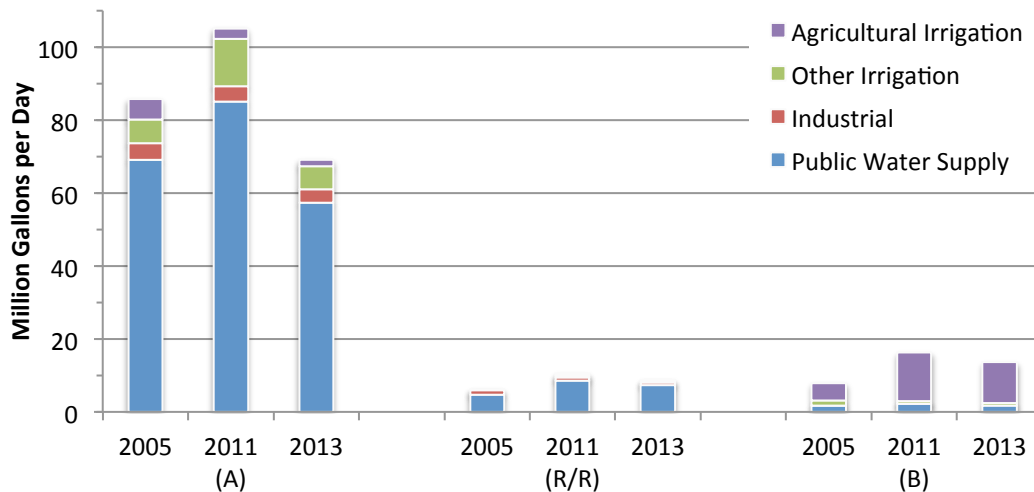


Figure 5-1 Groundwater Withdrawal History by Regulatory Area.
Data comes from the FBSD Annual Reports (2006, 2013).

Municipal water supply clearly dominates groundwater demands in the eastern half of FBC. Agricultural groundwater usage is unregulated across the county. Area A uses ten times more groundwater each day than the Richmond/ Rosenberg (R/R) subarea. When translated to consumption by actual area (table 5-1), we see that rates for Area A and subarea- R/R are much closer than Figure 5-1 illustrates. Agricultural usage

dominates in Area B, which only uses about nine to thirteen million gallons per day in 2011 and 2012 (FBSD, 2013).

Table 5-1 Groundwater Consumption by Area

	Area (km²)	2013 Pumping Rate (MGD)	Gallons/day*km²
FBC	2,295	91.5	39,869
Area A	1,126	69.1	61,340
Area A-R/R	191	8.7	45,669
Area B	978	13.7	14,008

Groundwater levels dropped twelve meters within the Evangeline aquifer from 2005 to 2014 near the R/R area. The cone of depression appears to be unrelated to historic and widespread pumping in the Houston metropolitan area. Further investigation was necessary to determine whether the change in aquifer levels was indicative of pumping patterns that would be affected by regulations (municipal versus agricultural) and be associated with subsidence.

Pumping data were obtained from a municipal groundwater well near the town of Rosenberg, from 2005 to 2014. The well is located about 30 meters north of USGS well JY-65-26-908, and halfway between PA10 and TXRO. Annual groundwater-withdrawal data from the City of Rosenberg Well #7 are shown in Figure 5-2. It also accounts for 11-15 % of the R/R sub-area's groundwater-withdrawal budget in 2011 and 2013, respectively.

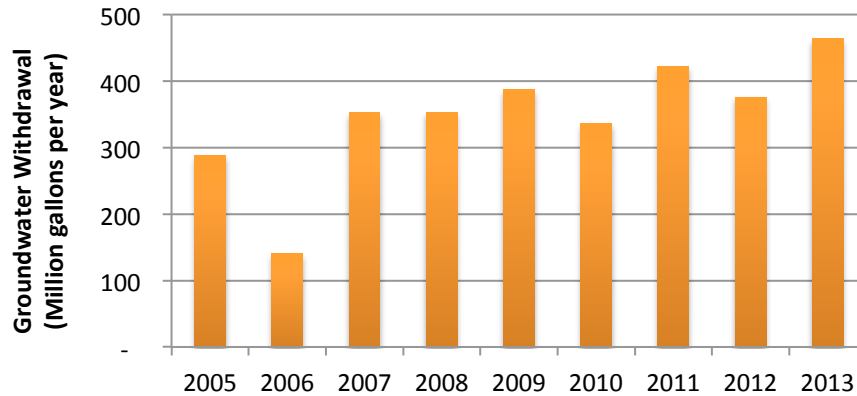


Figure 5-2 Annual Groundwater Withdrawal Data: City of Rosenberg Well #7. Volumes of groundwater extracted from 2005 to 2014. Data provided by John Maresh.

On average, about 350 million gallons (Mgal) per year are pumped from the R/R well, which is just short of 1.0 MGD. Groundwater production has steadily increased from 287,435,000 to 464,547,000 gallons per year over the study period. Well #7 is centrally located in relation to the drawdowns observed. The early stages of subsidence will be more readily observed through studying this isolated-drawdown feature and localized pumping.

Drawdown within the aquifer occurs when the rate of extraction exceeds the rate of recharge. Intersecting cones of depression compound, meaning the drawdown from each individual well adds to the drawdown induced by any other wells in the affected area (Fetter, 2001). Subsurface pressure changes can either be accommodated through a change in flow patterns, or deformation of the matrix (reduced storage). The resulting regional-scale drawdown feature is driven by closely spaced pumping-wells and increased production-volumes for an area, exemplified in Area A. Annual groundwater withdrawal for Area B is nominal, less than 0.5 MGD. The potentiometric surface is relatively unaffected, as illustrated in the following section.

5.2 Groundwater Levels

The observation of depressed groundwater levels in Fort Bend County (FBC) monitoring wells represent declines in the potentiometric surface. This observation is part of a much larger cone of depression that has been developing beneath the greater Houston metropolitan area, where the hydraulic head has dropped as much as 150 meters (~500 feet) beneath Houston from 1940 to 2000 (George et al., 2011). Groundwater regulations have aided in the rebound of the potentiometric surface. There has been an associated stabilizing or slight rebound of the land surface as the potentiometric surface returned to 30 to 40 meters BLS in the Chicot and Evangeline aquifers, respectively (Kearns et al., 2015).

The U.S. Geological Survey provided groundwater level observations for FBC through the Groundwater Watch program. The potentiometric surface of both the Chicot and Evangeline aquifers are shown below in map view for 2005, 2011 and 2014, (Figure 5-3). The input values are available in Appendix I. Measurements were originally reported in feet below land surface, but have been converted to meters for consistency with the rest of this report.

Figure 5-3 shows groundwater data collection points (triangles) and interpolated groundwater levels (raster surface) extrapolated across the county. There are 27 wells screened in the Chicot aquifer, 32 in the Evangeline and 6 screened in both (Appendix I). Aquifer levels are dynamic and fluctuate in response to pressure differentials induced by natural flow patterns or pumping. When one aquifer has been heavily pumped, a sharp change in gradient is evident, indicating the aquifers are not currently in equilibrium.

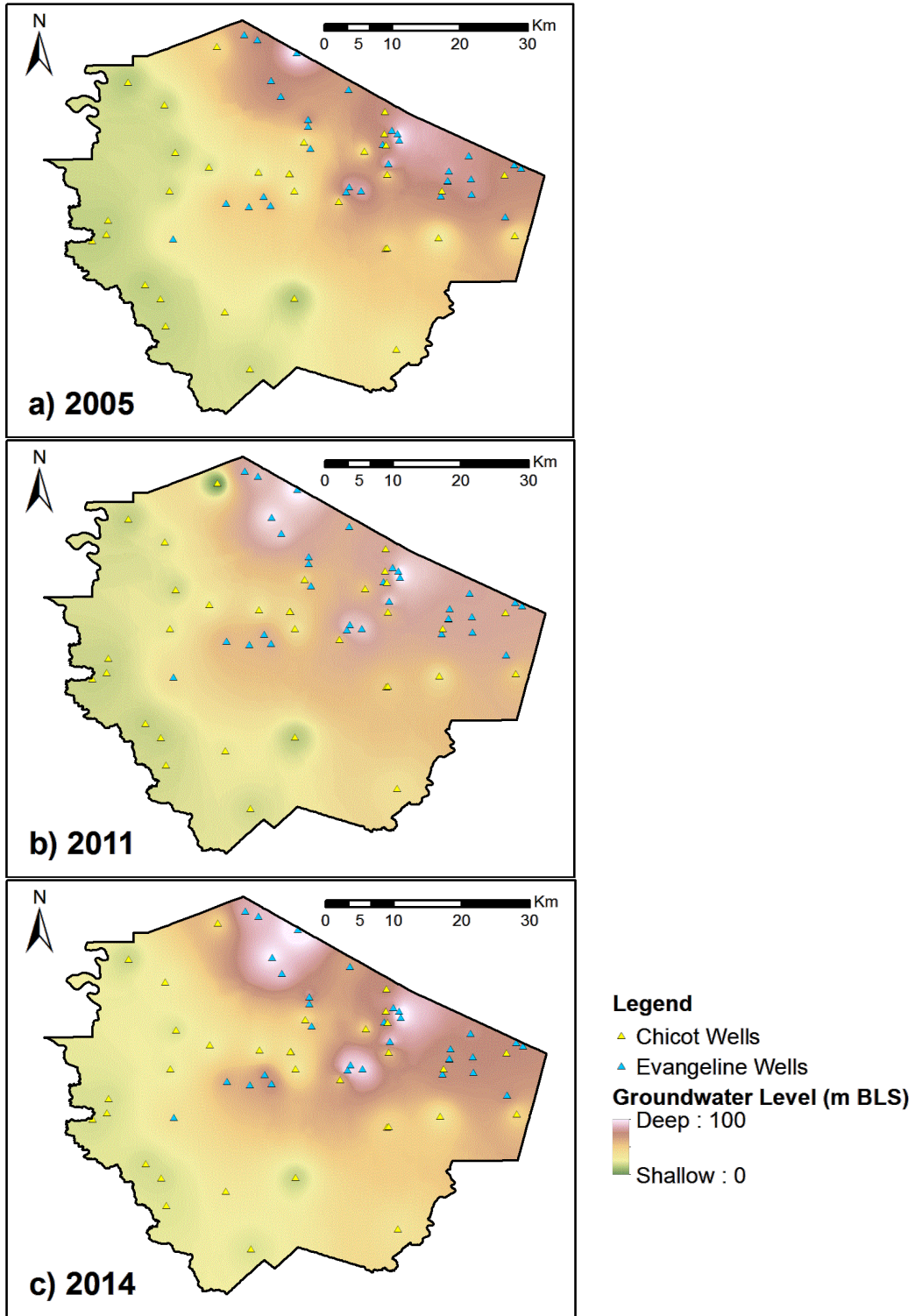


Figure 5-3 Groundwater Level Maps: Fort Bend County.
 Color shading is representative of the potentiometric surface at the beginning of each year.
 Data provided by the USGS Groundwater Watch.

Two colocated monitoring wells (JY-65-27-324 and JY-65-27-302) are screened in the Chicot and Evangeline aquifers, respectively, 165 meters apart vertically, (Figure 5-4). Measurements from the Evangeline aquifer show a steady lowering of the hydraulic head through 1985. In contrast, when the Chicot aquifer began to be monitored at this location in 1985, the hydraulic head was 20 meters higher than the monitoring well screened at a deeper interval. The difference in hydraulic head between the two aquifers decreased over the next ten years, indicating that the shallower unit was helping recharge the deeper unit until equilibrium was obtained in 2006 and maintained around 60 meters BLS through 2011, (Figure 5-4).

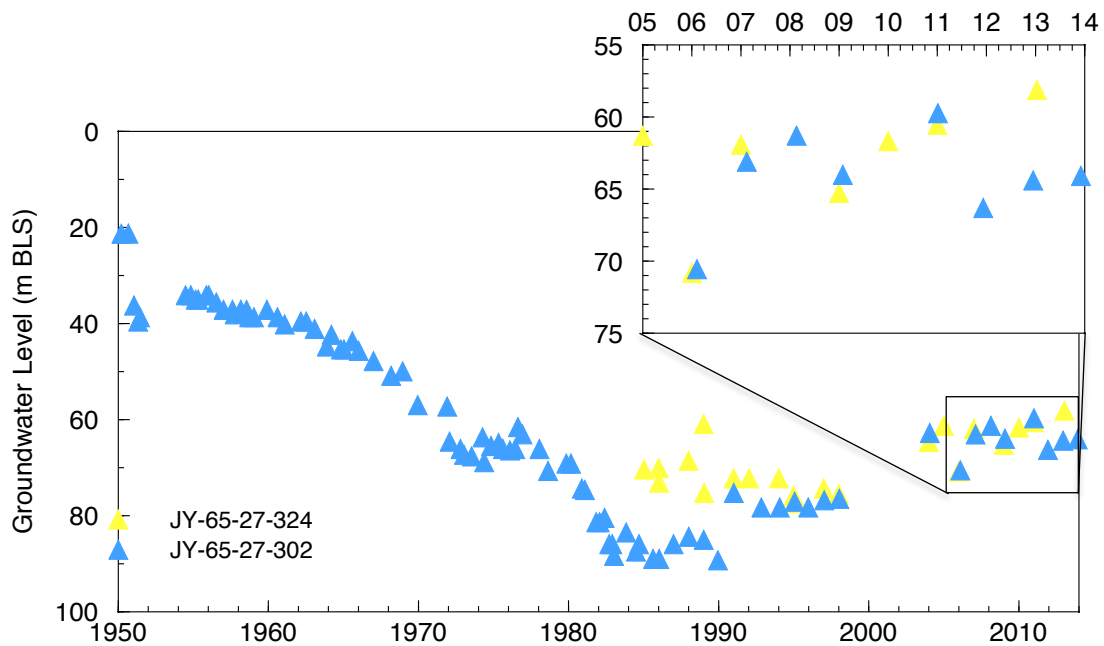


Figure 5-4 Chicot and Evangeline Aquifer Level Changes.

This figure shows two monitoring wells 400 meters apart and 3.7 km W-SW of PA04. JY-65-27-324 and JY-65-27-302 are screened in the Chicot and Evangeline aquifers, respectively. Notice the steady decline of hydraulic head within the Evangeline aquifer with time, which then rebounded, reestablishing equilibrium with the Chicot aquifer.

In 2011, pressures with the two aquifers begin to draw apart, with measurements differing by about seven meters. According the US Drought Monitor website (accessed April 2014), a widespread drought officially began in October of 2010 and lasted through December of 2011. The prolonged and increased reliance on groundwater resources during the drought strained the aquifer system.

A graph of 2011 groundwater levels observed at every monitoring well within FBC is shown in figure 5-5. Measurements ranged from 13 to 96 meters BLS for the Chicot and Evangeline aquifers. The observed drawdown from 2011 to 2012 ranges from 0.2 to 22 meters.

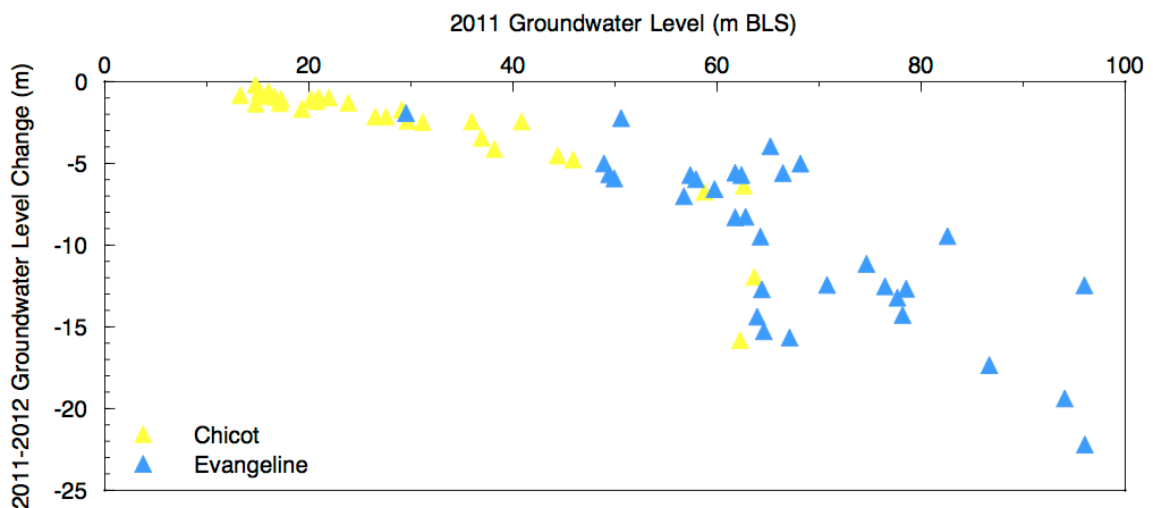


Figure 5-5 2011 Groundwater Levels Graph: Fort Bend County. Graph showing groundwater levels at the beginning of 2011 in relation to the magnitude of change over the drought year. Data provided by the USGS Groundwater Watch.

There is a strong linear relationship observed between 2011 groundwater levels and the magnitude of change; wells with lower hydraulic head (groundwater level) measurements show greater amounts of drawdown (change) in a single year. Smaller changes and shallower groundwater level measurements tend to be associated with wells

finished in the Chicot aquifer, while deeper measurements and larger magnitudes of change tend to be associated with the Evangeline aquifer.

These results, however, may represent an inherent bias in the dataset imposed by anthropogenic causes rather than aquifer characteristics. Municipal wells that produce large volumes of water tend to be screened in deeper units. In addition, data is normally collected during winter months, when there is a lull in groundwater usage for both municipal and agricultural purposes. Municipalities and farmers heavily pump groundwater resources during the summer months when rainwater is scarce and demand is high.

There is an anomaly in the relationship for wells measuring a hydraulic head about 65 meters BLS. Water level change is no longer a function of groundwater levels in wells, which ranges from 3 to 16 meters for wells screened in both the Chicot and Evangeline aquifers. When observing the aerial distribution of these data points, (Figure 5-3b), they fall along the periphery of areas of major drawdown. The observed change around 65 meters BLS, (Figure 5-3b) is interpreted to be a change in pressure gradient within the aquifer.

Spatially confined and heavily populated areas in the county such as Katy, Sugarland, and Greatwood began 2011 with a depressed hydraulic head, and reported a greater amount of drawdown over the year compared to surrounding areas. A location (JY-65-20-712) in Sugarland logged the groundwater level at 95 meters BLS at the beginning of 2011, then dropped 25 meters over the year. Wells are generally stable on the western edge of the county, which has the lowest population density and least growth.

5.3 GPS Measured Surface Deformation

All GPS data collected by the NGS and FBSD was processed through 2014 using GIPSY's Precise Point Positioning-Single Receiver Phase Ambiguity technique. Positions are reported in Northing, Easting and Vertical displacement from each station's respective initial (t_0) position within the Stable Houston Reference Frame (Wang et al., 2013). A complete collection of the GPS time-series analyzed in this study is included in Appendix II. An RMS accuracy of 6 to 7 mm was achieved for the vertical component and 2 to 3 mm in the horizontal direction for solutions within the SHRF (Wang et al., 2013). Spatial and temporal surface deformation patterns are discussed below.

Negative vertical deformation is referred to as subsidence, while positive displacement is rebound. Total observed subsidence for the four GPS stations operational from 2005 to 2014 is listed in Table 6-1, and shown in Figure 6-6a with horizontal displacement vectors. In most cases, horizontal displacement appears to be elastic, rather than permanent deformation. Maximum horizontal displacements range from six to fifteen centimeters (cm). Though the magnitude of displacement for horizontal components is nominal compared to the vertical component, major offsets tend to coincide between at least two of the three components.

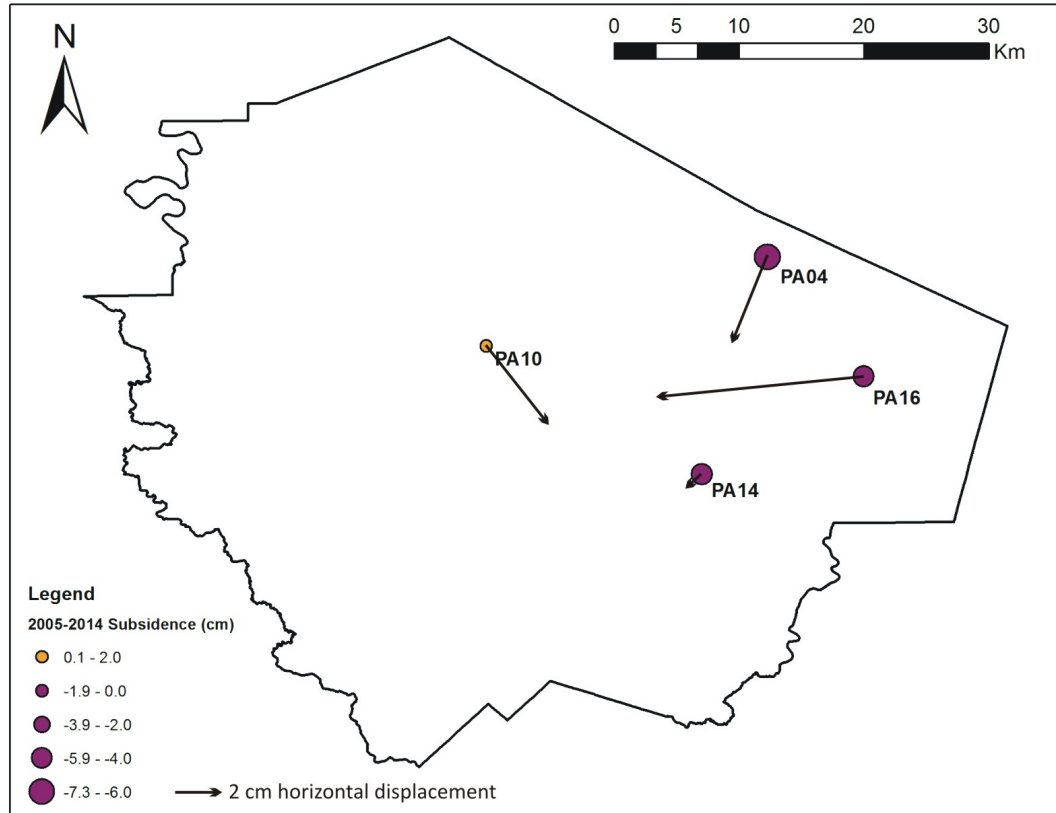


Figure 5-6 GPS Observations: 2005-2014.
Four stations have been operational from 2005-2014. Directional displacement points to the southeast corner of the county.

Multiple studies have used horizontal displacement to interpret surface deformation trends (Bawden et al., 2012; Burbey et al., 2006; Burbey, 2001). Horizontal displacements within the study area are sporadic and difficult to interpret, as seasonal fluctuations have an inconsistent magnitude and direction. PA04 (and PA14, PA16, PA40, PA57, PA62, PA67) moved steadily in one direction, despite seasonal fluctuations. PA30 was moving southwest at a rate of less than 1.0 cm/year and then rapidly changed direction in 2011, migrating to the northwest at a rate of 1.8 cm/year. TXRO exhibits a similar pattern beginning in 2009.

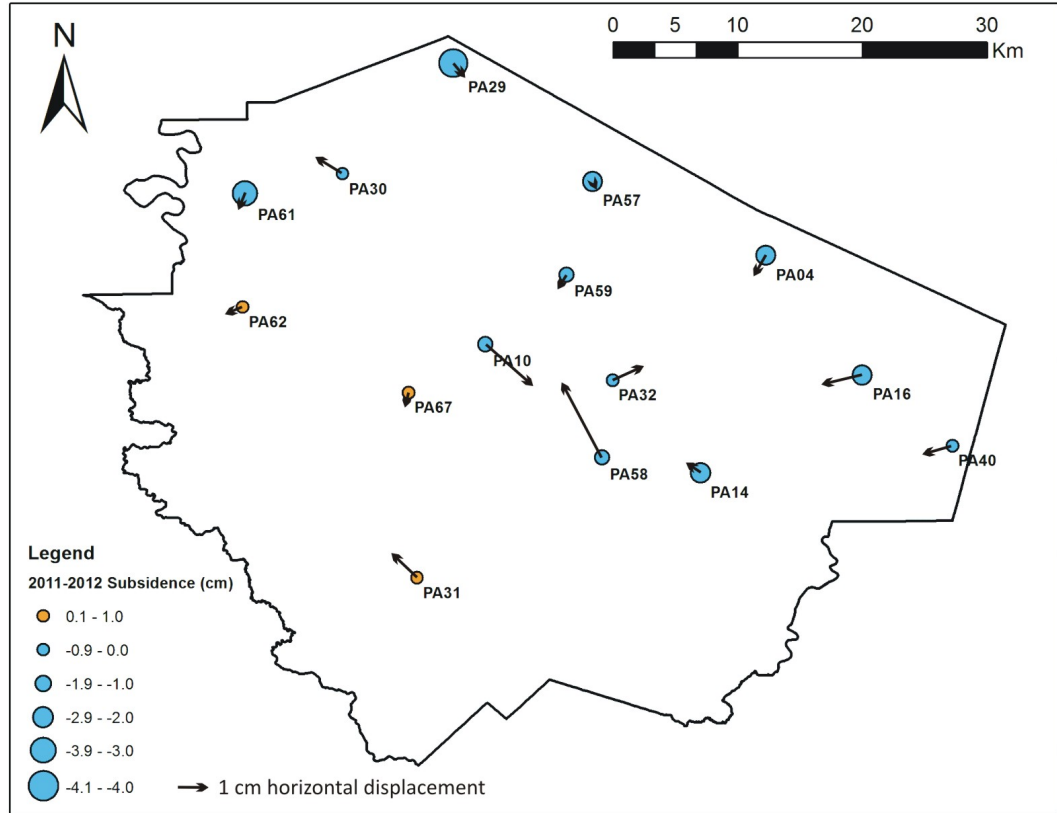


Figure 5-7 GPS Observations: 2011-2012.

This figure shows all 15 stations utilized throughout the study period. Directional displacement is relatively the same. In 2011, tiny arrows are within the range of error and considered stable, as are the smallest circles.

Significant subsidence in Fort Bend County has been observed in the southeastern region of FBC from 2005 to 2014. The more significant rates of subsidence are concentrated along the northern border of FBC. PA31, PA61, and PA62, located on the western edge of FBC where groundwater levels are within 20 meters of the surface, show stable vertical components. Horizontal displacements indicate two unique bowls of subsidence focused around Richmond- Rosenberg and Sugarland-Missouri City.

The vertical and horizontal temporal relationships are as follows: Some stations gradually subside, while others display a stair-step pattern of intermittent periods of rapid

subsidence buffered by relative stability. Sites that were previously sinking at a relatively stable rate, such as PA10 and PA16, began to alternate between periods of stability and rapid subsidence in 2005.

For example, PA10 steadily subsided 3.5 cm over ten years, averaging about 3.5 mm of vertical deformation per year. In contrast, PA04 shows steady subsidence up to 2005. From 2005 to 2010, the station subsides eight centimeters, averaging 16 mm per year. Upon closer inspection, there is an observed stair-step pattern: the station rapidly subsides 4.5 cm in one year, is stable for two years, and then rapidly subsides another 6.0 cm over a year and a half.

Rates of subsidence decrease to the south and west, as groundwater levels increase. The relationship between subsidence and groundwater levels is not clear at first, as the most rapidly subsiding stations are not necessarily located where groundwater levels are the lowest. This relationship will be further discussed in the following chapter.

6 Groundwater Levels and Surface Deformation

The scientific community has long accepted that extracting large volumes of fluids from shallow, soft-sediment aquifers can lead to subsidence. Multiple sources (InSAR, GPS, and extensometer) of data indicate subsidence is due to groundwater withdrawal in the greater Houston metropolitan area (Kasmarek et al., 2014; Buckley et al., 2003; Coplin and Galloway, 1999). Recent work by Jiang (2015), Burrough (2013), and Ortega (2013) determined that groundwater withdrawal drives aquifer compaction and observed land surface subsidence in and around the Houston metropolitan area.

Land surface subsidence has slowed or even begun to rebound around Southwest Houston and along the Ship Channel, where regulations have barred groundwater withdrawal. Subsidence has not been eradicated though; instead, it has migrated north and west to areas of increased groundwater pumping like Montgomery and Fort Bend County (FBC). As mentioned earlier in this study, urban development is strongly correlated with areas of heavy pumping and drawdown within the aquifer. These counties present an opportunity to study the early drivers of subsidence.

This study shows that the Chicot and Evangeline aquifers compact due to increased rates of groundwater withdrawal when the hydraulic head is more than 30 meters below land surface (BLS). To better understand the evolution of subsidence relating to groundwater withdrawal, the spatial variability and regional subsidence trends in FBC will be addressed first.

6.1 Spatial Variability of Subsidence in Relation to Hydraulic Head

As development patterns have changed in the Houston area, there has been a corresponding shift in the potentiometric surface. Pre-development hydraulic heads were artesian, while modern measurements range from 0 to 95 meters BLS. Texas relied more heavily on groundwater resources during the 2011 drought, amplifying surface deformation related to groundwater withdrawal. Figure 6-1 illustrates the potentiometric surface at the beginning of 2011 with GPS measured subsidence over the year.

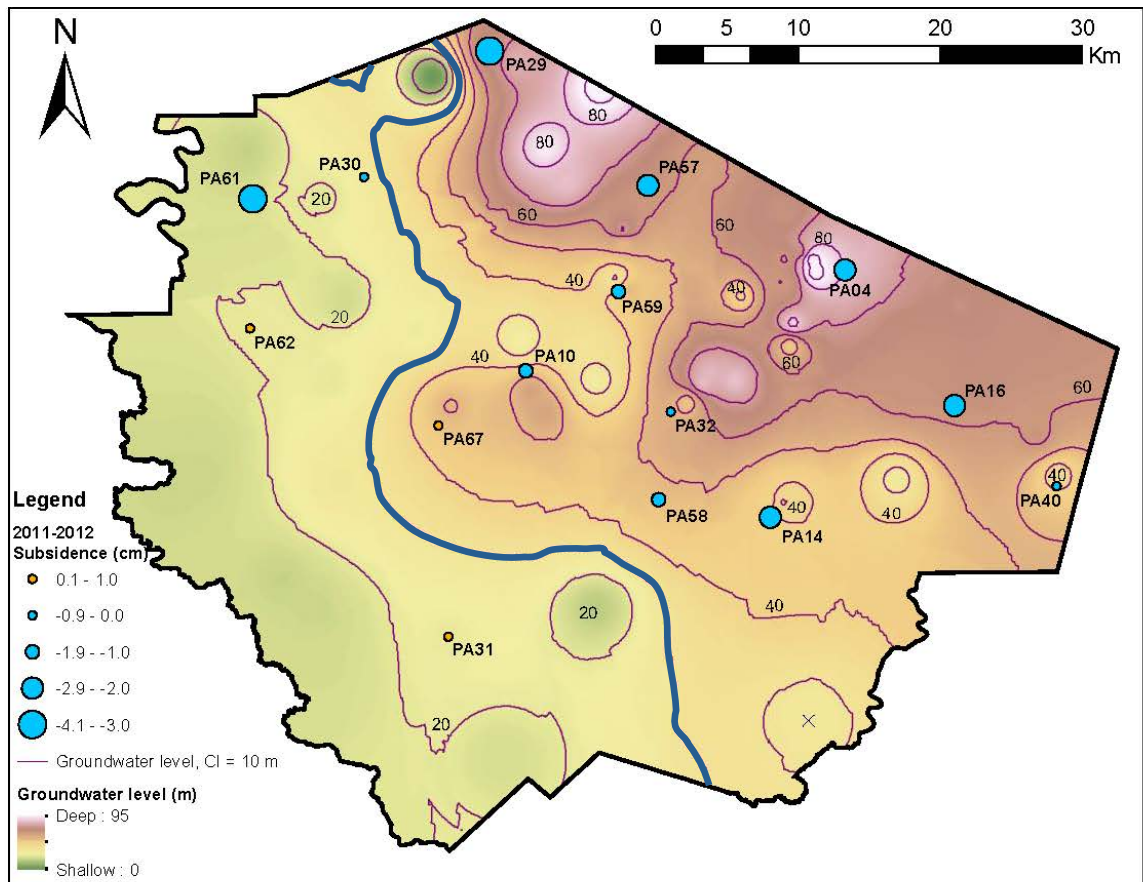


Figure 6-1 2011 Potentiometric Surface and Land Surface Deformation. Hydraulic head is contoured in purple; the dark blue line indicates the threshold, hypothesized to be approximately 30 meters below land surface, and graduated symbols represent the magnitude of subsidence from 2011-2012.

There is a general deepening of the potentiometric surface from west to east. Major pumping centers are associated with depressed hydraulic head measurements. Subsidence was observed to occur during periods when nearby groundwater levels were rebounding, dropping, and stable. Stations recording significant (≥ 1.0 cm/year) subsidence are clustered closest to Katy and Houston. GPS stations on the eastern half of the county were observed to be either rebounding or subsiding below the instrument's detection limits (± 0.7 cm/year) and are therefore considered stable.

The magnitude of subsidence does not consistently parallel the magnitude of drawdown in either the Chicot or Evangeline aquifer. Therefore, a more simplistic question was asked of the dataset: is subsidence observed below a specific hydraulic head? The answer is yes. Subsidence during the 2011 drought was observed to occur at GPS stations where the potentiometric surface was deeper than 30 meters BLS. The hypothesized threshold in FBC may fluctuate between 25 and 40 meters BLS in other years.

To better understand the correlation between groundwater withdrawal and surface subsidence, individual GPS stations and nearby monitoring wells were analyzed. Figure 6-2 shows station PA14 and co-located monitoring wells that are finished in the Chicot and Evangeline aquifers, respectively. Monitoring well JY-65-35-302, screened in the Chicot aquifer, remains fairly stable around 34 meters BLS, and JY-65-35-304 screened in the Evangeline fluctuates between 36 and 65 meters BLS. PA14 is stable from 2007 to 2008 when the hydraulic head drops 15 meters in the Evangeline aquifer, and subsides from 2013 to 2014 when groundwater levels rebound in both aquifers.

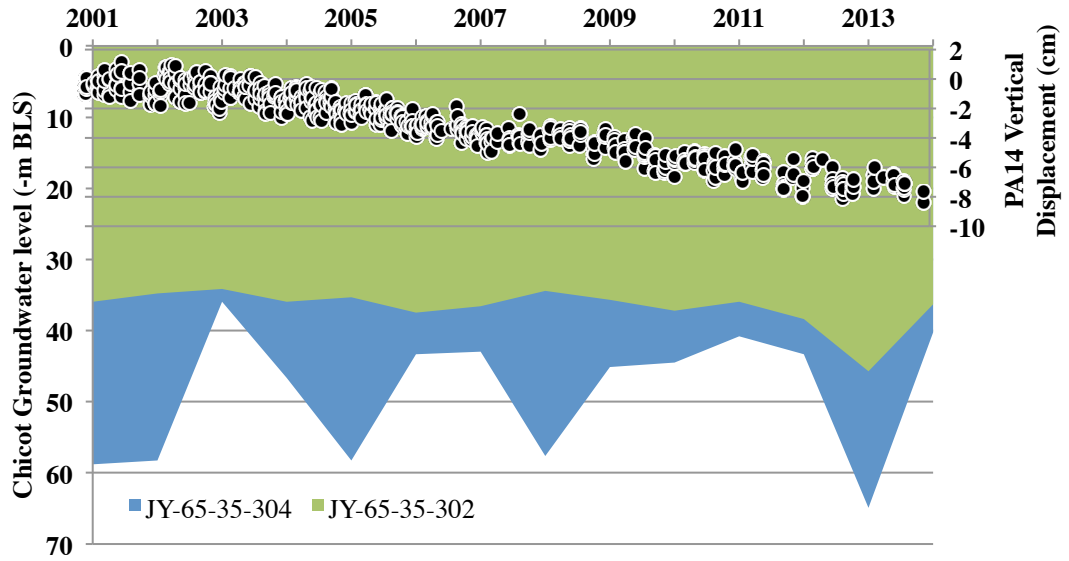


Figure 6-2 Smithers Lake: Surface Deformation and Groundwater Levels.
Note how quickly the aquifer reestablishes equilibrium- the potentiometric surface rebounded over 20 meters in 2002 and 2014. Subsidence is consistent from 2001 to 2007, then begins intermittent periods of subsidence.

PA14, near Smithers Lake illustrates the continuation of subsidence regardless of hydraulic head fluctuations below the proposed threshold of 30 meters BLS. This value is consistent with a recent study by Kearns et al. (2015), which found that land surface subsidence stabilized or even rebounded near the Houston Ship Channel once pumping stopped and the potentiometric surface was restored within 30 meters of the land surface.

Station PA32 is stable in 2011, when hydraulic head is 51 meters BLS. Previous years record a negligible seasonal signal. Monitoring well JY-65-27-505 is screened 256 meters BLS, near the interface between the Chicot and Evangeline aquifer. Two pumping wells (570 and 832) are located 80 meters southwest of PA32. Well 570 had minimal withdrawal from 2006 to 2011 before being shut off in 2011. Well 832 had a negligible pumping permit for 5 MGD (FBSD, 2015, *personal communication*). The lack of pumping corresponds with a period of surface stability, suggesting that the hydraulic

head and groundwater-pumping patterns contribute to observed subsidence. Significant groundwater pumping within close proximity is expected to be a key factor for inducing subsidence.

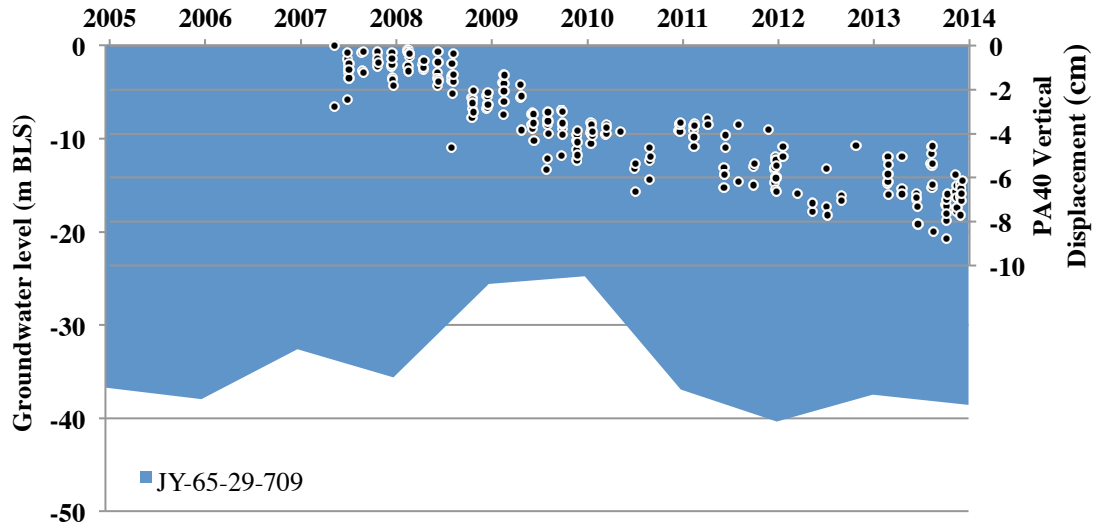


Figure 6-3 Arcola: PA40 and JY-65-29-709.

There is a time delay between the rise in hydraulic head in 2009 and reversal of subsidence halfway through the year that does not resume until 2011.

Monitoring well JY-65-29-709 (Figure 6-3) is located one kilometer south of station PA40, near Arcola, on the downthrown side of a normal fault. The hydraulic head remains between 25 and 40 meters BLS from 2005 to 2014, rising above 30 meters BLS in 2009. At GPS station PA40; subsidence is recorded both before and through 2009 when hydraulic head rises to 25 meters BLS, (Figure 6-3). A steady vertical displacement of 3.1 cm is recorded in 2009 and accompanied by an anomalous 2.0 cm displacement to the southwest. This suggests that there may be a delay in the equilibration of pore fluid pressure and the surrounding aquifer.

In the southeast corner of the county, PA16 has a steady vertical subsidence profile. Groundwater levels at the nearby monitoring well (JY-65-28-607) fluctuate from 60 to 70 meters BLS. Intermittent periods of deformation contribute to 10.0 cm of subsidence over fifteen years. Though horizontal deformation patterns are unusual- the northing component is fairly stable, changing no more than 3.0 cm over the 15-year station history. In contrast, the easting component has logged over 16.0 cm of displacement over the same period. Upon observing the character of displacement, one notices that the station is fairly stable, drifting 2.0 to 3.0 cm over a 5-year time span, and then shifting 3.0 cm westward in a day.

This rapid change suggests a different control, such as tectonic motion. Surrounding stations do not exhibit similar deformation, eliminating the possibility of plate motion. Another potential driver is the Blue Ridge salt dome, a nearby caprock just 18 meters BLS. A more detailed study is necessary to determine the control on displacement at this location.

GPS station PA61 present another exception to the proposed threshold- these stations continue to record subsidence in areas where the hydraulic head is less than 30 meters BLS and pumping volumes are negligible. Both PA40 and PA61 are located within a kilometer of regional faults (Ewing, 1991). The data is antiquated and the study area would benefit from a focused LiDAR study and further Station PA61 recorded a rapid (~4.0 cm) subsidence event during the 2011 drought. The hydraulic head at the time at JY-65-17-505 was measured to be 20 meters BLS in the Chicot aquifer. The GPS station is otherwise stable, and groundwater levels remain above the proposed threshold.

Pumping data provided by the FBSD (2015, *personal communication*) indicated that two wells, operated by Twinwood Farms, are located within 300 meters of PA61. Neither well has pumping activity recorded after January 2011.

The observed rapid subsidence event may be attributed to changes in the local environment and shallow soil conditions. Historic imagery from Google Earth indicates that the GPS station is located 90 meters north of a wetland pond that dried up in January 2011, as the land was cleared, (Figure 6-3). More data is necessary to form a conclusion concerning the rapid subsidence observed at PA61 in 2011.

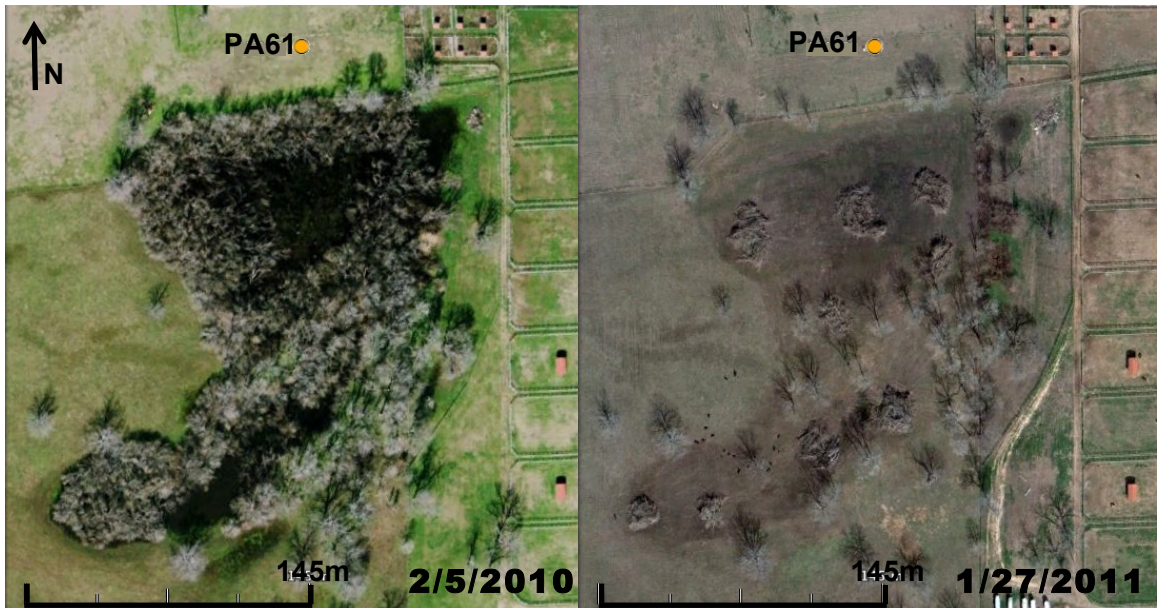


Figure 6-4 Aerial View of PA61 in Simonton.

The isolated, rapid subsidence event observed at PA61 in 2011 may be attributed to the clearing and drainage of the wooded pond located 90 meters south.

6.2 Temporal Variability of Subsidence in Richmond and Rosenberg

A USGS study of the Houston-Galveston region identified a unique subsidence feature around Sugarland utilizing InSAR scenes from 1996 to 1997 (Bawden et al., 2012). A later GPS study by Yu et al. (2014) indicated the possibility of a unique subsidence feature focused around the Richmond/Rosenberg (R/R) area. Groundwater levels in the Evangeline aquifer were also significantly depressed in this area, suggesting this is an area of recent change. Further analysis will increase understanding of the early drivers of subsidence in the Houston metropolitan area.

GPS stations PA10 and TXRO, shown in Figure 6-5, are both located near the city of Rosenberg. TXRO captures periodic subsidence, with a significant event halfway through 2009. This CORS station also displays a classic, seasonal signal in all three components. A similar, though subdued, and irregular seasonal signal is discernable at PA10. Subsidence rates recorded at PA10 appear to be constant through 2010, when a pattern of rapid subsidence and rebound begins.

Horizontal deformation at TXRO shifts in 2009 from relatively stable in both components to moving northwest (2.0 cm). That same year, PA10 begins to move southward. This minute, centimeter-scale change could indicate a change in the local stress regime. According to the FBSD Annual Report (2013), 2009 was the first year that groundwater withdrawals exceeded 8 MGD in Area A– R/R.

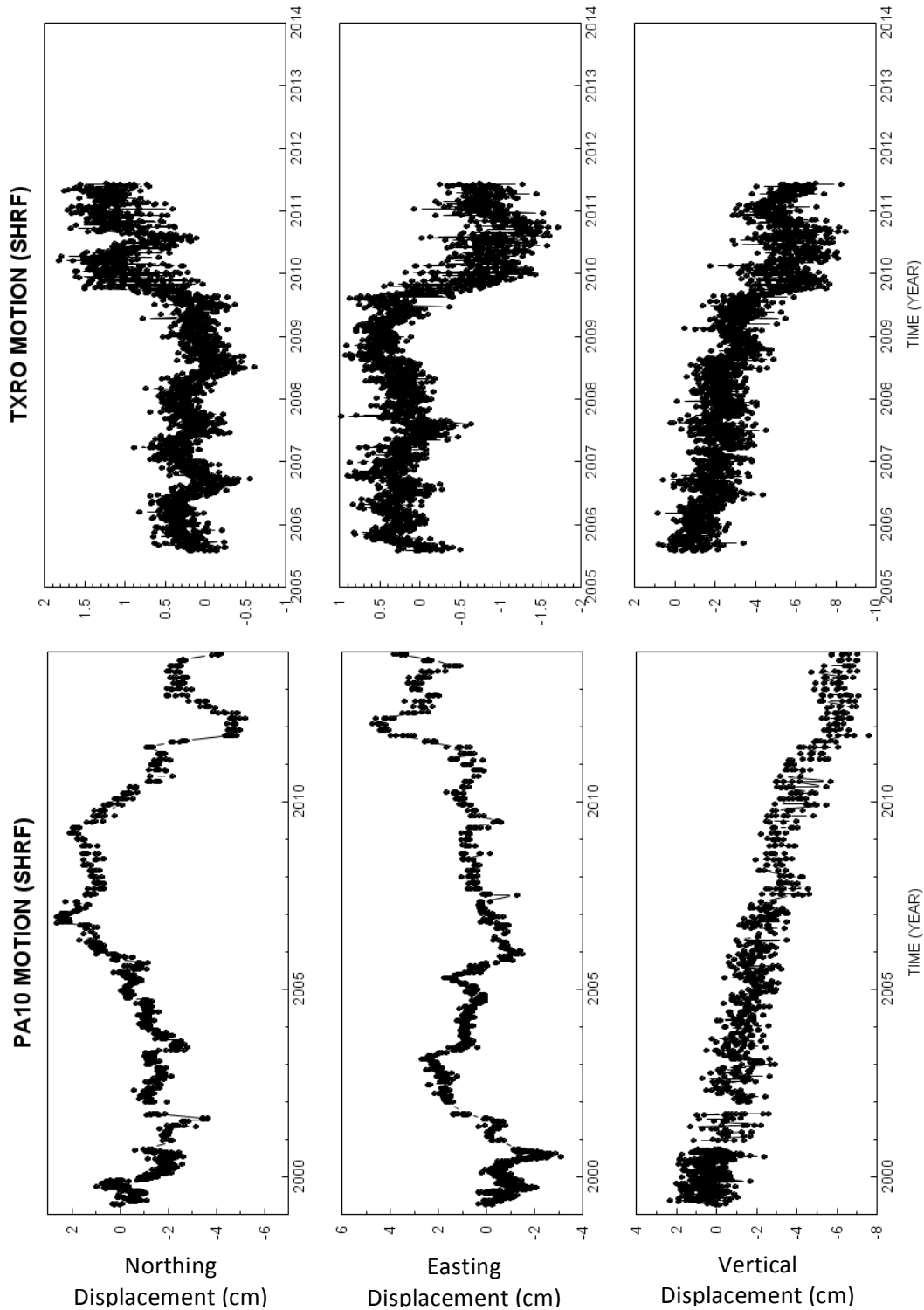


Figure 6-5 TXRO and PA10 Surface Deformation.
 Both stations are subsiding, and are fairly stable in the horizontal component through 2009. There is a drastic shift recorded in the horizontal direction, illustrating both stations beginning to move toward one another.

To further investigate the changing character of surface deformation patterns, it was necessary to obtain aquifer measurements and pumping data near PA10 and TXRO. There are two monitoring wells located near city of Rosenberg pumping wells. JY-65-26-908 and JY-65-26-812 roughly co-located with city pumping wells, shown in Figure 6-4. Evangeline aquifer levels dropped significantly— 12 to 16 meters— at these monitoring sites from 2005 to 2014, (Figure 6-6).

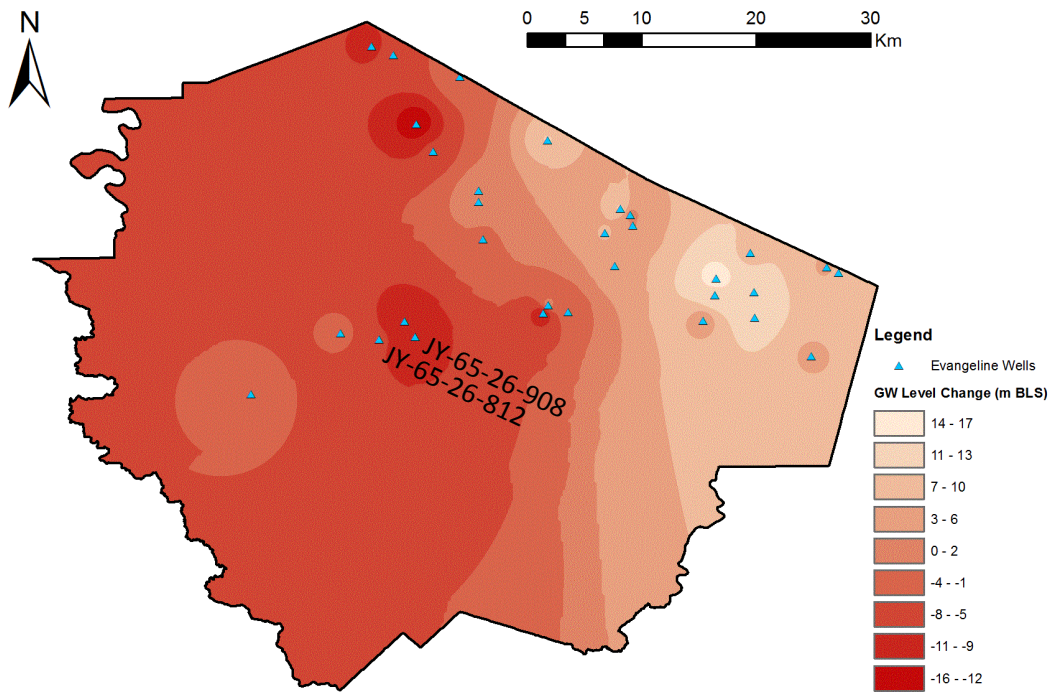


Figure 6-6 Evangeline Aquifer Level Changes: 2005-2014.

To better understand the relationship between groundwater withdrawal, hydraulic head and surface deformation, pumping data was obtained from the nearby city of Rosenberg pumping well #7. There are two separate trends visible in Figure 6-7: (1) groundwater withdrawal peaks in June, averaging 35.5 million gallons per month over the study period (2005-2014), and (2) annual groundwater withdrawals increase about 20 million gallons per year.

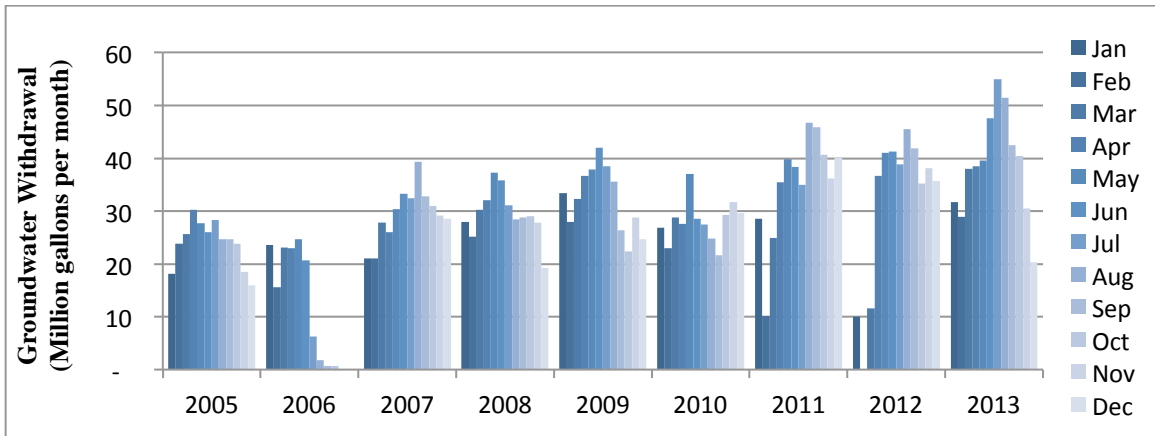


Figure 6-7 Monthly Groundwater Withdrawal at CoR Well #7.
 Graph of groundwater withdrawal by month (2005-2014) at the City of Rosenberg well site #7. Volumes extracted are greatest in 2009 and 2013. Annual pumping values during the 2011 drought are average. Data kindly provided by John Maresh, City of Rosenberg.

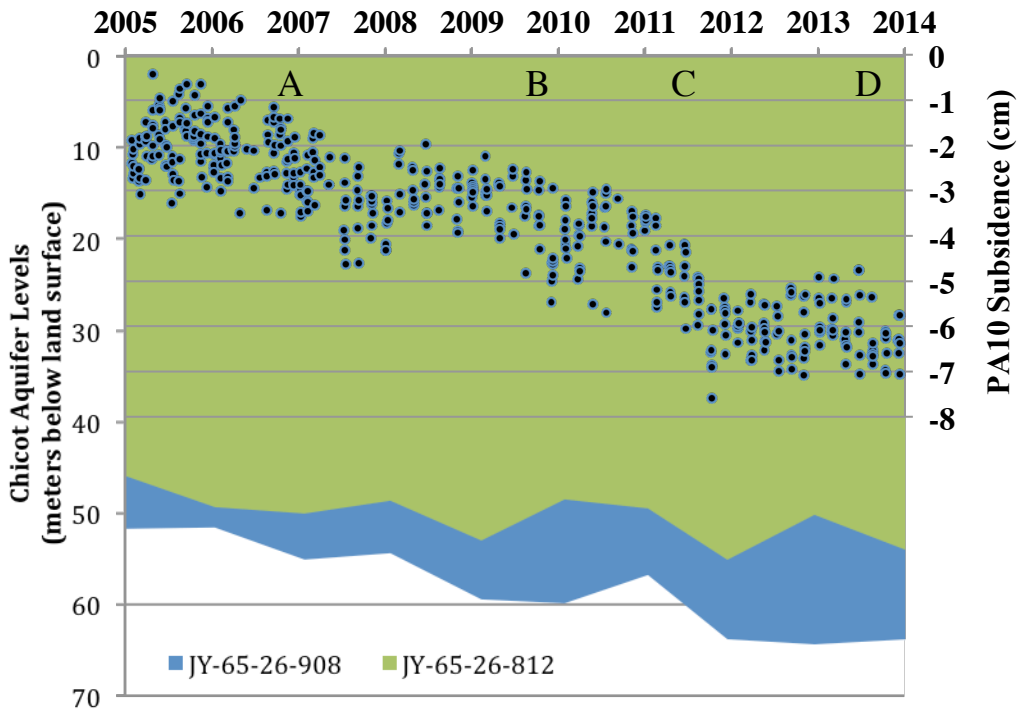


Figure 6-8 Rosenberg Groundwater Levels and Surface Displacement.
 This plot shows two Chicot aquifer monitoring wells located between PA10 and TXRO. TXRO is roughly 5km S-SW of PA10. JY-65-26-812 (green) is located 1.5 km southeast of PA10 and JY-65-26-908 (blue) is located 28 meters south. Vertical displacements at PA10 (black dots) are superimposed. Data courtesy of the USGS Groundwater Watch and FBSD.

Figure 6-8 shows subsidence at PA10 in relation to the changing hydraulic head. Rebound was observed in short-term aquifer measurements, but there is a long-term gradual decline within the aquifer at both locations. There is a clear correlation between potentiometric surface changes and land-surface measurements in Figure 6-8, but the temporal resolution makes it difficult to define the relationship between the two.

Table 6-1: Changes in Rosenberg Pumping Patterns and Aquifer Levels

Observed Period of Subsidence	Pumping Volume (gal)	Pumping Rate (gal/month)	Hydraulic Head Δ (m)	Subsidence (cm)
A. 1/2006 – 1/2008	492,770,000	20,532,083	-0.69	-0.8
B. 3/2009 – 2/2010	374,970,000	31,247,500	-4.56	-1.2
C. 7/2010 – 10/2011	510,108,000	23,186,727	4.20	-2.1
D. 1/2013 – 12/2013	464,547,000	38,712,250	3.95	-0.8

Table 6-1 synthesizes information from the two figures, showing periods of subsidence in relation to changing hydraulic head at JY-65-26-812 and pumping patterns at CoR well #7. The greatest pumping rates occur during periods B and D, when PA10 and TXRO displayed direction changes in the horizontal component, (Figure 6-5). This indicates that an increased pumping rate can affect both horizontal and vertical deformation at this location. Lee and Shen (1969) found that horizontal displacement related to subsidence is proportional the slope of the subsidence contour and the depth of the compacting interval.

The volume of water pumped and subsidence measured during the two-year period A and one-year period D is similar. The same amount of subsidence occurred in half the amount of time, at twice the rate of withdrawal during period D. This indicates that the volume of water extracted is directly related to the magnitude of subsidence.

Measured subsidence is greatest during the 2011 drought (period C). There is not a direct correlation between pumping rates and changes to the hydraulic head. The drought began October 2010, causing the wintertime pumping patterns to mirror summertime rates so that hydraulic heads were already depressed by January 2011. Extreme drought conditions across the state of Texas lead to a fifteen month period of increased pumping across the region (U.S. Drought Monitor, 2014). The hydraulic head appears to be affected on a regional scale by prolonged, high-volume pumping that exceeded recharge.

As seen in the previous section, this lead to increased *rates* of subsidence across the country, meaning that an increased rate of withdrawal correlates with greater-magnitude subsidence event. The delay between changes in hydraulic head and surface deformation may be the reason why changes to hydraulic head in Table 6-1 do not correlate with the observed pumping and deformation patterns. There is also the possibility that the combined effects of groundwater and oil and gas withdrawal contributing to the observed deformation, as suggested by Khan et al. (2014) in northwest Houston.

6.3 Groundwater Levels in Relation to Geologic Features

The effect of salt diapirs and faults in relation to subsidence has been a source of debate within the scientific community since the 60's. Many studies supported the idea that increased fault activity within the Houston metropolitan area is driven by fluid withdrawal (Van Sicken, 1967; Kreitler et al., 1977; Verbeek and Clanton, 1981; Holzer and Gabrysch, 1987). Kreitler (1977) promoted the idea that the observed fault motion was actually differential compaction due to faults compartmentalizing drawdown within the aquifer. Holzer (1984) then suggested that creeping faults were induced by groundwater withdrawal.

Carl Norman (2004) advocates for faulting and subsidence in the Houston area being unrelated, due to the completely different timescale of deep-seated tectonic processes that control fault motion versus shallow-aquifer compaction. Another worker in nearby Louisiana advocates for a tectonic control on subsidence and fault motion (Dokka et al., 2006). Both ideas are further supported by LiDAR data, which shows no geographic correlation supporting faulting being related to subsidence in the Houston area (Engelkemeir and Khan, 2008). Fracture or faulting patterns observed in the Houston region were not consistent with subsidence features, suggesting that stress is well distributed throughout the aquifer (Engelkemeir and Khan, 2008; Holzer, 1984).

Regional faults shown in Figure 6-9 appear to compartmentalize areas of drawdown within the aquifer (Ewing, 1991). The issue is still open for debate, and would be an excellent topic for future studies.

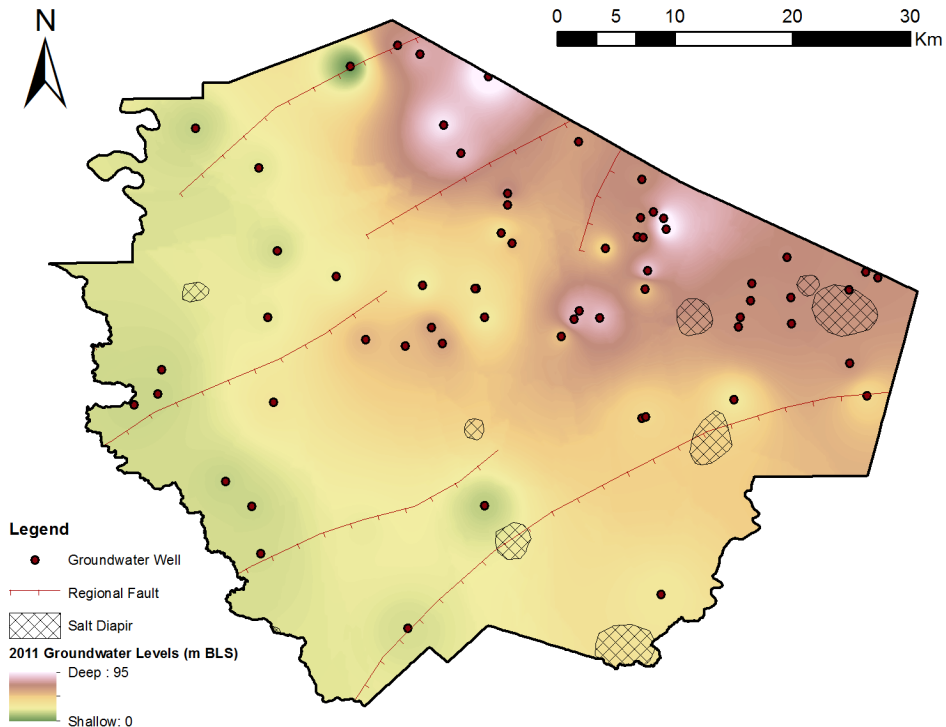


Figure 6-9 Groundwater levels for the Chicot and Evangeline Aquifers, January 2011. (USGS Groundwater Watch, 2014; Ewing 1991).

Two GPS stations, PA57 and PA59 are located on either side of a fault and exhibit similar subsidence trends, indicating fault-motion is not responsible for displacement in this area. Both PA29 and PA61 are located a few hundred meters up dip of the northern-most fault trace. These two stations display over 2.0 cm vertical displacements in 2011. PA30, to the south, is stable. Horizontal displacements are toward one another, which, if the motion were attributed to the fault, could indicate this fault is compartmentalizing subsidence or moving north.

7 Conclusions

This study investigated land-surface deformation related to groundwater withdrawal in Fort Bend County, Texas. GPS observations were processed and analyzed within the Stable Houston Reference Frame from 2005 through 2014. Analysis of GPS observations, localized groundwater pumping patterns, and hydraulic head measurements were used to arrive at the following conclusions.

1. *Regional control*: Regional subsidence trends are driven by groundwater withdrawal. Subsidence was observed to occur at GPS stations where the potentiometric surface was more than 30 meters below the land surface and significant groundwater pumping occurred. PA40 presents an exception to this trend, but analysis suggests that there is a delay between changes in hydraulic head and the surface deformation response. Considerable subsidence is not observed in areas where the potentiometric surface is shallower than 30 meters BLS. One exception occurs near Simonton, in northwest FBC, but the rapid subsidence event is attributed to the draining of a nearby pond.
2. *Spatial Variability*: Areas closer to Houston and Katy are subsiding about 2.0 centimeters per year (cm/year), the central region of FBC is subsiding about 1.0 cm/year, and areas to the west are stable or less than 0.7 cm/year. The potentiometric surface mirrors this trend, with the hydraulic gradient shallowing to the west. The potentiometric surface is observed to be more than 65 meters BLS closer to Houston and in areas associated with a dense population.

3. *Temporal variability*: Localized subsidence trends are driven by intervals of increased groundwater pumping rates. The increased pumping rates correlated with significant deformation in both horizontal and vertical components. The most prominent period affecting GPS stations across Fort Bend County was during the 2011 drought, when nine out of fifteen GPS stations recorded more than one cm of subsidence. The GPS data presented in this study verifies the Sugarland subsidence feature, observed by Bawden et al. (2012) using InSAR. A unique bowl of subsidence is proposed to form around Richmond/Rosenberg starting in 2009.; further investigation and data is necessary to confirm this feature.

The results of this research would benefit from further pumping tests and controlled lab-experiments to determine the hydromechanical properties of aquitards in Houston to determine their response to changes in aquifer pressure through groundwater withdrawal. The role of horizontal deformation is still poorly understood, but would benefit from regional-scale modeling of the groundwater system and further LiDAR studies.

The hydraulic characteristic of faulting in the Houston metropolitan area is still an area of academic debate; the author suggests a combined GPS study and pumping test is necessary to conclusively determine hydraulic characteristics and deformation trends across faults in the Houston metropolitan area. The results of this research can be used in managing regional groundwater use in relation to subsidence and can be extended to understanding ground surface deformation of the Gulf Coast Aquifer System in other regions.

8 References

- Anderson, J. B., and Rodriguez, A. B. (2001). The Episodic Evolution of Galveston Bay; Implications for Future Response to Global Change. *State of the Bay Symposium V* (pp. 125-131). Galveston, TX: Galveston Estuary Program.
- Baker Jr, E. (1979). Stratigraphic and Hydrogeologic Framework of Part of the Coastal Plain of Texas. *USGS Open-File Report 77-712*.
- Bar-Sever, Y. E., Kroger, P. M., and Borjesson, J. A. (1998). Estimating horizontal gradients of tropospheric path delay with a single GPS receiver. *Journal of Geophysical Research*, 103(B3), 5019–5035.
- Bawden, G. W., Johnson, M. R., Kasmarek, M. C., Brandt, J., and Middleton, C. S. (2012). Investigation of Land Subsidence in the Houston-Galveston Region of Texas by Using the Global Positioning System and Interferometric Synthetic Aperture Radar, 1993–2000. Denver, CO: *U.S. Geological Survey Scientific Investigations Report 2012–5211*.
- Bertiger, W., Desai, S. D., Haines, B., Harvey, N., Moore, A. W., Owen, S., and Weiss, J. P. (2010). Single receiver phase ambiguity resolution with GPS data. *Journal of Geodesy*, 84(5), 327-337. doi:10.1007/s00190-010-0371-9
- Bird, D. E., K. Burke, S. A. Hall, and J. F. Casey. (2005). Gulf of Mexico tectonic history: hotspot tracks, crustal boundaries, and early salt distribution. *AAPG bulletin*, 89.3, 311-328.
- Blewitt, G. (1989). Carrier phase ambiguity resolution for the Global Positioning System applied to geodetic baselines up to 2000 km. *Journal of Geophysical Research: Solid Earth (1978–2012)*, 94(B8), 10187-10203.
- Blewitt, G., and Lavallée, D. (2002). Effect of annual signals on geodetic velocity. *Journal of Geophysical Research: Solid Earth*, 107(B7), ETG-9.
- Boehm, J., and Schuh, H. (2004). Vienna mapping functions in VLBI analyses. *Geophysical Research Letters*, 31(L01603). doi:10.1029/2003GL018984.
- Bos, M., and Scherneck, H. (2011). Free Ocean Tide Loading Provider. Retrieved 01 30, 2014, from <http://holt.oso.chalmers.se/loading/index.html>
- Buckley, S. M., Rosen, P., Hensley, S., and Taplay, B. D. (2003). Land subsidence in Houston, Texas, measured by radar interferometry and constrained by extensometers. *Geophysics Research*, 108(B11). doi:10.1029/2002JB001848
- Burbey, T. J. (2001), Stress-strain analyses for aquifer-system characterization. *Groundwater*, 39: 128–136. doi: 10.1111/j.1745-6584.2001.tb00358.x

- Burbey, T. J., Warner, S. M., Blewitt, G., Bell, J. W., and Hill, E. (2006). Three-dimensional deformation and strain induced by municipal pumping, part 1: Analysis of field data. *Journal of Hydrology*, 319(1), 123-142.
- Bureau of Economic Geology. (1992). Geologic Map of Texas: University of Texas at Austin, Virgil E. Barnes, project supervisor, Hartmann, B.M. and Scranton, D.F., cartography, scale 1:500,000.
- Burrough, T. M. (2013). Spatial and Temporal Variability in Vertical Deformation in Willowbend, TX Derived from Long-Term GPS and Extensometer Observations. *Master's thesis*, University of Houston.
- Burkett, V. R., Zilkoski, D. B., and Hart, D. A. (2002). Sea-Level Rise and Subsidence: Implications for Flooding in New Orleans, Louisiana. *Subsidence Interest Group Conference: Proceedings of the Technical Meeting. Galveston, TX: U.S. Geological Survey.*
- Campbell, M. D., Campbell, M. D. Wise, H. M., and Bost, R. C. (2014). Growth Faulting and Subsidence in the Houston, Texas Area: Guide to the Origins, Relationships, Hazards, Potential Impacts and Methods of Investigation. *Houston Geological Society*. Retrieved 01 15 2015, from <http://ela-iet.com/HouFaultGuideDecember2014.pdf>
- Chowdhury, A. H., and Turco, M. J. (2006). Geology of the Gulf Coast aquifer, Texas. Texas Water Development Board Report 365. Retrieved 02 13, 2012, from http://www.twdb.state.tx.us/publications/reports/numbered_reports/doc/R365/ch02-Geology.pdf
- Coplin, L. S., and Galloway, D. (1999). Houston-Galveston, Texas. Land subsidence in the United States: *US Geological Survey Circular*, 1182, 35-48.
- Davis, J. L., Herring, T. A., Shapiro, I., Rogers, A., and Elgered, G. (1985). Geodesy by radio interferometry: Effects of atmospheric modeling errors on estimates of baseline length. *Radio Science*, 20(6), 1593-1607.
- Dixon, T. H., and R. K. Dokka (2008). Earth scientists and public policy: Have we failed New Orleans?, *Eos Trans. AGU*, 89(10), 96-96.
- Dokka, R. K., G. F. Sella, and T. H. Dixon. (2006). Tectonic control of subsidence and southward displacement of southeast Louisiana with respect to stable North America, *Geophysical Research Letters*, 33.
- Eckl, M. C., Snay, R. A., Soler, T., Cline, M. W., and Mader, G. L. (2001). Accuracy of GPS-derived relative positions as a function of interstation distance and observing-session duration. *Journal of Geodesy*, 75(12), 633-640.
- El-Rabbany, A. (2006). Introduction to GPS: The Global Positioning System 2nd Edition. Norwood: Artech House.

- Engelkemeir, R. M., and Khan, S. D. (2008). Lidar mapping of faults in Houston, Texas, USA. *Geosphere*, 4(1), 170-182.
- Engelkemeir, R., Khan, S. D., and Burke, K. (2010). Surface deformation in Houston, Texas using GPS. *Tectonophysics*, 490(1-2), 47-54.
- Ewing, T. E. (1983). Growth faults and salt tectonics in the Houston diapir province—relation, timing and exploration significance. *Gulf Coast Association of Geologists Society Transactions*, 33, 83-90.
- Ewing, T. E. (1991). Structural framework of the Gulf of Mexico basin: The geology of North America. *Geological Society of America*, J, 31-52.
- FBSD (2015). Personal Communication, April 1, 2015. Telephone correspondence.
- FBSD (2013). Fort Bend Subsidence District Regulatory Plan, accessed 04 01 2014 from: [http://www.fbsubsidence.org/docs_reports/2014/20130828%20FBSD%20Regulatory%20Plan%20ADOPTED%20-%20\(FINAL\).pdf](http://www.fbsubsidence.org/docs_reports/2014/20130828%20FBSD%20Regulatory%20Plan%20ADOPTED%20-%20(FINAL).pdf)
- Fetter, C.W. (2001), Applied Hydrogeology. 4th Edition. Prentice-Hall, Upper Saddle Creek, NJ.
- Firuzabadi, D., and King, R. W. (2012). GPS precision as a function of session duration and reference frame using multi-point software. *GPS Solutions*, 16, 191–196.
- Fogg, G. E. (1986). Groundwater flow and sand body interconnectedness in a thick, multiple-aquifer system. *Water Resources Research*, 22(5), 679–694.
- Gabrysch, R. K. (1969). Land Surface Subsidence in the Houston-Galveston Region, Texas. Tokyo, Japan: *International Symposium on Land Subsidence*.
- Gabrysch, R. (1984). Ground-Water Withdrawals and Land-Surface Subsidence. Austin: Texas Department of Water Resources.
- Gabrysch, R. K., and Bonnet, C. W. (1975). Land Surface Subsidence in the Houston-Galveston Region, Texas. Austin, TX: *Texas Water Development Board Report 188*.
- Galloway, W. E. (2001). Cenozoic evolution of sediment accumulation in deltaic and shore-zone depositional systems, northern Gulf of Mexico Basin. *Marine and Petroleum Geology*, 18(10), 1031-1040.
- Galloway, D. L., and Burbey, T. J. (2011). Review: Regional land subsidence accompanying groundwater extraction. *Hydrogeology Journal*, 19, 1459 - 1486. doi:10.1007/s10040-011-0775-5
- Galloway, D., Jones, D., and Ingebritsen, S. (1999). Land Subsidence in the United States. Denver, CO: U.S. Geological Survey Circular 1182.
- George, P. G., R. E. Mace, and R. Petrossian. (2011). The Gulf Coast Aquifer. Aquifers of Texas, Texas Water Development Board Report 380.

- González, J. L., and Tornqvist, T. E. (2006). Coastal Louisiana in crisis: subsidence or sea level rise?. *EOS, Transactions American Geophysical Union*, 87(45), 493-498.
- Grant, A. and Rodriguez, L. (2006). 5 years after Allison, is city safer from flooding?. *Houston Chronicle*, June 4, 2006. Accessed 04 21 2015 from <http://www.chron.com/news/houston-texas/article/5-years-after-Allison-is-city-safer-from-1851965.php>
- Hamlin, H. S. (2006). Salt domes in the Gulf Coast aquifer, in Mace R. E., Davidson, S. C., Angle, E. S., and Mullican, W. F., III, eds., *Aquifers of the Gulf Coast of Texas: Texas Water Development Board Report 365*, p. 217–230.
- Holzer, T. L. (1984) Ground Failure Induced by Ground-water Withdrawal from Unconsolidated Sediments. *Reviews in Engineering Geology*, 6, 67-106.
- Holzer, T. L., and R. K. Gabrysch. (1987). Effect of water-level recoveries on fault creep, Houston, Texas. *Groundwater*, 25(4), 392-397.
- Holzer, T. L., and A. I. Johnson. (1985). Land subsidence caused by ground water withdrawal in urban areas. *GeoJournal*, 11(3), 245-255.
- Huffman, A.C., Kinney, S.A., Biewich, L.R., Mitchell, H.R., and Gunther, G.L. (2004). Salt Diapirs in the Gulf Coast. U.S. Geological Survey, DS 90-A, version 1.0- Miocene of Southern Louisiana. <http://pubs.usgs.gov/ds/2004/90/A/about.htm>
- Jiang, J. J. (2015). Rapid Land Subsidence Associated with Severe Drought: A Case Study in Houston Area, Texas. *Master's thesis*, University of Houston.
- Jorgensen, D. G. (1975). Analog-Model Studies of Groundwater Hydrology in the Houston District, Texas. Austin, TX: U.S. Geological Survey and the Texas Water Development Board.
- Jurkowski, G., Ni, J., and Brown, L. (1984). Modern uparching of the Gulf coastal plain. *Journal of Geophysical Research: Solid Earth* (1978–2012), 89(B7), 6247-6255.
- Kasmarek, M. (2015). Personal Communication, March 24, 2015. Telephone correspondence.
- Kasmarek, M. C., Johnson, M. R., and Ramage, J. K. (2014). Water-Level Altitudes 2013 and Water-Level Changes in the Chicot, Evangeline, and Jasper Aquifers and Compaction 1973–2013 in the Chicot and Evangeline Aquifers, Houston–Galveston Region, Texas. Denver, CO: *U.S. Geological Survey Scientific Investigations Map 3308*.
- Kasmarek, M. C., and Robinson, J.L. (2004). Hydrogeology and Simulation of Ground-Water Flow and Land-Surface Subsidence in the Northern Part of the Gulf Coast Aquifer System, Texas. No. 2004-5102. *U.S. Geological Survey*.

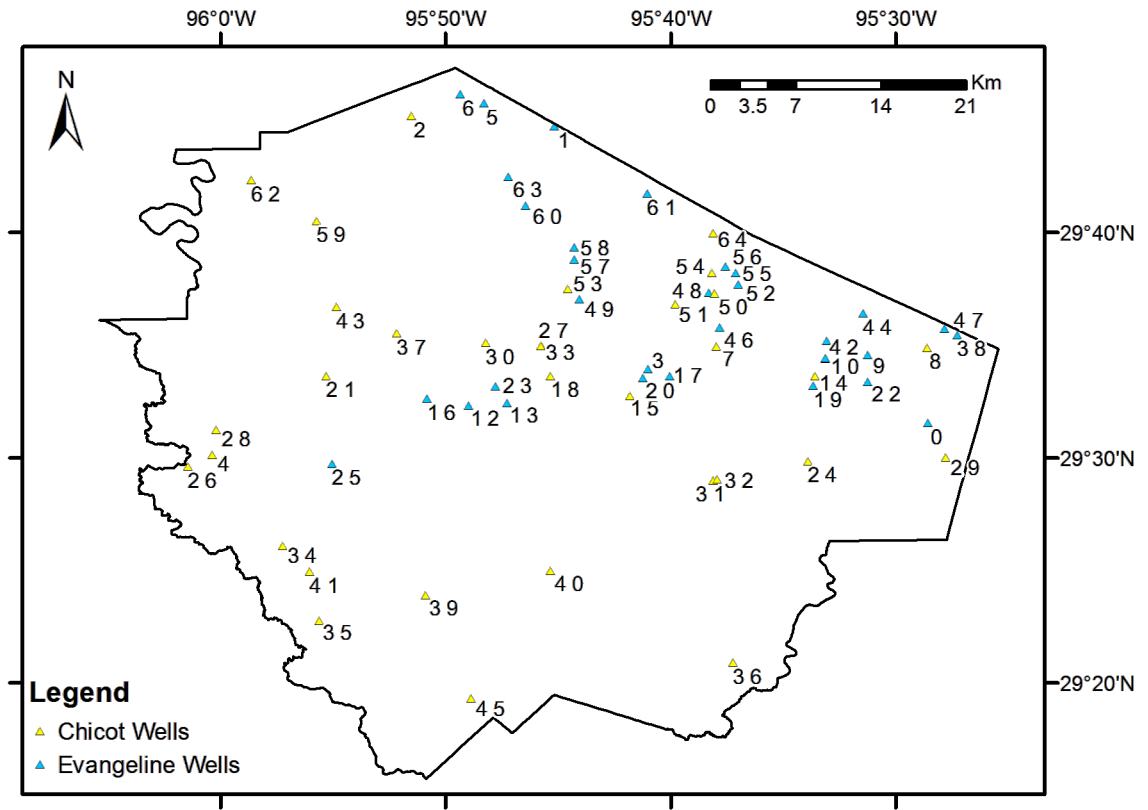
- Kasmarek, M. C., and Strom, E. W. (2002). Hydrogeology and Simulation of Ground-Water Flow and Land-Surface Subsidence in the Chicot and Evangeline Aquifers, Houston Area, Texas. Austin, TX: U.S. Geological Survey Water-Resources Investigations Report 02-4022.
- Kearns, T.J., Wang, G., Boa, Y., Jiang, J. and Lee, D. (2015). Current land subsidence and groundwater level changes in the Houston metropolitan area, Texas (2005-2012). *Journal of Surveying Engineering*. 05015002.
- Kedar, S., Hajj, G. A., Wilson, B. D., and Heflin, M. B. (2003). The effect of the second order GPS ionospheric correction on receiver positions. *Geophysical Research Letters*, 30(16), 1829. doi:10.1029/2003GL017639
- Khan, S. D., Huang, Z. and Karacay, A. (2014). Study of ground subsidence in northwest Harris County using GPS, LiDAR, and InSAR techniques. *Natural Hazards*. 73(3), 1143-1173.
- Knox, P. R., Young, S. C., Galloway, W. E., Jr., E. T., and Budge, T. (2006). A stratigraphic approach to Chicot and Evangeline aquifer boundaries, central Texas Gulf Coast. *Gulf Coast Association of Geological Societies Transactions*, 56, 371-393.
- Kouba, J. (2002). The GPS toolbox - ITRF transformations. *GPS Solutions*, 5(3), 88-90.
- Kreitler, C. W. (1977). Fault control of subsidence, Houston, Texas. *Groundwater*, 15.3, 203-214.
- Kreitler, C. W., Guevera, E., Granata, G., and McKalips, D. (1977). Hydrogeology of Gulf Coast aquifers, Houston-Galveston area, Texas. *Gulf Coast Association of Geological Societies Transactions*, 27, 72-89.
- Leake, S., and Prudic, D. (1991). Documentation of a Computer Program to Simulate Aquifer System Compaction using the Modular Finite-Difference Ground-Water Flow Model. Denver, CO: U.S. Geological Survey Techniques of Water-Resources Investigations Book 6 Chapter A2.
- Lyard, F., Lefevre, F., Letellier, T., and Francis, O. (2006). Modelling the global ocean tides: modern insights from FES2004. *Ocean Dynamics*, 56, 394-415.
- Maupin, M.A., Kenny, J.F., Hutson, S.S., Lovelace, J.K., Barber, N.L., and Linsey, K.S. (2014). Estimated use of water in the United States in 2010. *U.S. Geological Survey Circular 1405*, 56 p., <http://pubs.usgs.gov/circ/1405/>
- Matsuzaka, S. (2012, 05 24-25). Geodesy and Geodetics. Retrieved 12 09, 2014, from <http://ggim.un.org/docs/meetings/Hangzhou%20Forum/session%203/Geodesy%20and%20Geodetic%20reference%20system.pdf>
- Meyer, W.G. (1939). Stratigraphy and historical geology of Gulf Coast Plain in vicinity of Harris County, Texas. *American Association of Petroleum Geologists Bulletin*, 23(2), 145-211.

- Middleton, C. (2014). Personal communication, November 5, 2014. Email correspondence.
- Nolan, B.T., Healy, R.W., Taber, P.E., Perkins, K., Hitt, K.J., and Wolock, D.M. (2007). Factors influencing ground-water recharge in the eastern United States, *Journal of Hydrology*, 332, 187–205.
- Norman, C. (2004). Are surface faults activated by subsidence induced by groundwater pumpage? *Geological Society of America Abstracts with Programs*, 36(1), 27.
- Oden, T.D., and Delin, G.N. (2013). Groundwater recharge to the Gulf Coast aquifer system in Montgomery and Adjacent Counties, Texas. U.S. Geological Survey Fact Sheet 2013–3043, 6 p., <http://pubs.usgs.gov/fs/2013/3043/>.
- Ortega, J. A. (2013). Groundwater Withdrawal and Aquifer Compaction: A Case Study in Addicks, Texas. *Master's thesis*, University of Houston.
- Paine, J. G. (1993). Subsidence of the Texas coast: inferences from historical and late Pleistocene sea levels. *Tectonophysics*. 222.3, 445-458.
- Pearson, C., McCaffrey, R., Elliott, J. L., and Snay, R. (2010). HTDP 3.0: Software for coping with the coordinate changes associated with crustal motion. *Journal of Surveying Engineering*, 136(2), 80-90.
- Pearson, C., and Snay, R. (2013). Introducing HTDP 3.1 to transform coordinates across time and spatial reference frames. *GPS solutions*, 17(1), 1-15.
- Pratt, W. E., and Johnson, D.W. (1926). Local subsidence of the Goose Creek oil field. *The Journal of Geology*, 577-590.
- Ray, J., Rebischung, P., and Schmid, R. (2011). Dependence of IGS products on the ITRF datum. *Proceedings of IAG Commission 1 Symposium on Reference Frames for Applications in Geosciences*. Marne-la-Vallée, France.
- Remondi, B. W. (1985). Global positioning system carrier phase: Description and use. *Bulletin of Geodesy*, 59, 361-377.
- Rizos, C., Janssen, V., Roberts, C., and Grinter, T. (2012). Precise Point Positioning: Is the era of differential GNSS positioning drawing to an end? In: *Proceedings of FIG Working Week 2012*, 6-10 May 2012, Rome, Italy.
- Shah, S. D., and Lanning-Rush, J. (2005). Principal Faults in the Houston Metropolitan Area. Denver, CO: *U.S. Geological Survey Scientific Investigations Map 2874*. Retrieved from <http://pubs.usgs.gov/sim/2005/2874/>
- Shah, S.D., Houston, N.A., and Braun, C.L. (2007). Hydrogeologic Characterization of the Brazos River Alluvium Aquifer, Bosque County to Fort Bend County, Texas. *U.S. Geological Survey Scientific Investigations Map 2989*, Sheets 1 to 5.

- Snay, R. A. (1999). Using the HTDP software to transform spatial coordinates across time and between reference frames. *Surveying and Land Information Systems*, 59(1), 15-25.
- Soler, T., and Snay, R. A. (2004). Transforming positions and velocities between the International Terrestrial Reference Frame of 2000 and North American Datum of 1983. *Journal of Surveying Engineering*, 130(2), 49-55.
- Theis, C.V. (1940). The source for water derived from wells. *Civil Engineering*, 10 (5), 277-280.
- Trimble. (2010). NetR9 (version 4.15) GNSS Reference Receiver User Guide. Dayton, Ohio: *Trimble Navigation*.
- U.S. Census Bureau. (2010). 2010 Census TIGER/Line® Shapefiles. Retrieved 08 20, 2013, from <http://www.census.gov/cgi-bin/geo/shapefiles2010/main>
- U.S. Drought Monitor. (2014). 2011 Drought Maps. Retrieved 04 01 2014, from <http://droughtmonitor.unl.edu>
- U.S. Environmental Protection Agency. *The Determination of Mitigation Under the Clean Water Act Section 404(b)(1) Guidelines* (February 6, 1990), Retrieved 01 21 2015 from <http://water.epa.gov/lawsregs/guidance/wetlands/mitigate.cfm>
- U.S. Geological Survey. (2012). Geologic Maps of the US States. Retrieved 08 20, 2013, from <http://mrdata.usgs.gov/geology/state/>
- U.S. Geological Survey. (2013). USGS Groundwater Watch. Retrieved 08 01, 2014, from <http://groundwaterwatch.usgs.gov>
- Van Siclen, D. C. (1968). *The Houston Fault Problem*. Dallas, TX: American Institute of Professional Geologists, Texas Section.
- Verbeek, E. R., and Clanton, U. S. (1981). Historically active faults in the Houston metropolitan area, Texas. *Houston Area Environmental Geology: Surface Faulting, Ground Subsidence, Hazard Liability*, p 28-68.
- Wang, G. Q. (2013). Millimeter-accuracy GPS landslide monitoring using Precise Point Positioning with Single Receiver Phase Ambiguity (PPP-SRPA) resolution: A case study in Puerto Rico. *Journal of Geodetic Science*, 3(1), 22-31.
- Wang, G., Yu, J., Ortega, J. Saenz, G., Burrough, T., and Neill, R. (2013). A stable reference frame for ground deformation study in the Houston metropolitan area, TX. *Journal of Geodetic Science*. 3(3). DOI: 10.2478/jogs-2013-0021
- Wang, G. and Soler, T. (2013). Using OPUS for measuring vertical displacements in Houston, Texas. *Journal of Surveying Engineering*. 139(3), 126-134.

- Wang, G. and Soler, T. (2014). Measuring land subsidence using GPS: Ellipsoid height versus orthometric height. *Journal of Surveying Engineering*, 05014004.
- Wesselman, J. B. (1972). Ground-water resources of Fort Bend County, Texas. *Texas Water Development Board Report 155*.
- Williams, T.A., and Williamson, A.K. (1989). Estimating water-table altitudes for regional ground-water flow modeling, U.S. Gulf Coast: National Water Well Association, *Ground Water*, v. 27, no. 3, p. 333-340.
- Wilson, A. M., and Gorelick, S. (1996). The effects of pulsed pumping on land subsidence in the Santa Clara Valley, California. *Journal of Hydrology*, 174(3), 375-396.
- Winker, Charles D. (1982). Cenozoic shelf margins, Northwestern Gulf of Mexico. *Gulf Coast Association of Geological Societies Transactions*, 32, 427-448.
- Winslow, A.G., and W.W. Doyle. (1954). Land-surface subsidence and its relation to the withdrawal of ground water in the Houston-Galveston region, Texas. *Economic Geology*, 49(4), 413-422.
- Yerkes, R.F., Castle, R.O., 1969. Surface deformation associated with oil and gas field operation in the United States. In: Tison, L.J. (Ed.), *Land Subsidence 1*, Vol. 88. 1st International Association of Scientific Hydrology Publication, Wallingford, pp. 55–64.
- Young, S. C., J. Pinkard, R. L. Basset, and Chowdhury, A. (2014) Hydrochemical evaluation of the Texas Gulf Coast Aquifer System and implication for developing groundwater availability model: Report prepared by *INTERA, Inc. for the Texas Water Development Board*, Austin.
- Yu, J., Wang, G., Kearns, T. and Yang, L. (2014). Is there deep-seated subsidence in the Houston- Galveston area? *International Journal of Geophysics*, 2014.
- Zilkoski, D. B., Hall, L. W., Mitchell, G. J., Kammula, V., Singh, A., Chrismer, W. M., and Neighbors, R. J. (2001). The Harris-Galveston Coastal Subsidence District/ National Geodetic Survey Automated GPS Subsidence Monitoring Project. Galveston: *U.S. Geological Survey Subsidence Interest Group Conference*.

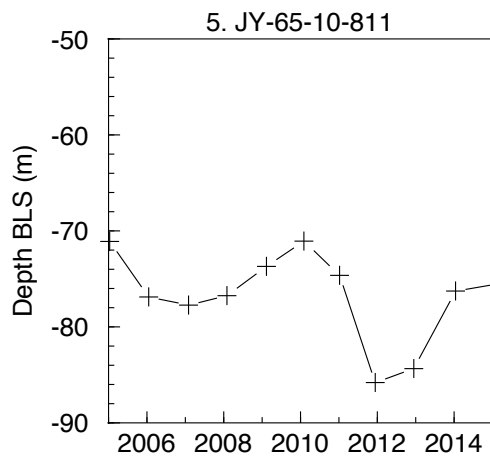
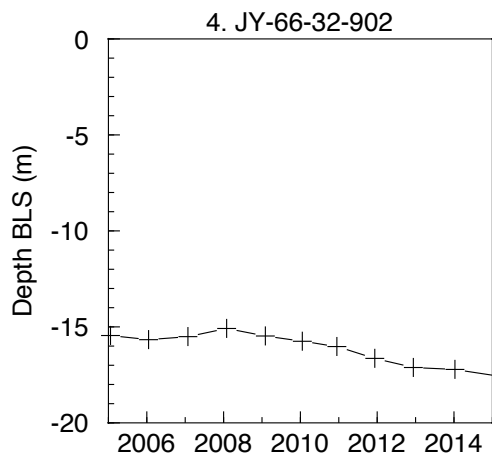
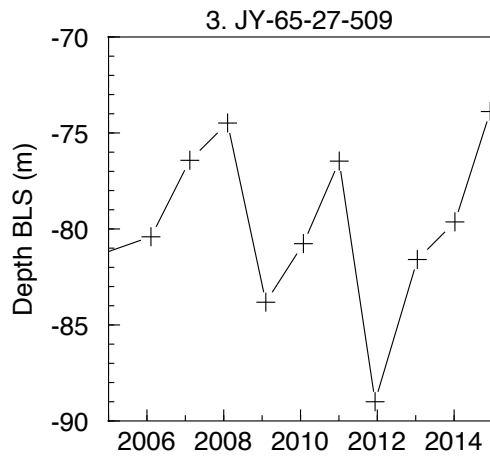
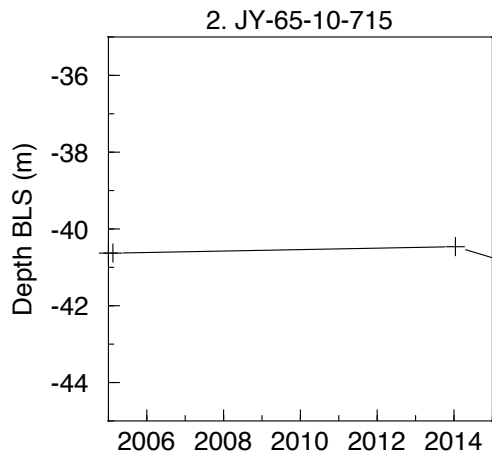
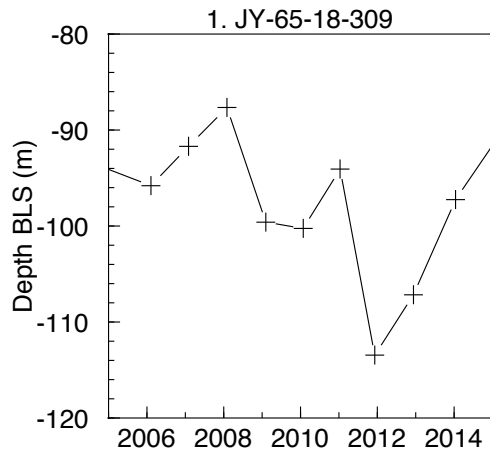
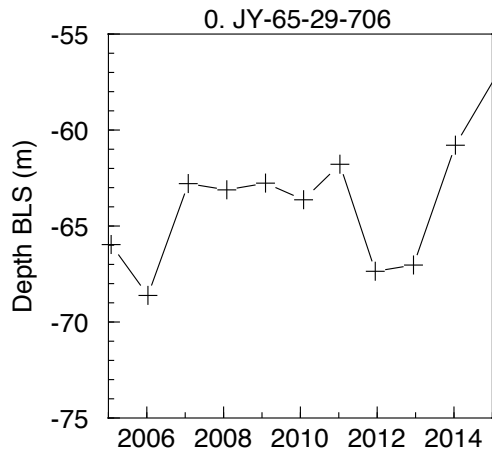
9 Appendix I: Groundwater Levels

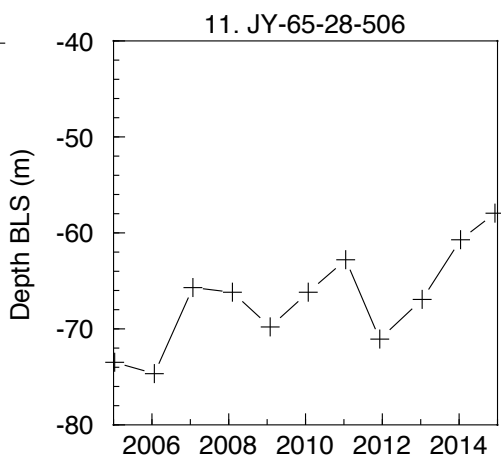
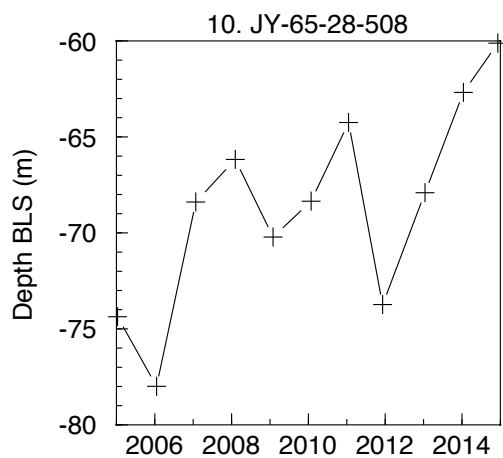
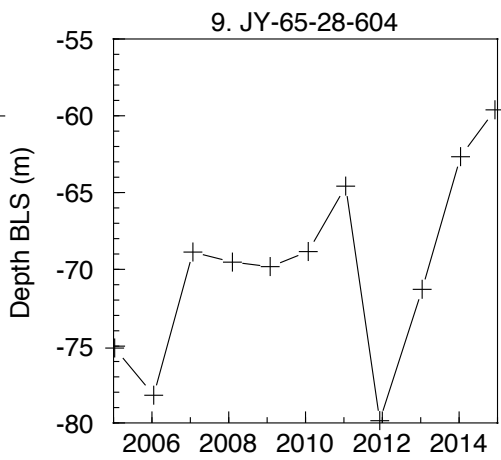
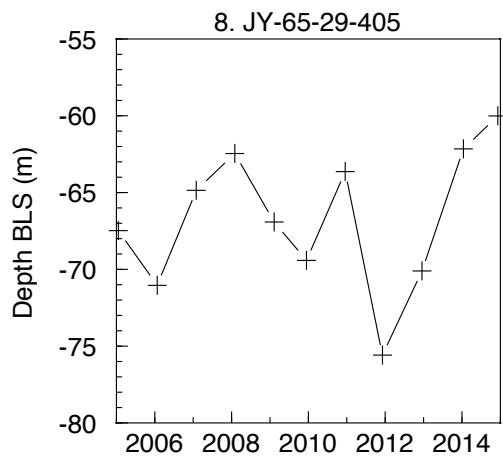
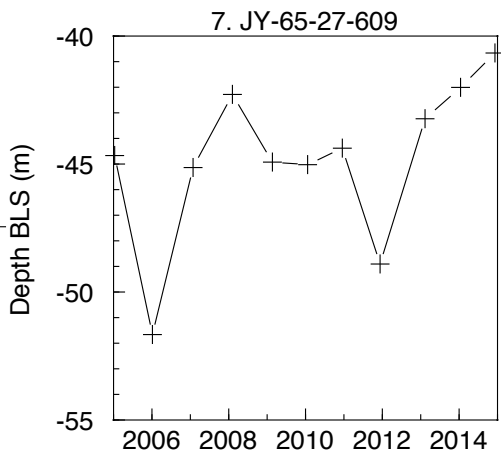
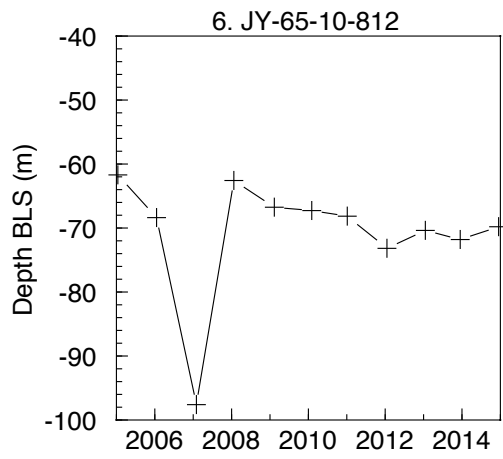


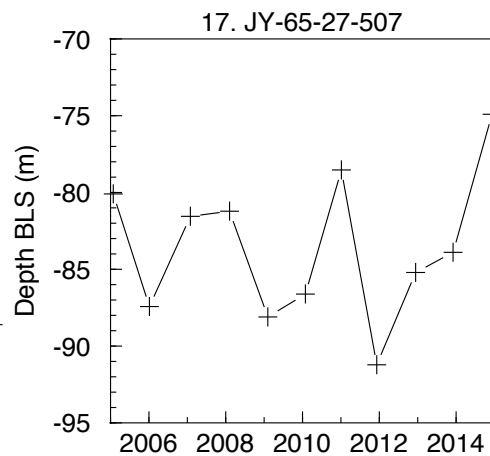
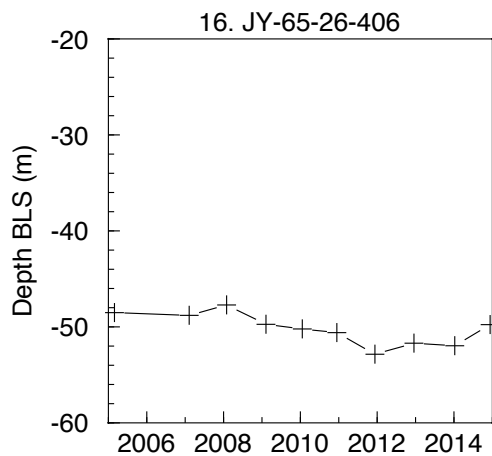
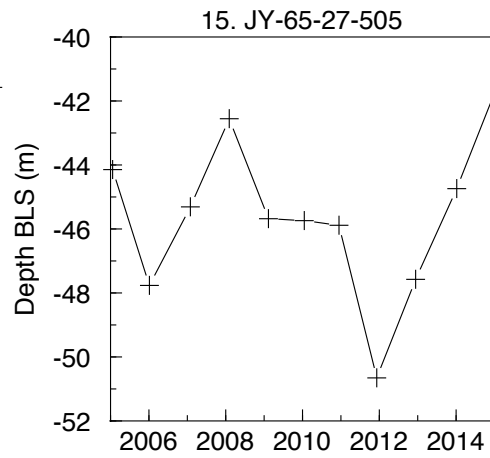
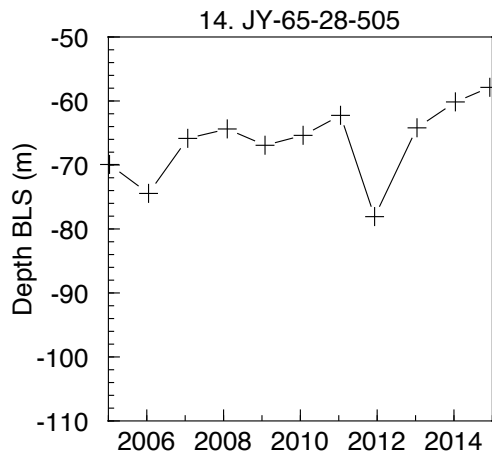
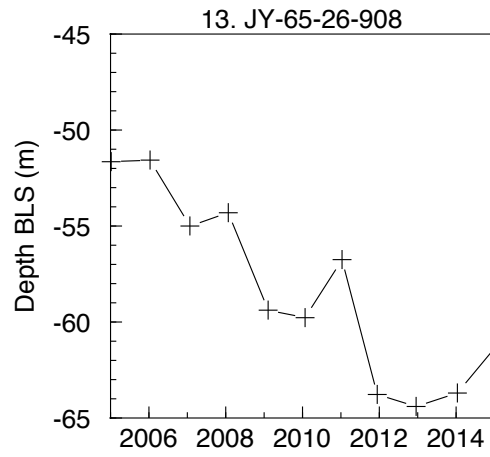
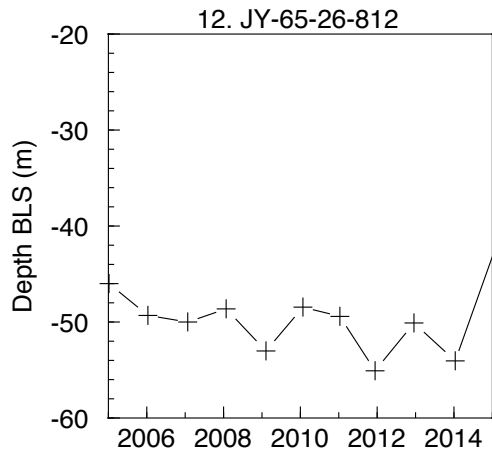
Map ID & Graph #	Site Name	Well Depth (meters)	Local Aquifer	GW Level Measurement (m BLS)					GW Level Change (m)	
				2005	2011	2012	2014	2011-2012	2005-2014	
0	JY-65-29-706	402.34	Evangeline	65.97	61.78	67.36	60.80	-5.58	5.18	
1	JY-65-18-309	359.66	Evangeline	95.81	94.07	113.46	97.25	-19.39	-1.44	
2	JY-65-10-715	140.21	Chicot	40.63	-	-	40.47	-	0.16	
3	JY-65-27-509	543.76	Evangeline	80.41	76.47	89.00	79.64	-12.53	0.77	
4	JY-66-32-902	92.66	Chicot	15.45	16.03	16.65	17.22	-0.62	-1.76	
5	JY-65-10-811	311.51	Evangeline	71.11	74.64	85.80	76.28	-11.16	-5.17	
6	JY-65-10-812	202.39	Evangeline	61.72	68.17	73.19	71.81	-5.02	-10.09	
7	JY-65-27-609	141.12	Chicot, Lower	44.67	44.38	48.91	42.01	-4.53	2.66	
8	JY-65-29-405	172.21	Chicot, Lower	67.49	63.64	75.59	62.16	-11.95	5.32	
9	JY-65-28-604	398.68	Evangeline	75.13	64.59	79.86	62.67	-15.27	12.46	
10	JY-65-28-508	402.34	Evangeline	74.37	64.25	73.74	62.69	-9.49	11.68	
11	JY-65-28-506	365.76	Evangeline	73.49	62.80	71.08	60.73	-8.28	12.76	
12	JY-65-26-812	400.20	Evangeline	46.00	49.42	55.09	54.05	-5.67	-8.05	
13	JY-65-26-908	481.58	Evangeline	51.65	56.76	63.78	63.71	-7.02	-12.05	
14	JY-65-28-505	327.36	Chicot And Evangeline	69.93	62.27	78.09	60.17	-15.82	9.76	
15	JY-65-27-505	256.03	Chicot And Evangeline	44.15	45.89	50.66	44.74	-4.77	-0.59	
16	JY-65-26-406	359.05	Evangeline	48.52	50.61	52.85	51.98	-2.24	-3.46	
17	JY-65-27-507	598.63	Evangeline	80.10	78.54	91.22	83.91	-12.68	-3.81	
18	JY-65-26-613	152.40	Chicot, Lower	24.39	23.86	25.15	23.41	-1.30	0.98	
19	JY-65-28-510	324.61	Evangeline	64.80	61.79	70.10	62.45	-8.31	2.35	
20	JY-65-27-506	591.92	Evangeline	72.21	77.67	90.89	85.76	-13.22	-13.55	
21	JY-65-25-506	234.70	Chicot And Evangeline	18.01	20.22	21.28	19.21	-1.06	-1.19	
22	JY-65-28-607	335.28	Evangeline	73.60	63.94	78.33	61.96	-14.39	11.64	
23	JY-65-26-520	488.90	Evangeline	51.52	57.38	63.10	62.97	-5.72	-11.45	
24	JY-65-36-201	114.30	Chicot, Lower	24.37	26.49	28.64	26.68	-2.15	-2.31	
25	JY-65-33-210	297.18	Evangeline	27.74	29.52	31.45	31.09	-1.93	-3.35	
26	JY-66-40-307	98.76	Chicot	14.45	15.16	15.77	16.19	-0.61	-1.74	
27	JY-65-26-603	157.89	Chicot, Lower	33.67	31.14	33.62	30.18	-2.48	3.49	

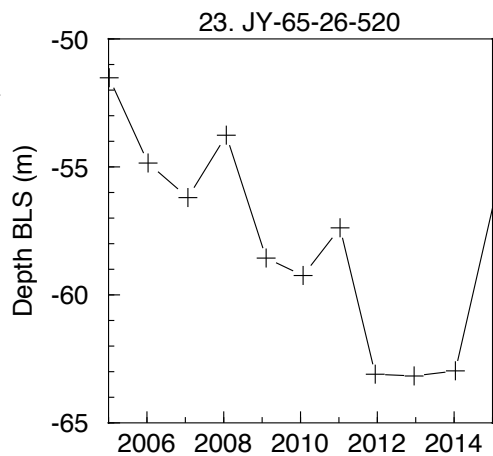
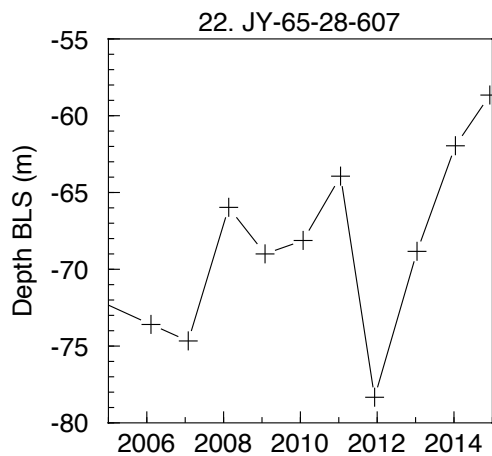
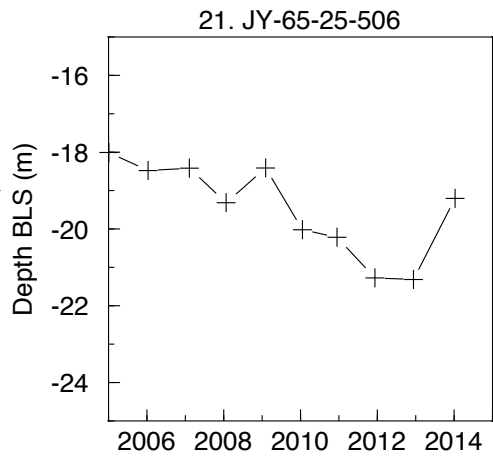
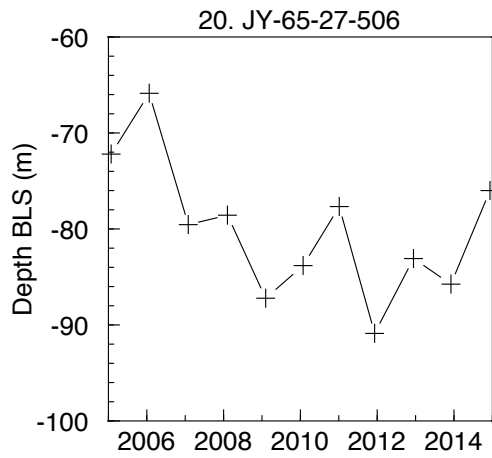
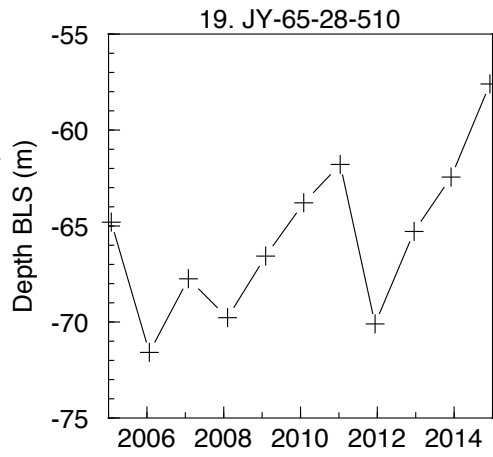
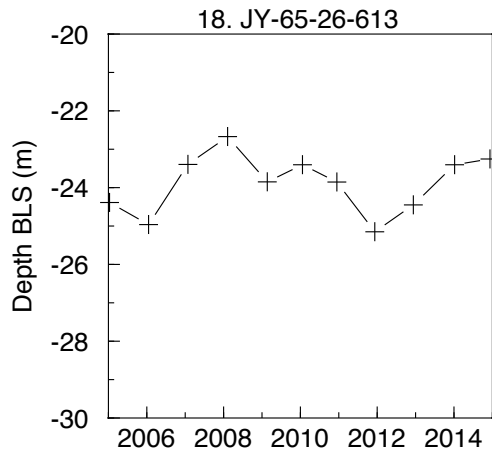
Map ID & Graph #	Site Name	Well Depth (meters)	Local Aquifer	GW Level Measurement (m BLS)					GW Level Change (m)	
				2005	2011	2012	2014	2011-2012	2005-2014	
28	JY-66-32-905	82.30	Chicot	14.81	15.30	16.15	17.75	-0.85	-2.93	
29	JY-65-29-709	159.72	Chicot, Lower	36.69	36.92	40.36	38.55	-3.44	-1.87	
30	JY-65-26-202	92.96	Chicot	20.27	21.95	22.94	22.14	-0.98	-1.87	
31	JY-65-35-304	259.99	Chicot	58.22	40.84	43.28	40.23	-2.44	17.98	
32	JY-65-35-302	213.97	Chicot	35.36	35.97	38.40	36.27	-2.44	-0.91	
33	JY-65-26-605	131.37	Chicot	29.37	29.64	32.04	29.38	-2.40	-0.01	
34	JY-65-33-502	179.83	Chicot	14.15	14.77	16.13	16.21	-1.36	-2.06	
35	JY-65-33-803	110.64	Chicot, Lower	15.79	17.14	18.46	18.17	-1.32	-2.37	
36	JY-65-44-101	266.40	Chicot And Evangeline	27.50	27.56	29.71	29.73	-2.15	-2.23	
37	JY-65-26-105	128.63	Chicot	19.20	20.95	21.92	21.26	-0.98	-2.06	
38	JY-65-29-209	320.04	Evangeline	68.82	62.39	68.11	61.37	-5.72	7.46	
39	JY-65-34-718	157.89	Chicot	0.00	20.74	21.95	21.41	-1.21	-21.41	
40	JY-65-34-901	193.85	Chicot	12.48	13.27	14.13	13.99	-0.85	-1.51	
41	JY-65-33-801	171.91	Chicot	15.34	15.34	16.21	16.59	-0.87	-1.25	
42	JY-65-28-214	338.33	Evangeline	78.88	64.40	77.11	61.83	-12.71	17.05	
43	JY-65-25-301	133.50	Chicot	15.73	16.63	17.56	17.42	-0.93	-1.69	
44	JY-65-28-312	382.83	Evangeline	74.55	67.12	82.78	66.19	-15.66	8.36	
45	JY-65-42-501	265.48	Chicot And Evangeline	17.43	17.27	18.33	17.87	-1.06	-0.44	
46	JY-65-27-326	525.48	Evangeline	86.88	82.59	92.05	81.41	-9.46	5.47	
47	JY-65-29-109	371.86	Evangeline	71.02	65.23	69.19	65.84	-3.96	5.18	
48	JY-65-27-302	477.01	Evangeline	70.57	59.75	66.33	64.11	-6.58	6.47	
49	JY-65-27-106	429.77	Evangeline	46.66	48.92	53.93	48.67	-5.01	-2.01	
50	JY-65-27-324	312.42	Chicot And Evangeline	61.32	60.55	0.00	58.14	60.55	3.18	
51	JY-65-27-322	124.05	Chicot, Lower	36.97	38.19	42.32	36.80	-4.13	0.17	
52	JY-65-20-711	507.49	Evangeline	94.61	96.01	108.48	92.38	-12.47	2.23	
53	JY-65-27-107	95.71	Chicot, Lower	26.69	29.11	30.83	28.65	-1.72	-1.95	
54	JY-65-19-909	167.34	Chicot, Lower	65.08	58.77	65.51	62.29	-6.75	2.79	
55	JY-65-20-712	457.20	Evangeline	100.44	96.05	118.26	99.89	-22.21	0.55	

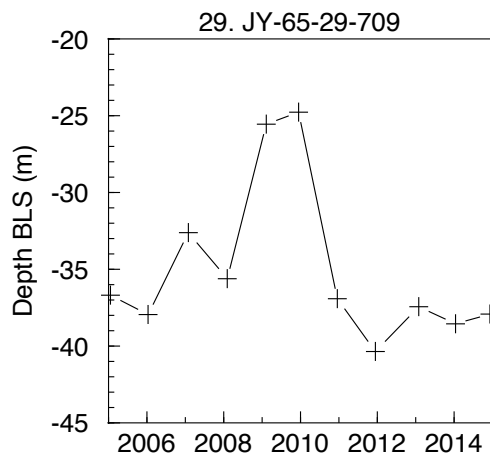
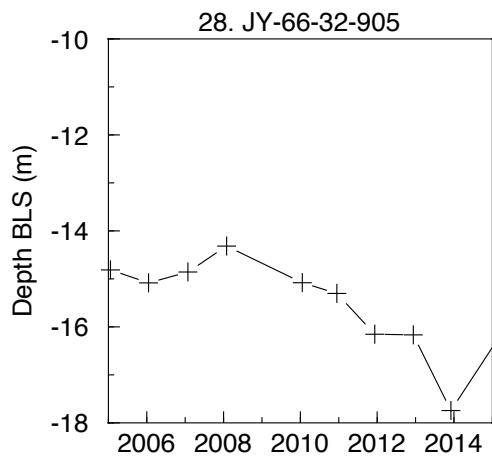
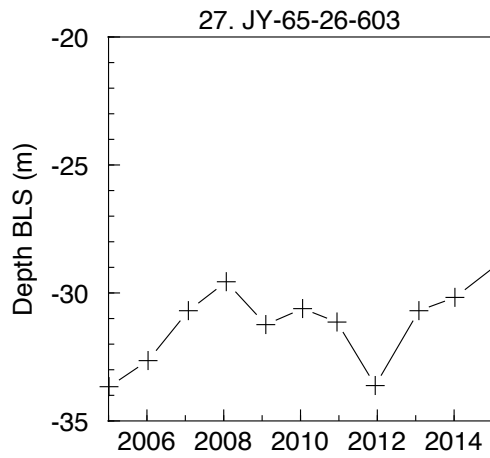
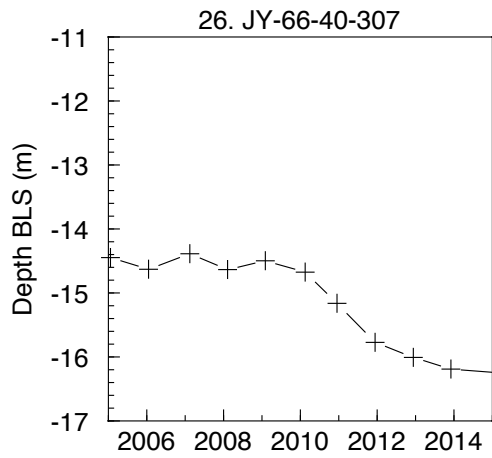
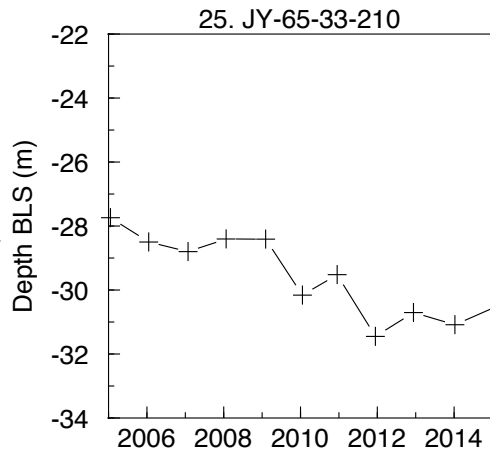
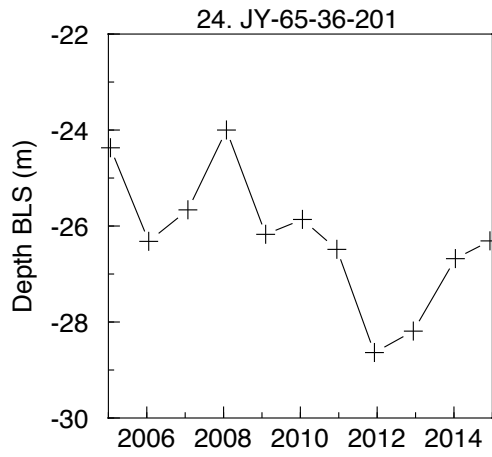
Map ID & Graph #	Site Name	Well Depth (meters)	Local Aquifer	GW Level Measurement (m BLS)					GW Level Change (m)	
				2005	2011	2012	2014	2011-2012	2005-2014	
56	JY-65-19-904	541.02	Evangeline	74.68	66.46	72.05	63.96	-5.60	10.71	
57	JY-65-19-707	265.18	Evangeline	51.63	49.93	55.85	48.86	-5.93	2.77	
58	JY-65-19-708	417.58	Evangeline	71.23	70.79	83.23	71.39	-12.44	-0.16	
59	JY-65-17-505	137.16	Chicot, Lower	16.37	19.31	21.00	21.60	-1.69	-5.22	
60	JY-65-18-611	365.76	Evangeline	69.16	78.18	92.46	77.14	-14.28	-7.98	
61	JY-65-19-509	267.61	Evangeline	63.91	57.93	63.92	54.06	-5.98	9.85	
62	JY-65-17-401	115.21	Chicot	13.13	14.75	14.96	15.10	-0.21	-1.98	
63	JY-65-18-609	332.23	Evangeline	70.76	86.68	104.03	86.62	-17.35	-15.86	
64	JY-65-19-907	274.93	Chicot	71.23	62.63	69.00	61.12	-6.37	10.11	

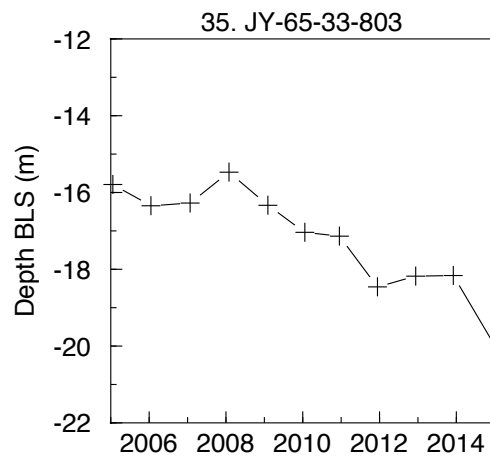
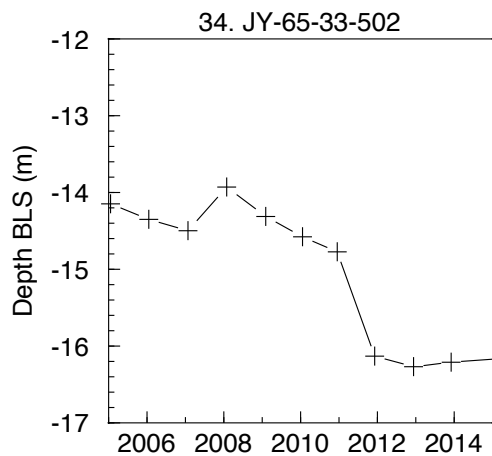
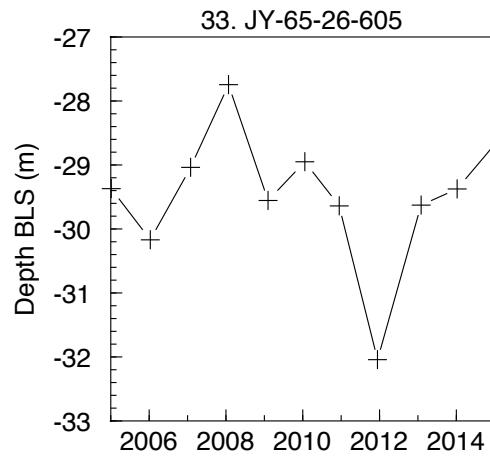
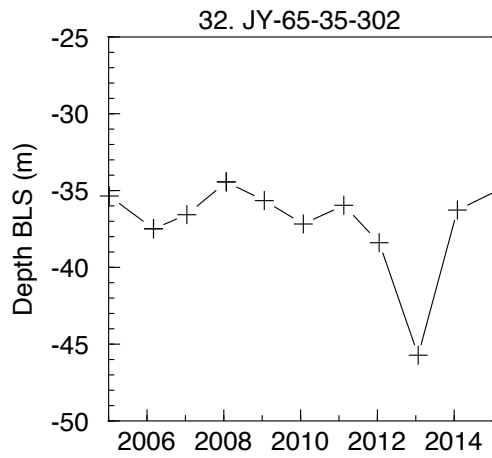
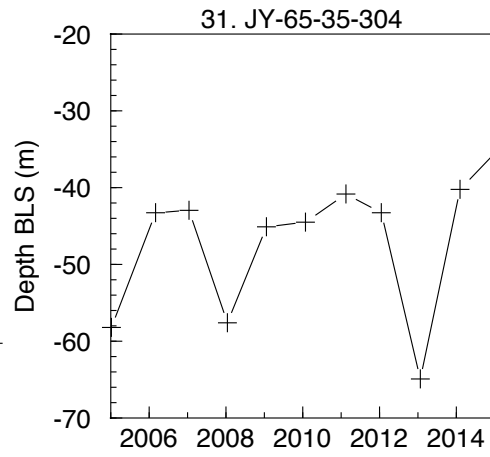
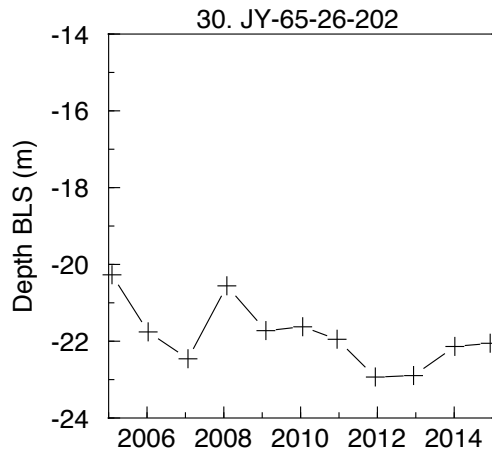


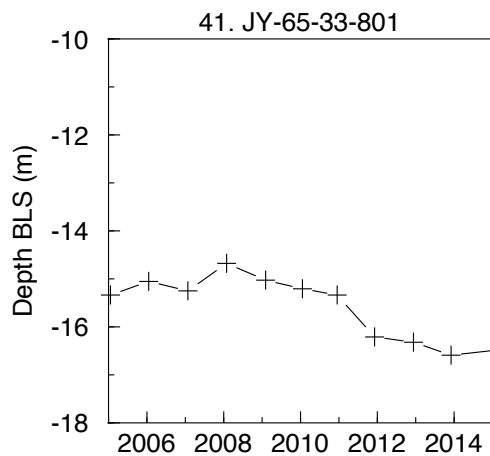
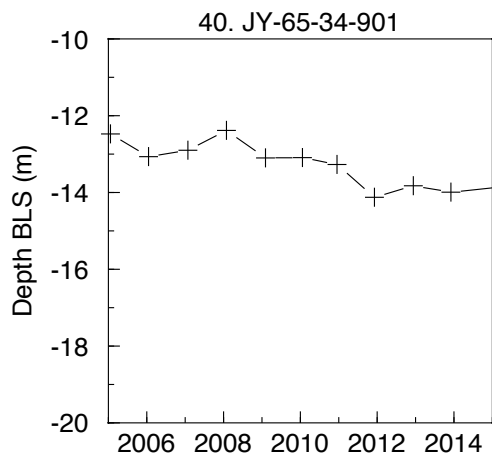
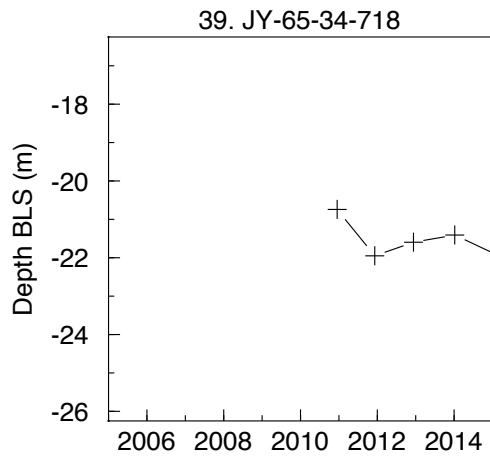
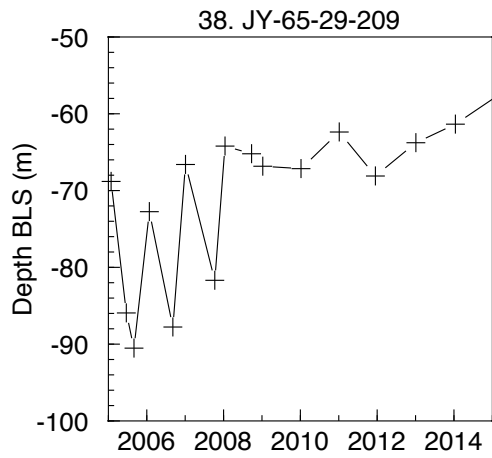
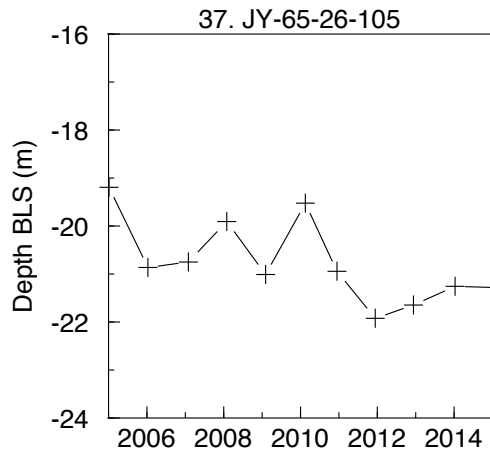
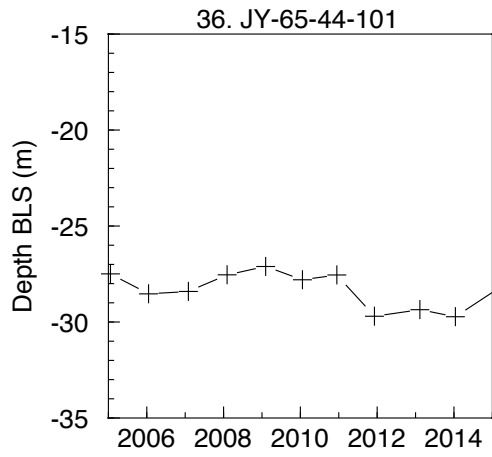


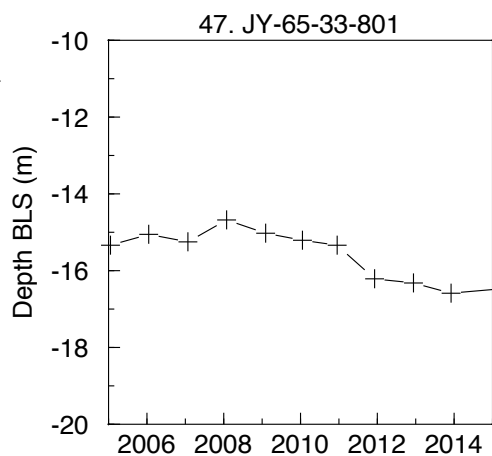
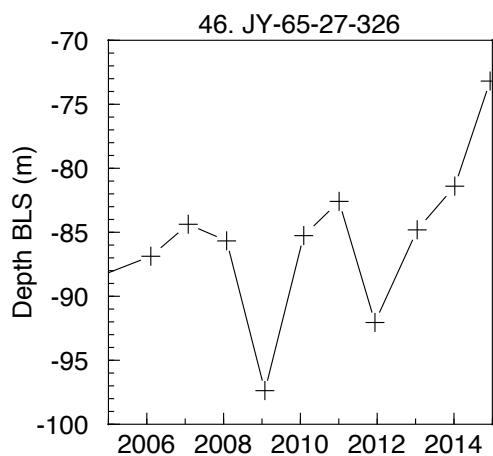
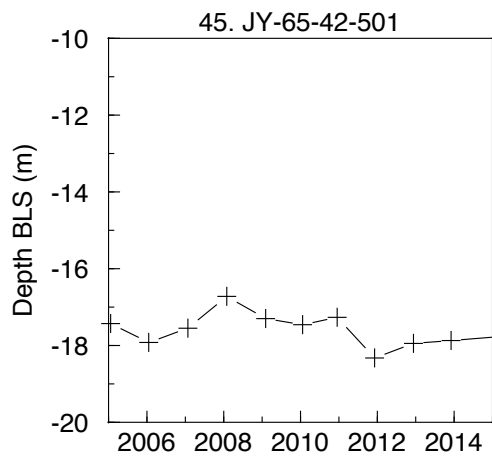
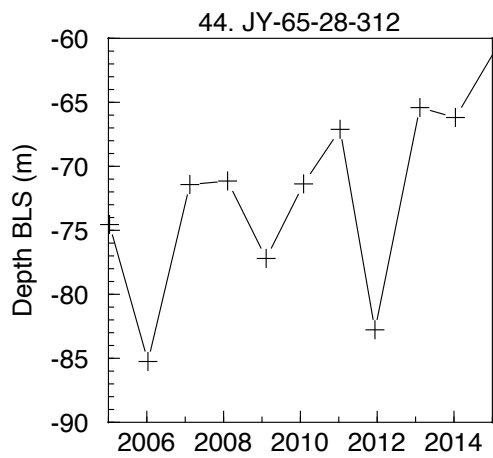
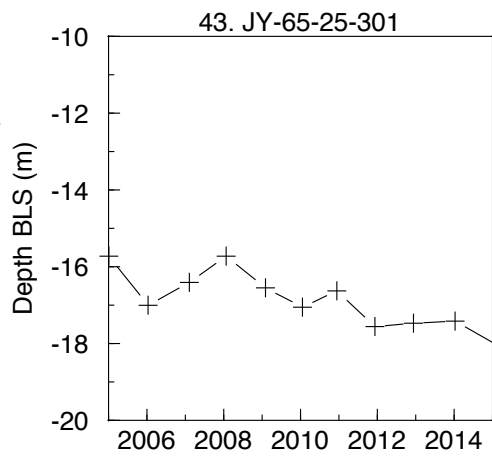
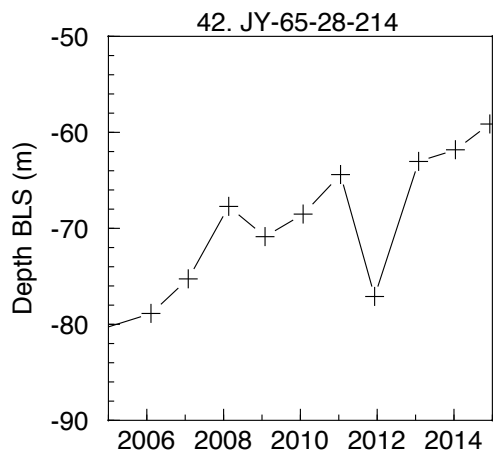


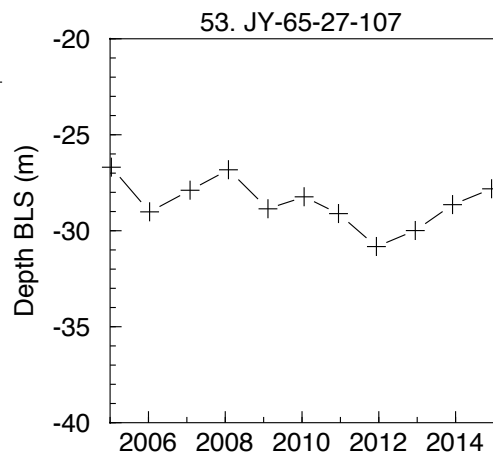
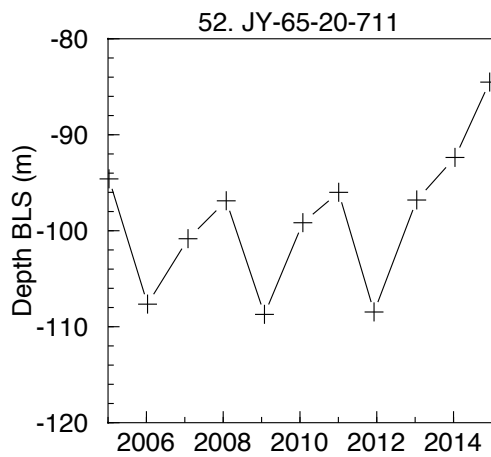
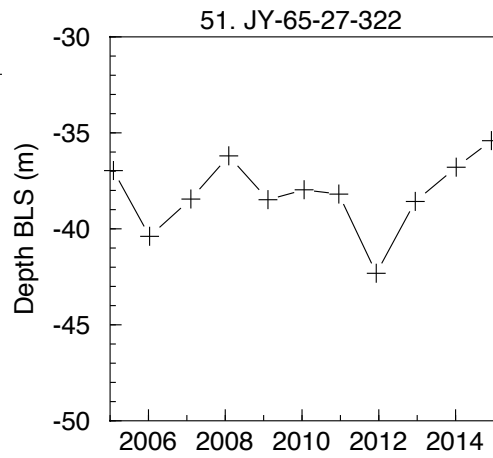
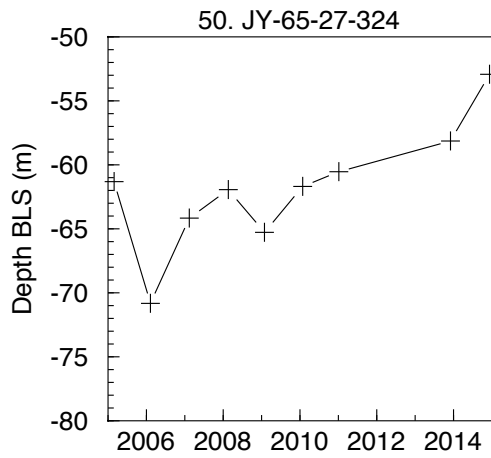
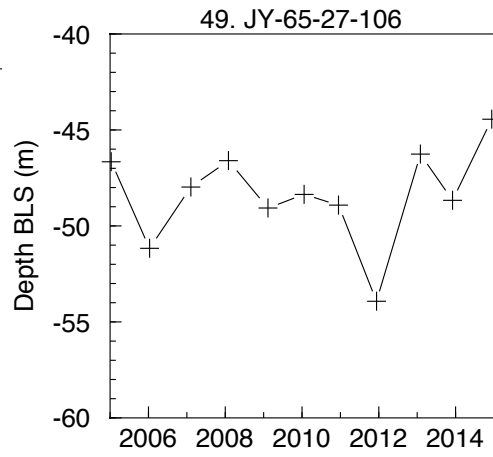
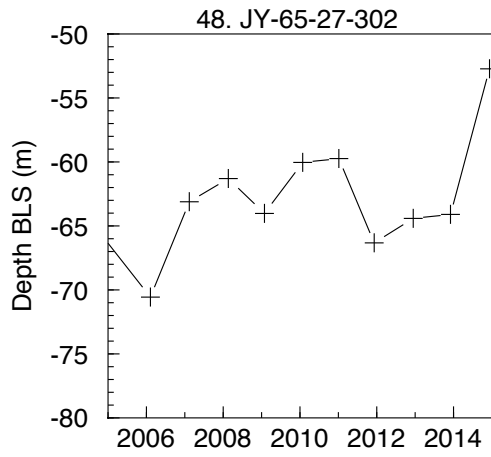


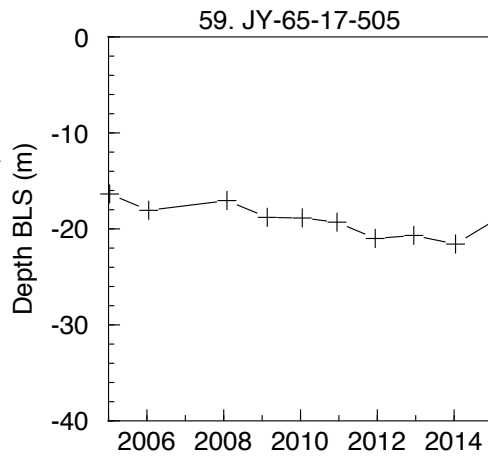
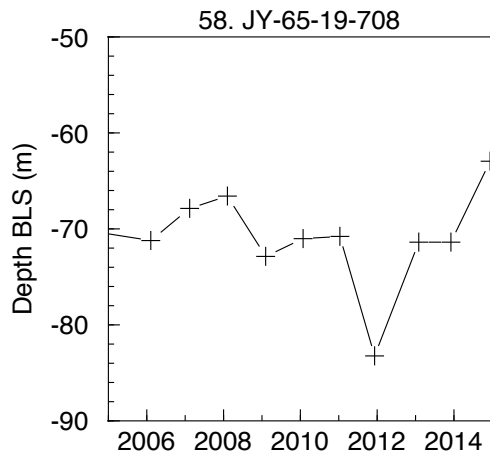
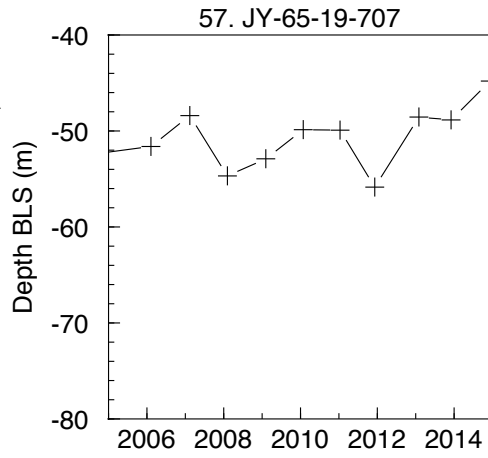
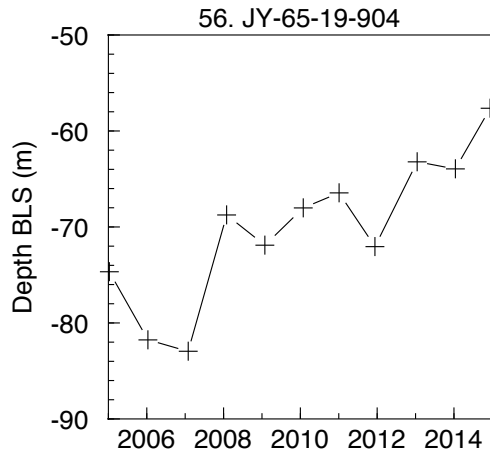
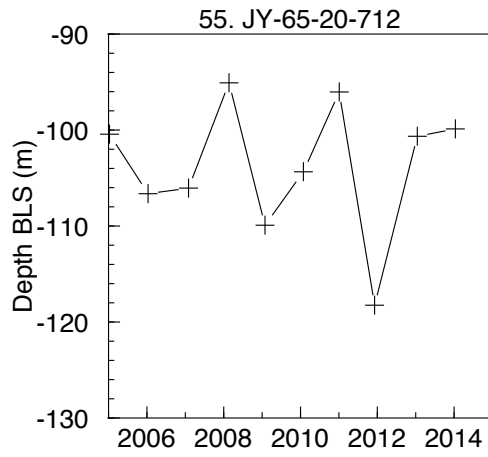
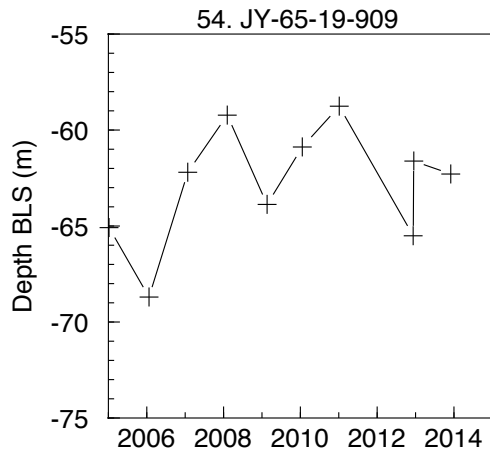


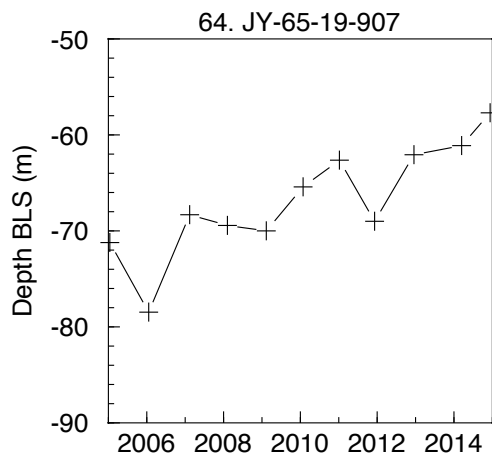
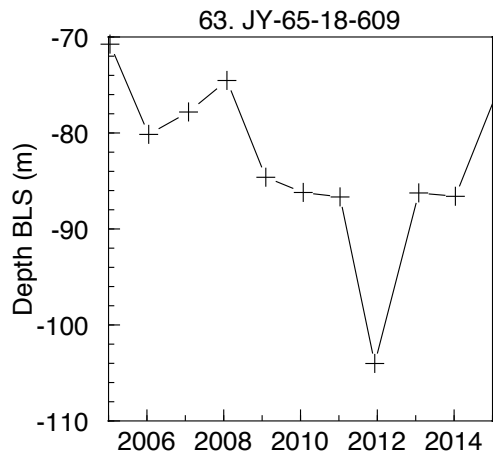
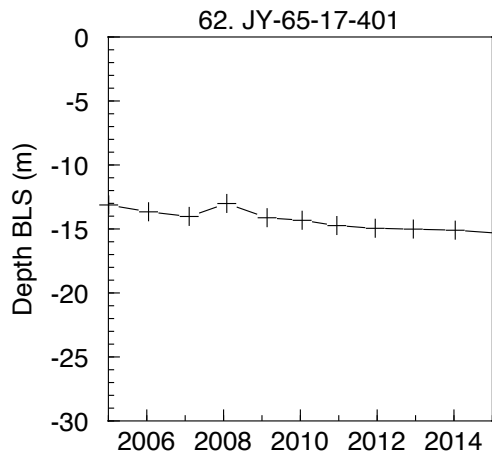
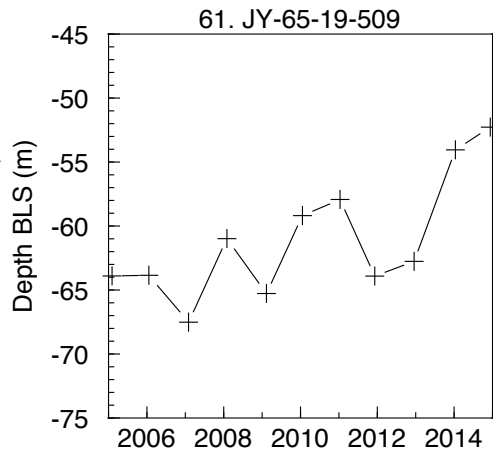
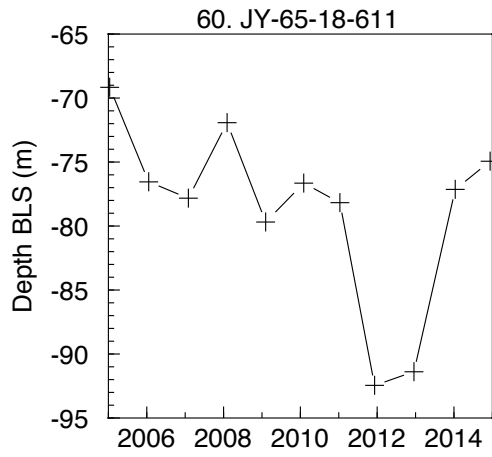




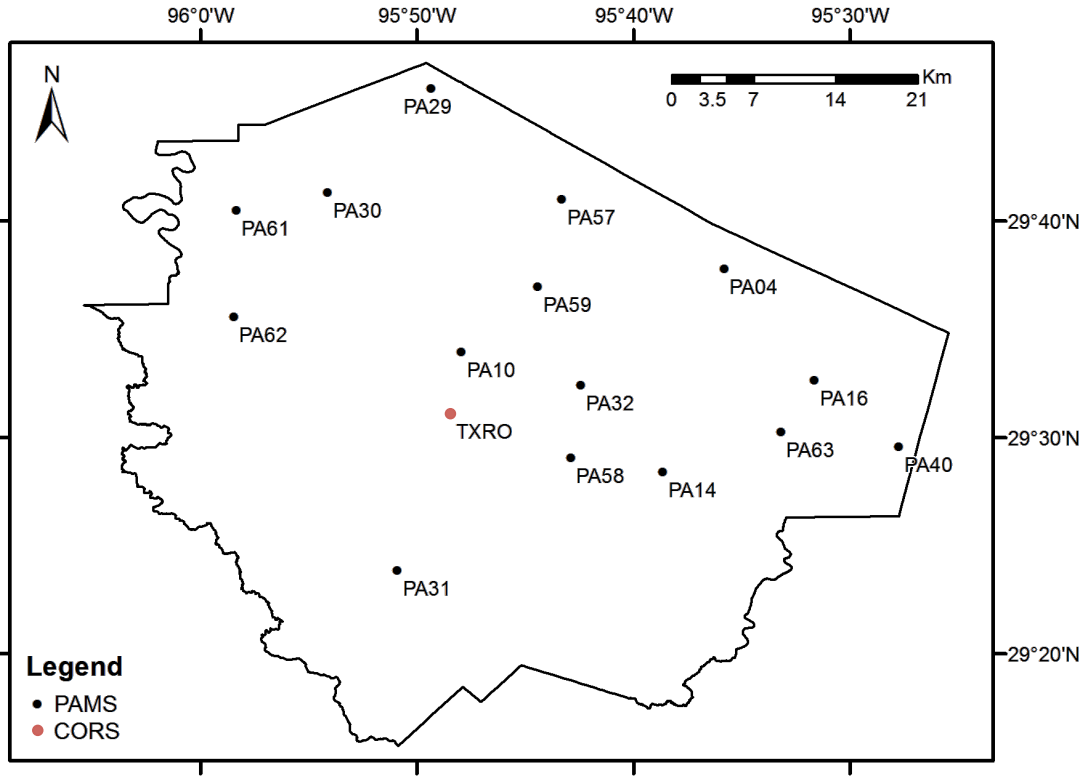




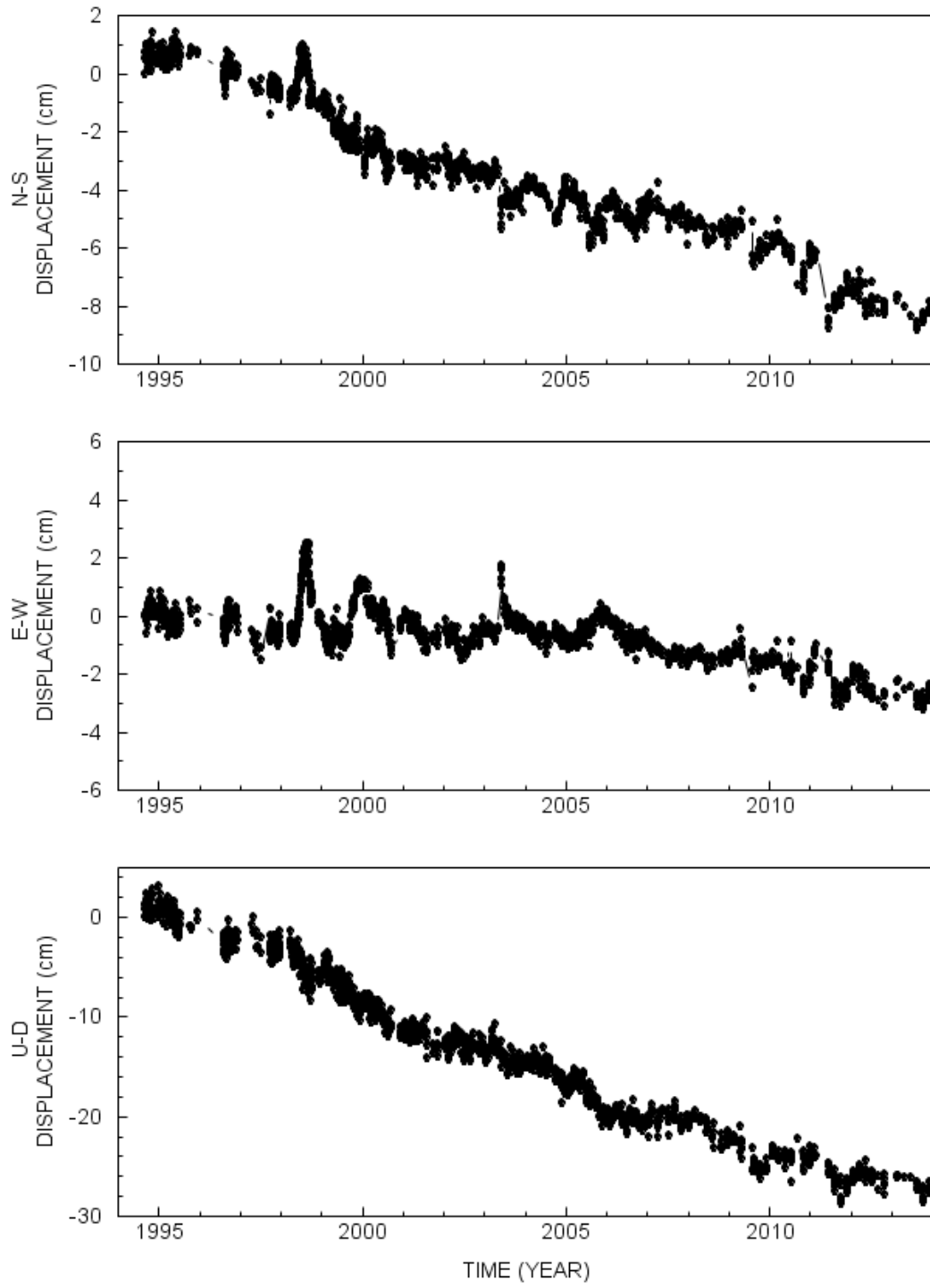




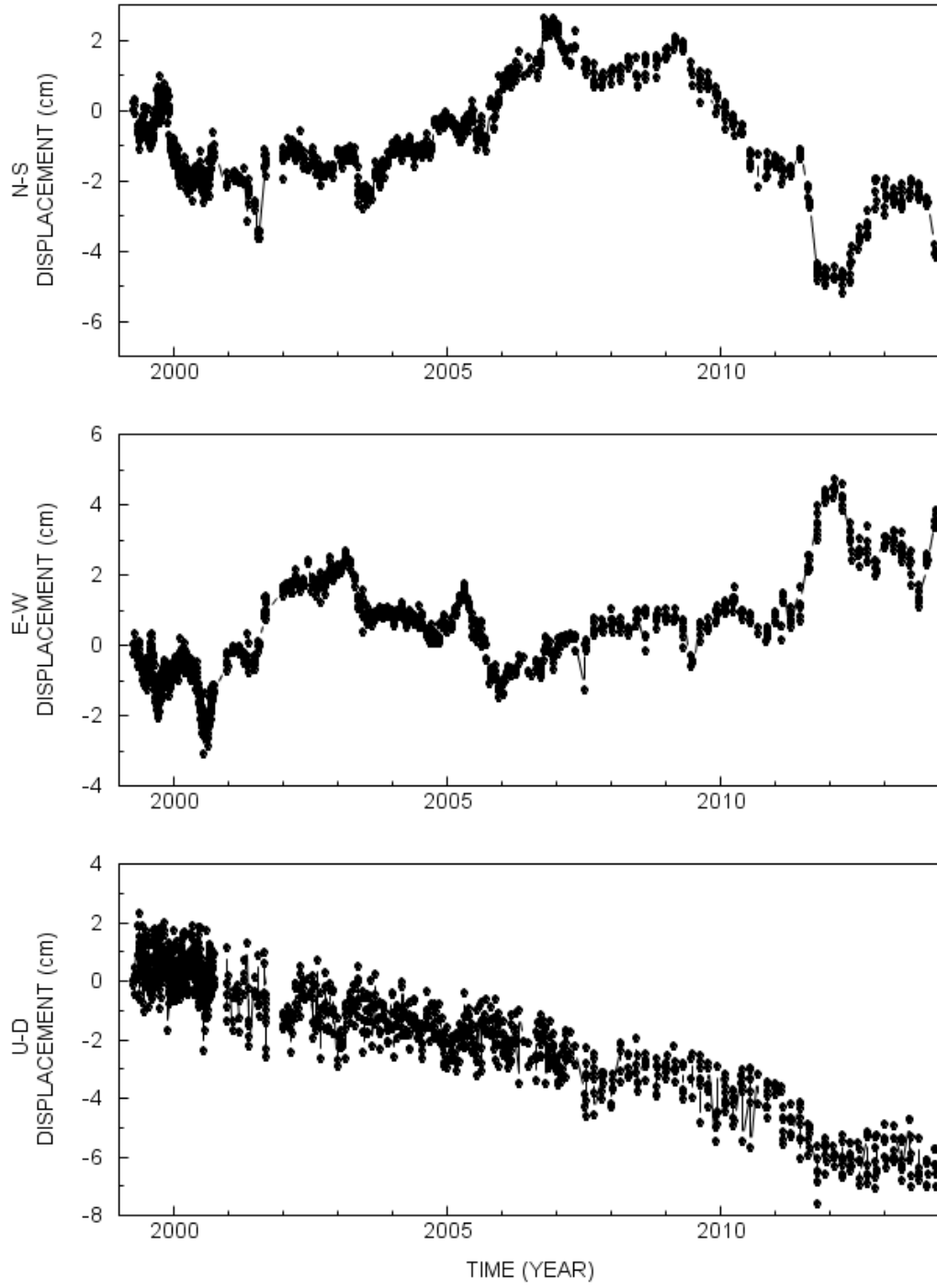
Appendix II: GPS Timeseries



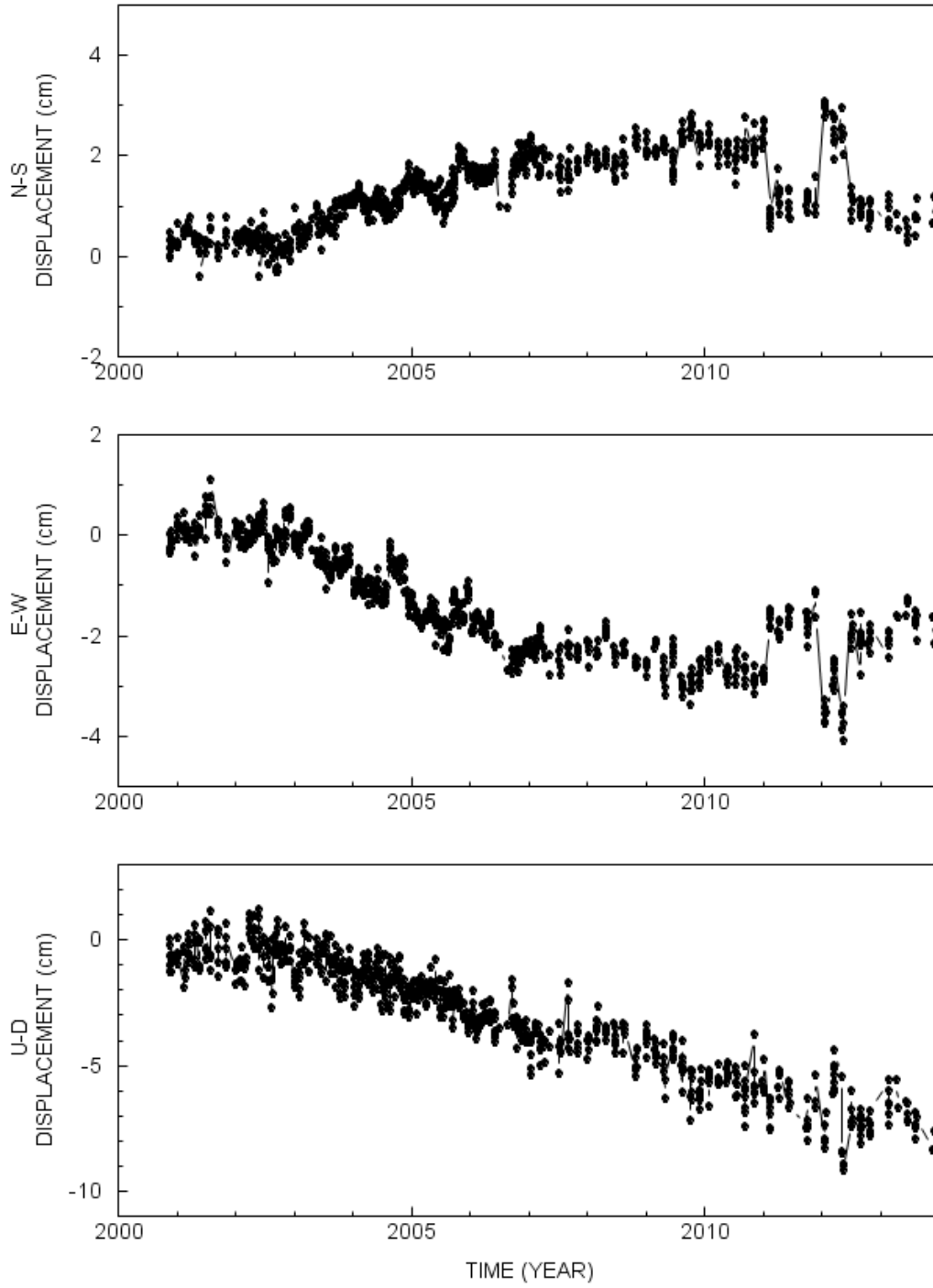
PA04 MOTION (SHRF)



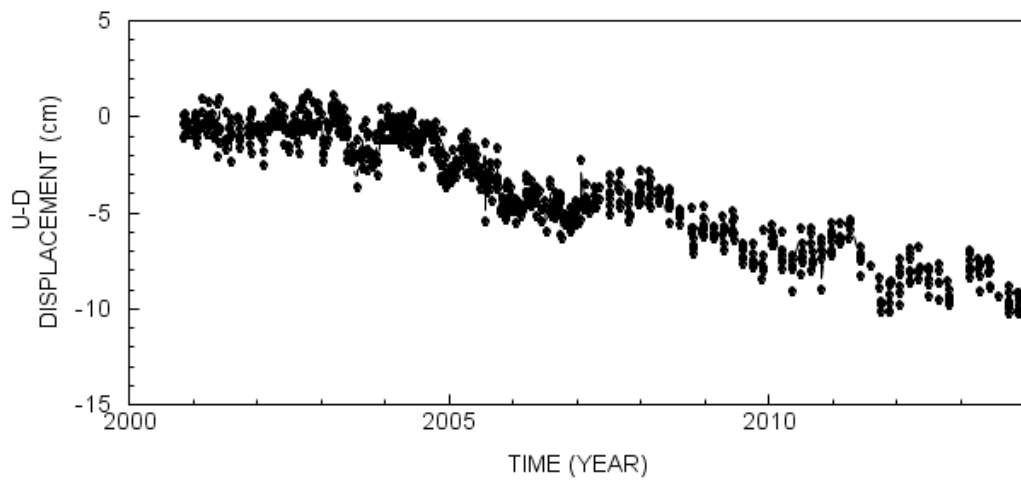
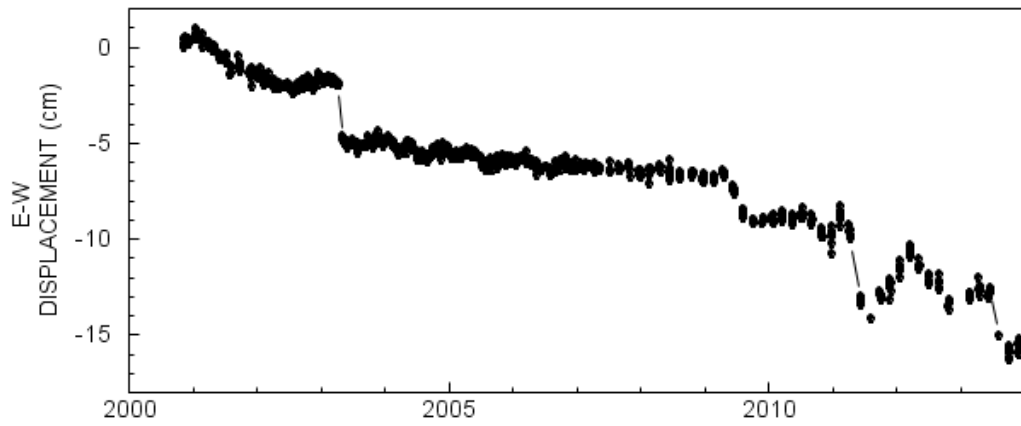
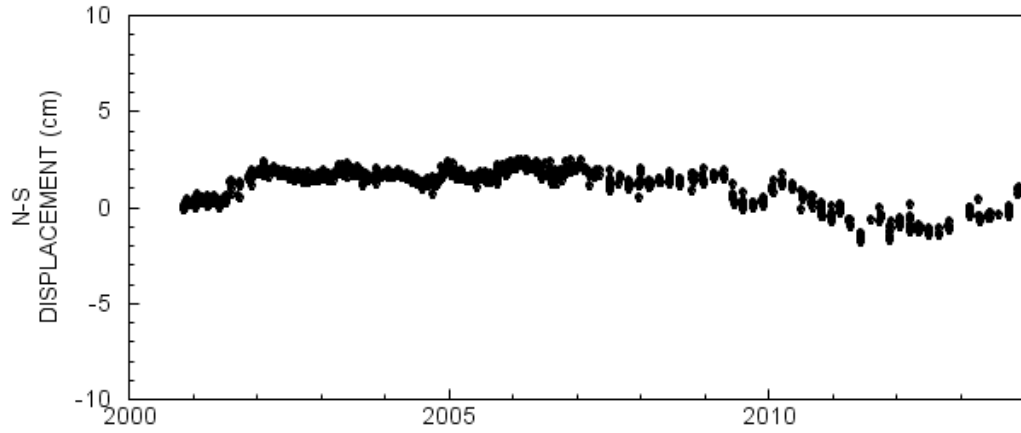
PA10 MOTION (SHRF)



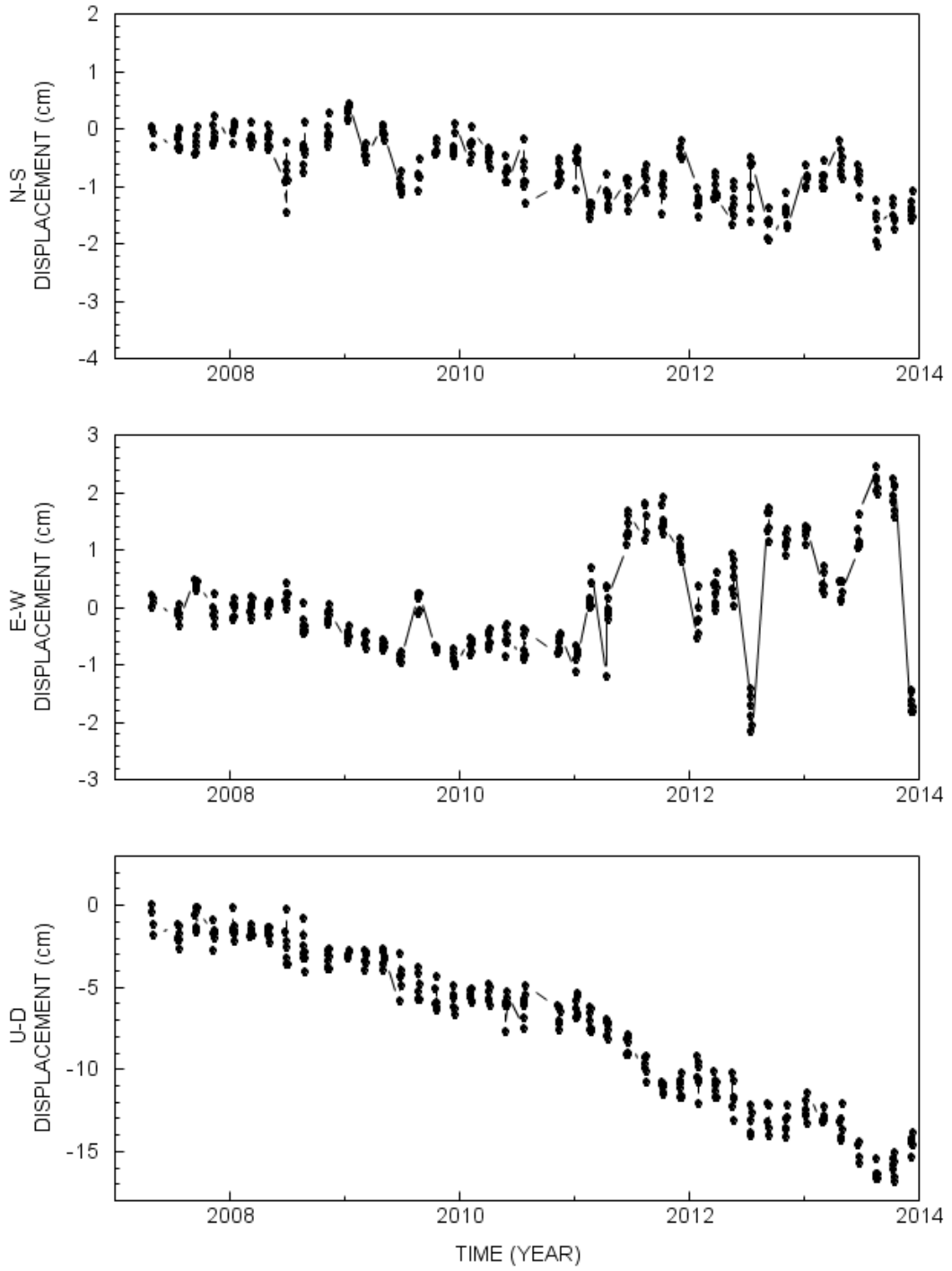
PA14 MOTION (SHRF)



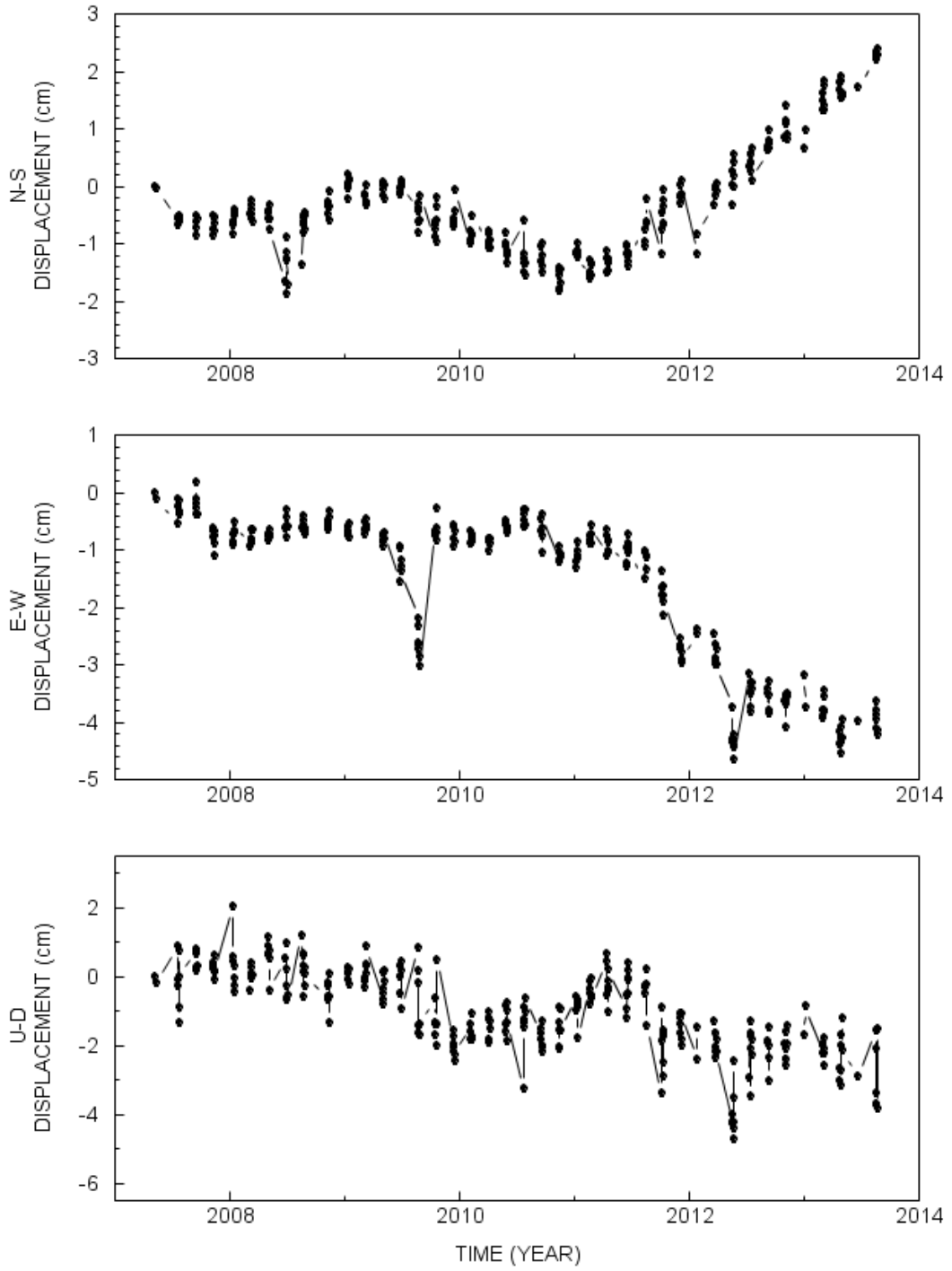
PA16 MOTION (SHRF)



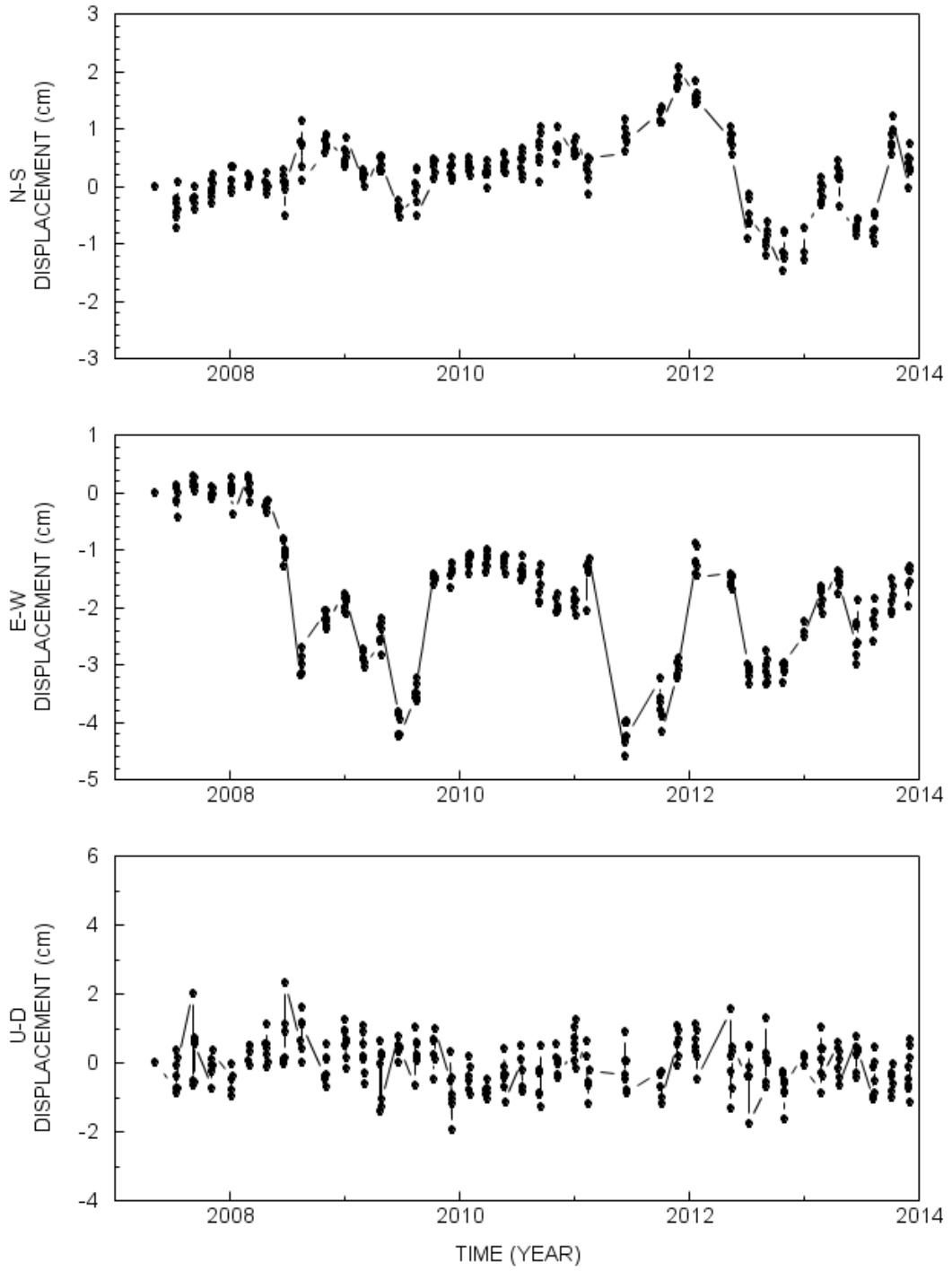
PA29 MOTION (SHRF)



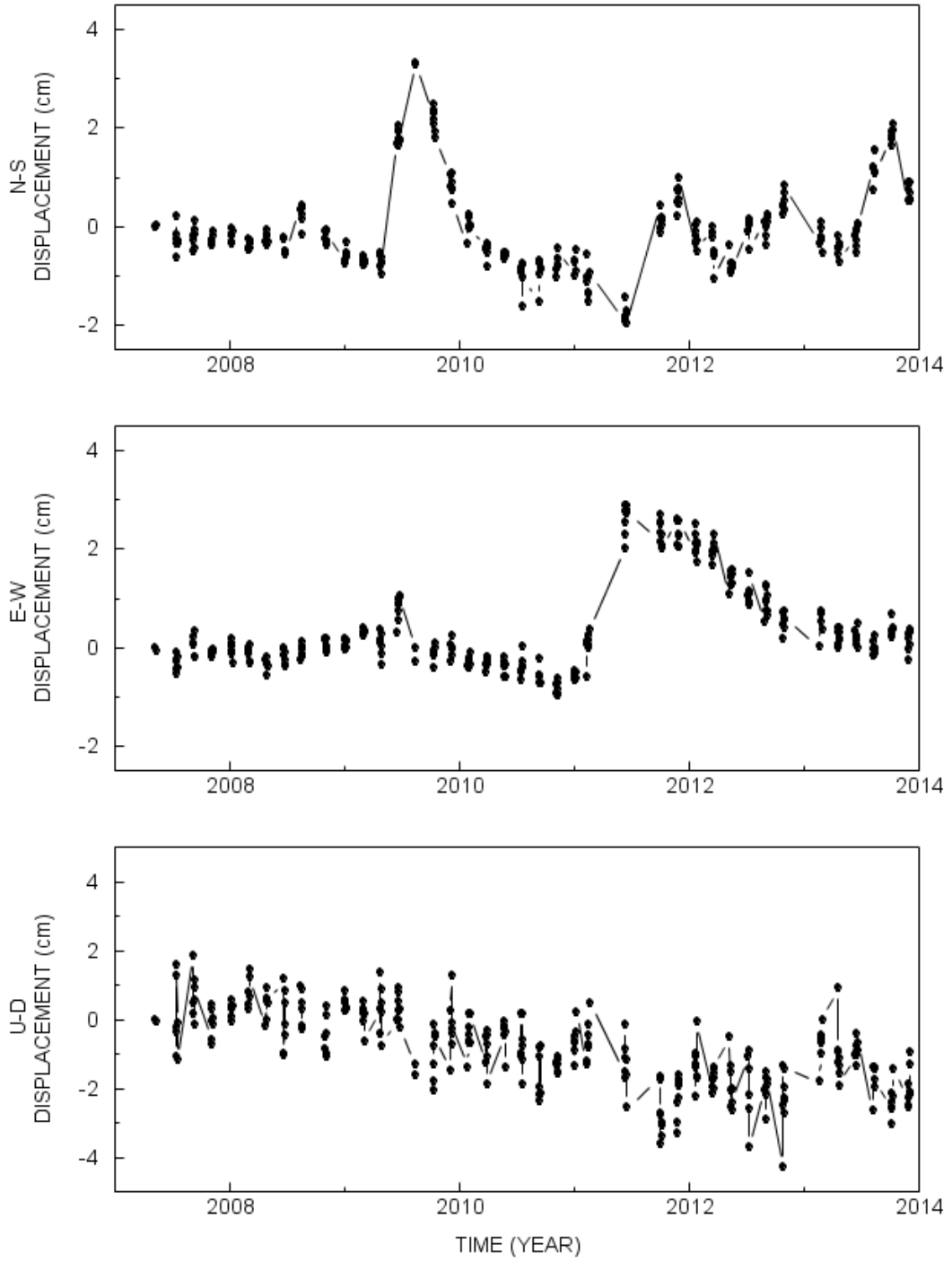
PA30 MOTION (SHRF)



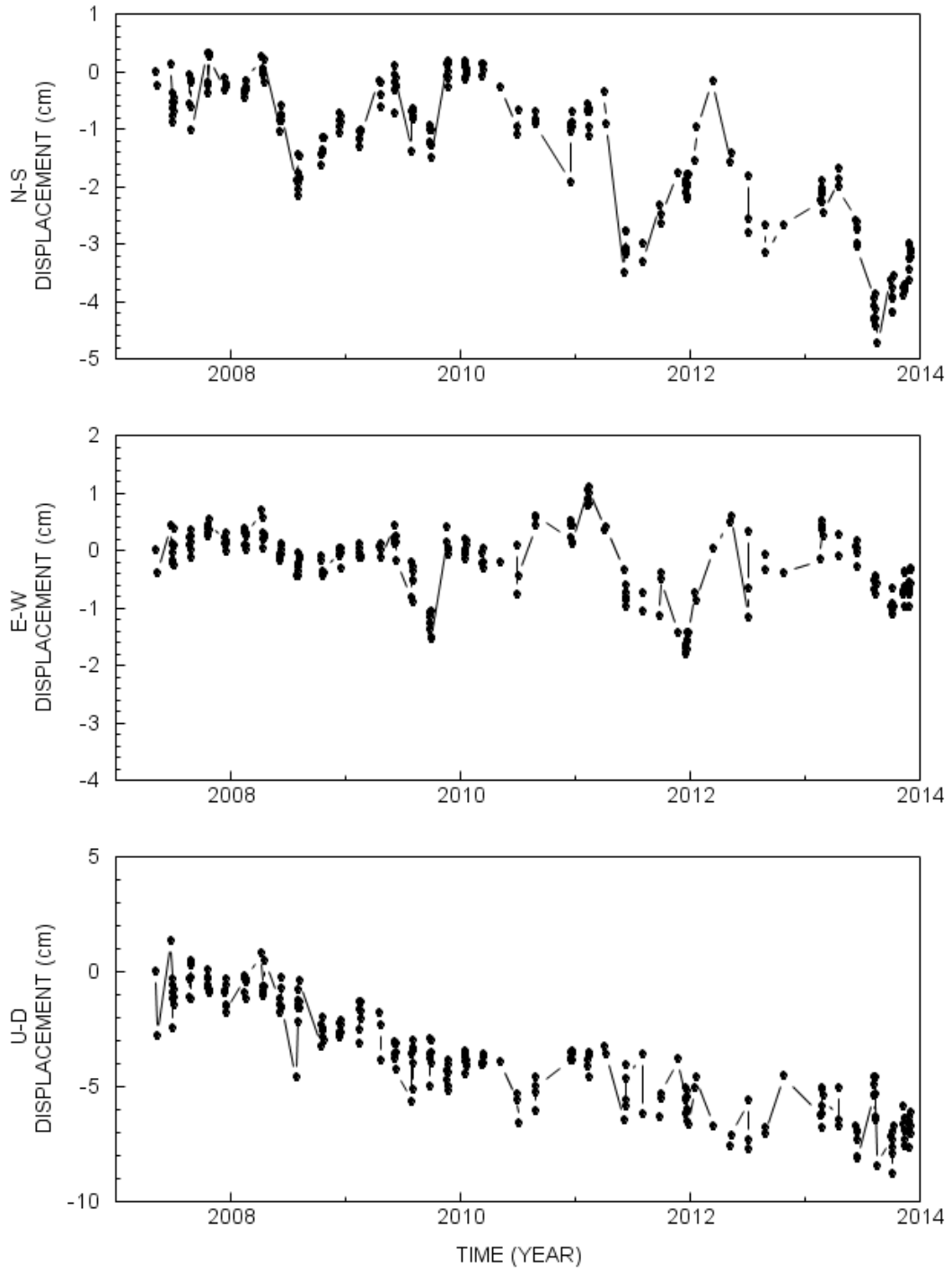
PA31 MOTION (SHRF)



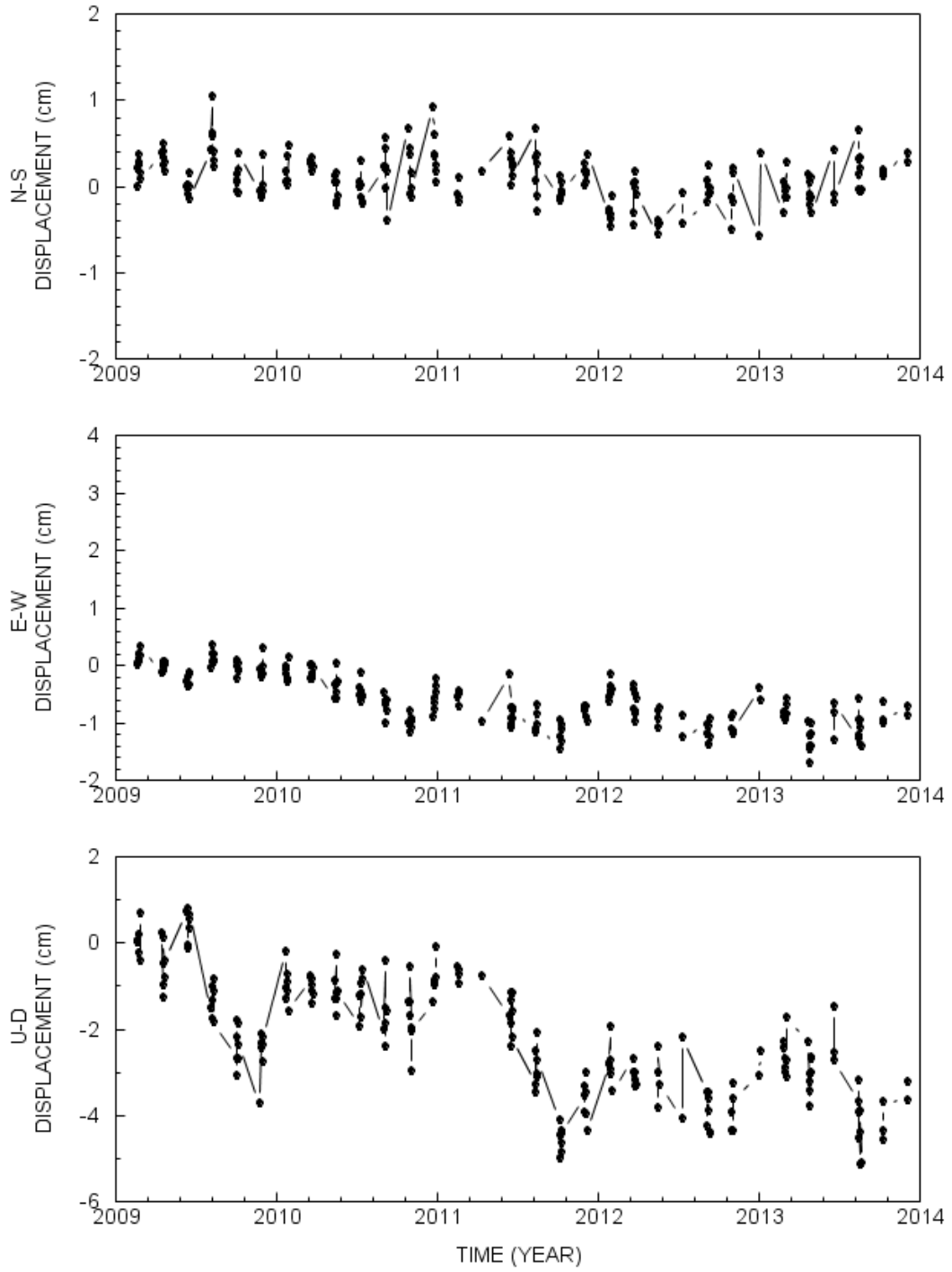
PA32 MOTION (SHRF)



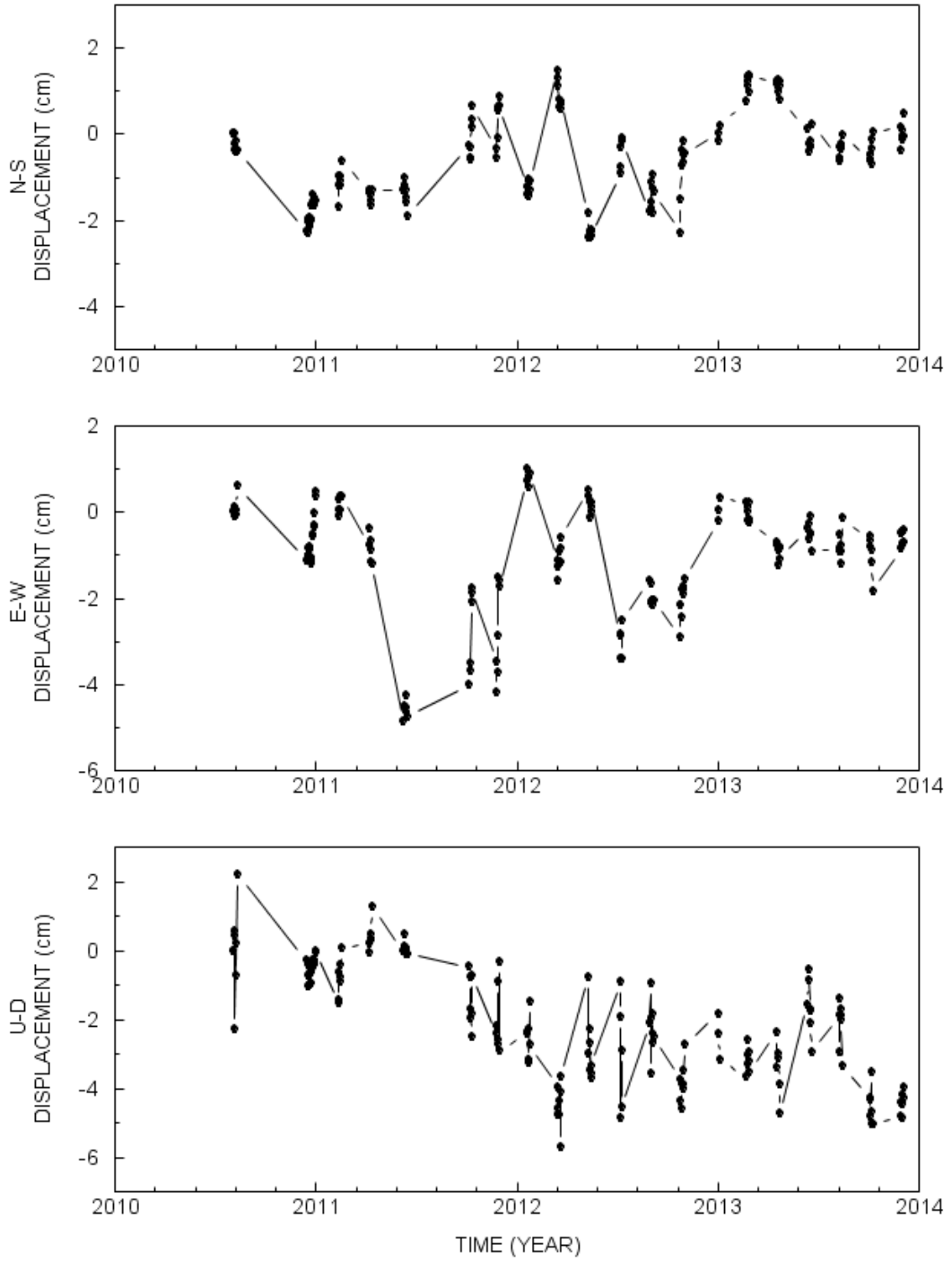
PA40 MOTION (SHRF)



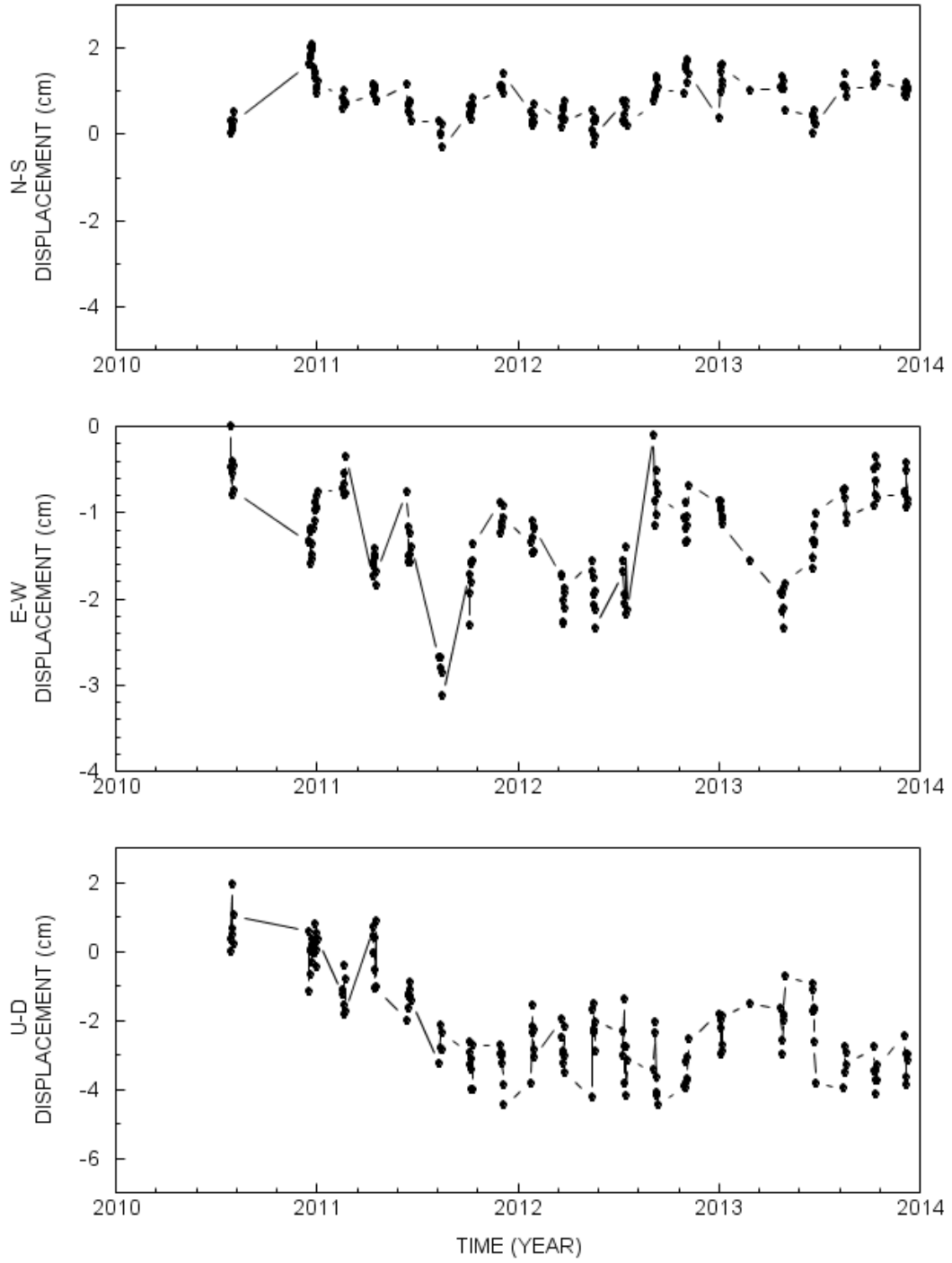
PA57 MOTION (SHRF)



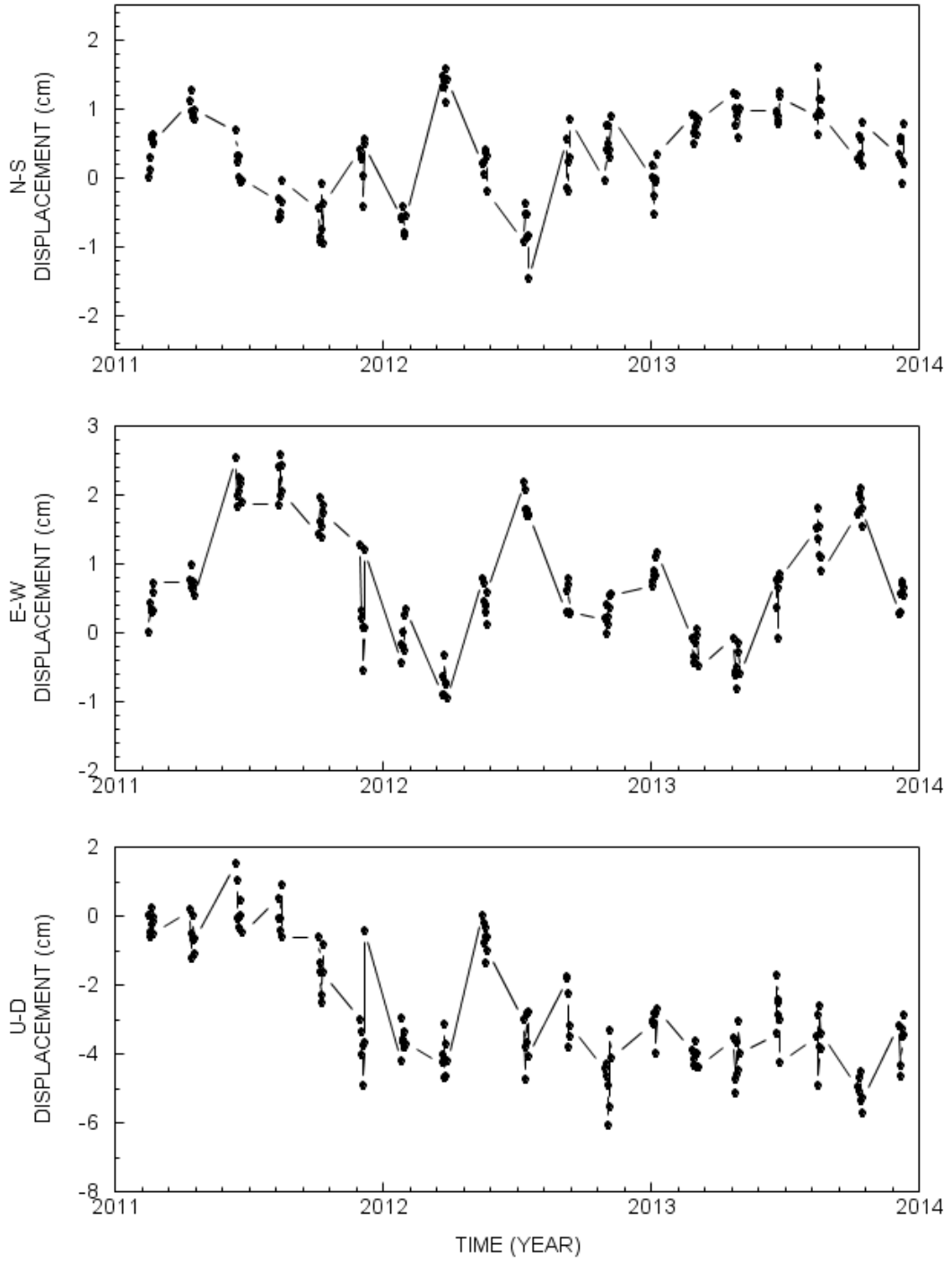
PA58 MOTION (SHRF)



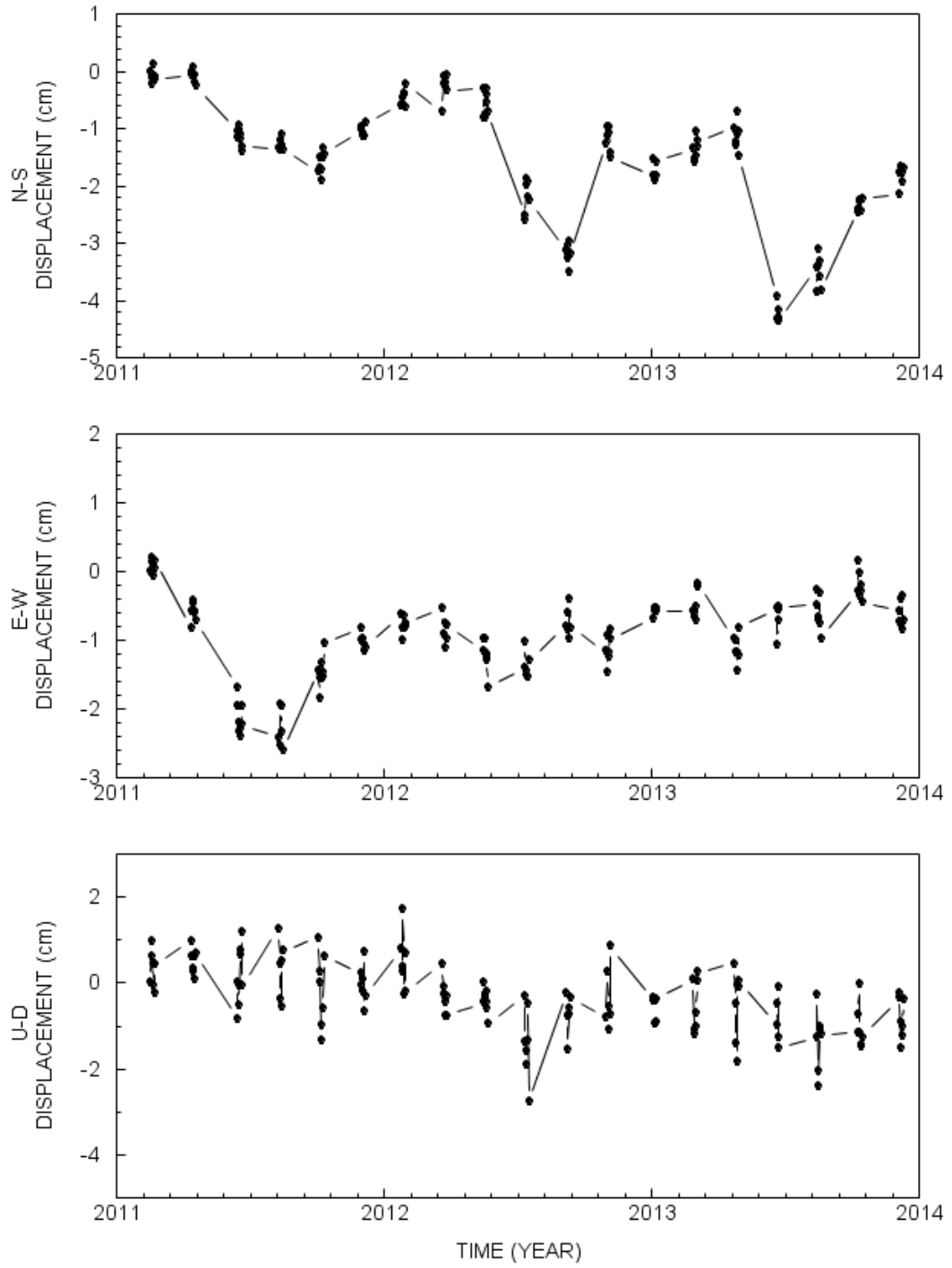
PA59 MOTION (SHRF)



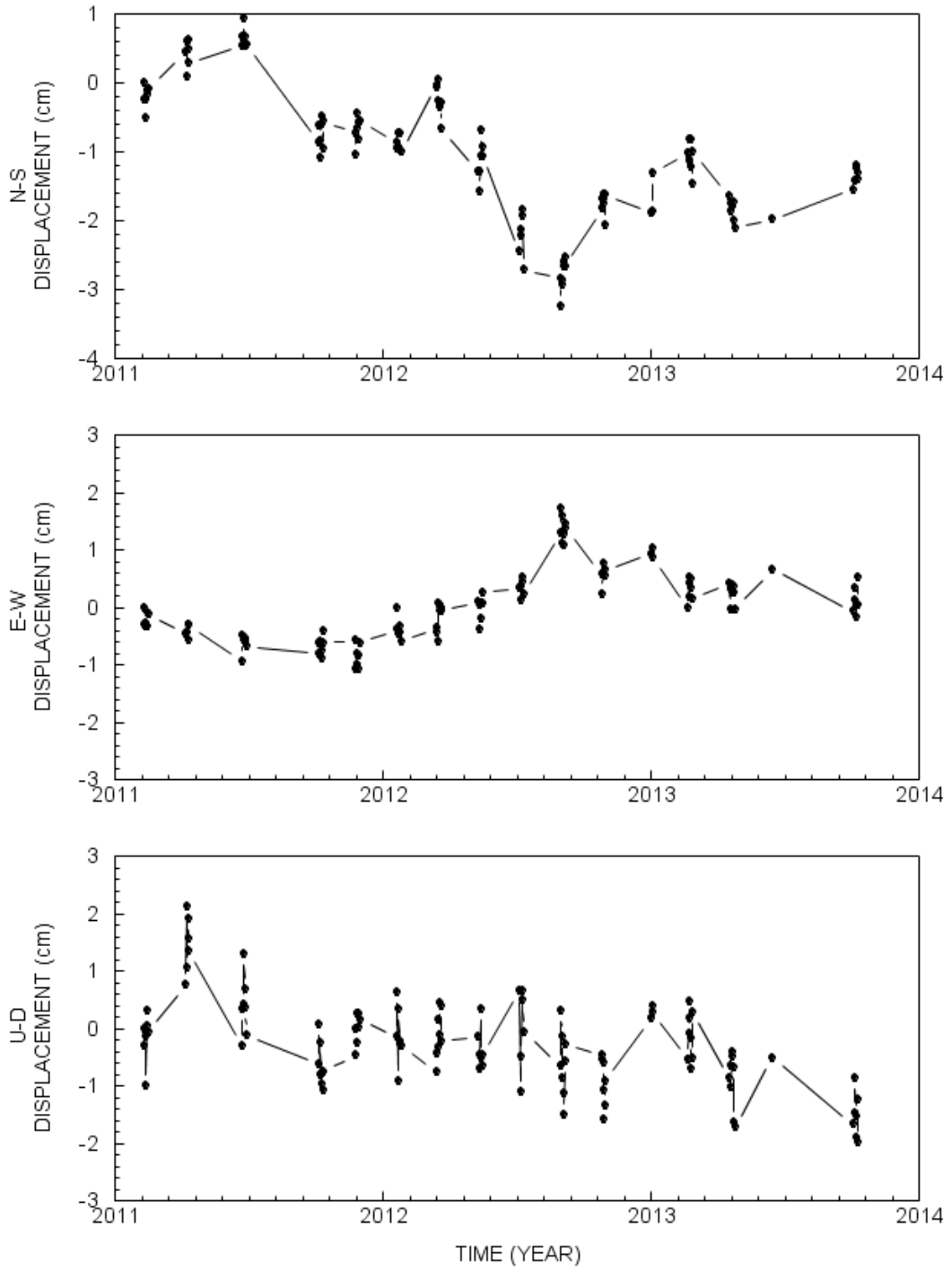
PA61 MOTION (SHRF)



PA62 MOTION (SHRF)



PA67 MOTION (SHRF)



TXRO MOTION (SHRF)

